EXPERIMENTAL EVALUATION OF THE MASSACHUSETTS INSTITUTE OF TECHNOLOGY LINCOLN LABORATORY ANECHOIC CHAMBER

T. G. Hickman
Senior Research Engineer
T. J. Lyon
Manager, Research and Analysis

Scientific-Atlanta, Inc.
Atlanta, Georgia

Submitted Under Contract AF 19(628) 5167
June 1968

EXPERIMENTAL EVALUATION OF THE MASSACHUSETTS INSTITUTE OF TECHNOLOGY LINCOLN LABORATORY ANECHOIC CHAMBER

T. G. Hickman
Senior Research Engineer
T. J. Lyon
Manager, Research and Analysis

Scientific-Atlanta, Inc.
Atlanta, Georgia

Prepared for
Massachusetts Institute of Technology
Lincoln Laboratory
Purchase Order Number A-1097

Submitted Under Contract AF 19(628) 5167
June 1968

TABLE OF CONTENTS

LIST OF ILLUSTRATIONS

LIST OF ILLUSTRATIONS - continued

1.0 INTRODUCTION

This report presents the results of an analytical and experimental program directed toward evaluation of an 84-foot tapered anechoic chamber at Massachusetts Institute of Technology Lincoln Laboratory. The program was cooperatively funded by Lincoln Laboratory under Contract AF 19(628) 5167 and Scientific-Atlanta, Incorporated; the experiments and analyses were conducted by the Research and Analysis Group of Scientific-Atlanta with the support and assistance of Lincoln Laboratory personnel under the direction of Mr. L. J. Ricardi and the direct supervision of Mr. D. J. Frediani, Jr. Emphasis of the program was placed on documentation of the chamber capabilities at representative frequencies in terms of typical required antenna measurement objectives.

This report is divided into four major sections. A theoretical discussion of the tapered chamber is presented in Section 2. Section 3 includes a discussion of coherent extraneous signal effects and describes the measurement techniques which were employed to document the effects of such signals in the test region. Section 4 discusses the measurement results and presents data to demonstrate the interference levels observed. Conclusions and recommendations are presented in Section 5.

Accepted for the Air Force
Franklin C. Hudson
Chief, Lincoln Laboratory Office

2.0 THEORETICAL ANALYSIS OF THE TAPERED CHAMBER

The presence of extraneous electromagnetic energy in any antenna test facility is a potential source of error for any kind of antenna testing. The elimination of this extraneous energy is therefore the primary objective in the design of the facility. In the case of an elevated outdoor antenna test range, this is accomplished by the selection of range length, tower heights, and source antenna beamwidths such that only sidelobe energy from the source antenna is allowed to illuminate the range surface. This sidelobe energy is frequently reflected skyward by the placement of conducting diffraction fences on the range surface, thereby leaving the area of the receiving aperture illuminated by essentially only direct path energy from the source antenna. This test facility closely approximates the free space illumination of a test antenna by a plane wave and is thus widely used as a testing environment.

It is not always practical to select these variables such that only sidelobe energy illuminates the surface of an antenna range, however, and the above described range is not useful in such cases. When low frequencies are involved, for example, and antennas such as yagis and log period structures are being tested, the broad beamwidths of antennas available as source antennas prohibit the exclusion of main lobe energy from the test range surface. In such cases this surface illumination is utilized. The surface is graded to a tolerance in keeping with the Rayleigh criterion such that it represents a microwave mirror to the incoming wave. The range length and tower heights are then adjusted such that the direct path wave and the wave reflected from the range surface add in phase at the test aperture thereby producing a smoothly varying cosinusoidal interference pattern peaked on the antenna under test.

This antenna test range, commonly referred to as a ground reflection range, also closely approximates the free space illumination of a test antenna by a plane electromagnetic wave and is commonly used as a test facility. The mere fact that the reflected wave can approximately equal the direct path wave in amplitude in no way detracts from its utility as a test facility, since the purity of the incident field is the important consideration and not how this purity was obtained. The scattering of energy into the test aperture in such a manner as to cause cyclic perturbations of the incident wave in the test aperture region, however, does

degrade the performance of the facility and sources of such scattering must be minimized. In the case of the ground reflection range, such scattering sources could be present as shrubs on the range surface, fences close to the range, drain gutters on the receive building, etc. These are the reflection levels that are referred to when extraneous energy levels are quoted on such an antenna test facility, and not the primary reflection from the range surface.

It is the opinion of this author that such an analogy can be made with respect to the tapered anechoic chamber in that whereas only one conducting surface contributes to the smoothly varying interference pattern at the test aperture in the case of the ground reflection range, four such conducting surfaces contribute thereto in the case of the tapered chamber.

Before looking at the tapered chamber, let us first look more closely at the ground reflection range. Consider the geometry of Figure 1. The range surface is assumed to present a reflection coefficient to the illuminating field of $e^{j\pi}$. In order that the direct-path signal[1], $\bar{E}_D$, and the reflected signal, $\bar{E}_R$, shall arrive at the test point in phase, we must have

$$R_R = R_D + N\lambda/2, \qquad N = 1, 3, 5, 7, \ldots \tag{2.1}$$

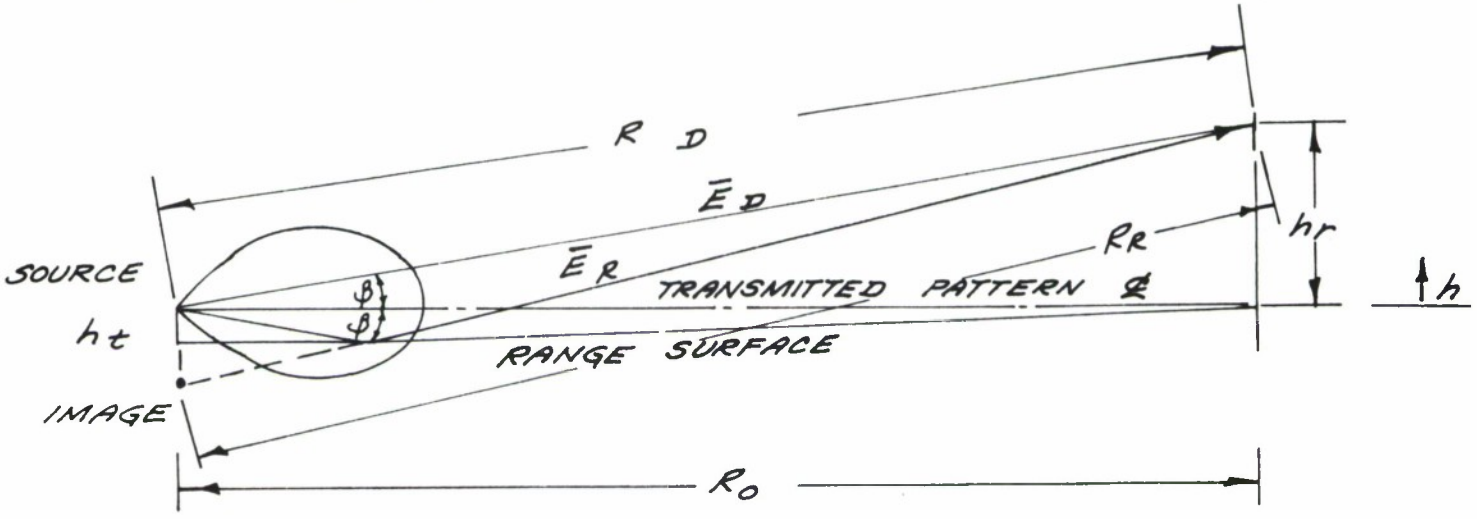

Figure 1. Ground-Reflection Antenna Range Geometry

[1] Phasors will be indicated by superscripted bars throughout this report.

For given test heights, one usually prefers the case N = 1, which produces the broadest possible lobe in the region of the test aperture. Reference to Figure 1 shows that for $h = h_r$,

$$R_D = \left[R_o^2 + (h_r - h_t)^2\right]^{\frac{1}{2}} \tag{2.2}$$

and

$$R_R = \left[R_o^2 + (h_r + h_t)^2\right]^{\frac{1}{2}} . \tag{2.3}$$

For $R_o >> h_r$ and h_t, equations (2.1) through (2.3) yield, for N = 1,

$$R_R - R_D \doteq \left[R_o + \frac{(h_r + h_t)^2}{2R_o}\right] - \left[R_o + \frac{(h_r - h_t)^2}{2R_o}\right] \doteq \frac{\lambda}{2} \tag{2.4}$$

or

$$h_t = \frac{\lambda R_o}{4h_r} \quad .* \tag{2.5}$$

Let us now look at the phasor addition of the two waves. We will consider R_o to be of sufficient length to consider the waves as planar.

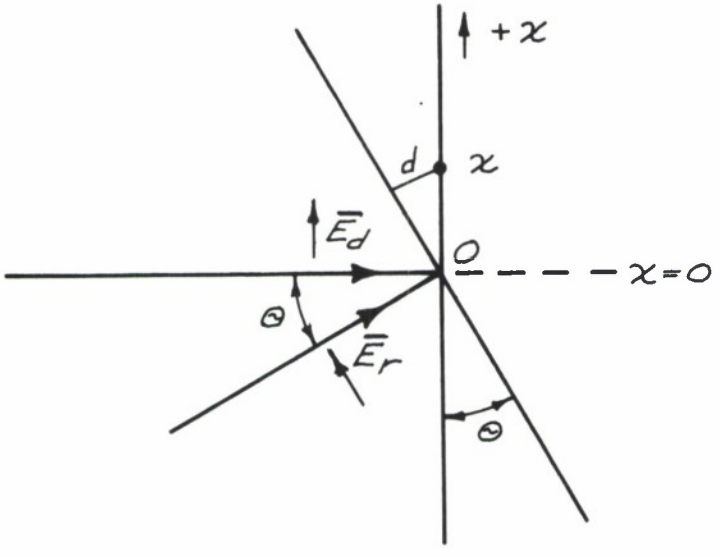

Figure 2. Two Plane Waves Coincident at a Point O.

*In practice, experimental optimization of the incident field will require a source height setting somewhat less than $\lambda R_o/4h_r$ due to the directive pattern of the source antenna.

The two fronts of constant phase shown in Figure 2 intersect at Point O, the origin, which corresponds to the maximum of the interference pattern. We will look at the resultant field at the general field Point X. Assume the waves to be of equal amplitude. This is approximately true in the ground reflection range because the beamwidths of the antennas are very broad; these antennas are pointing toward the base of the receive tower, and the coefficient of reflection of the ground under normal operating conditions is essentially -1. The phasors $\overline{E}_d$ and $\overline{E}_r$ can be expressed at the field Point X as

$$\overline{E}_d = Ee^{j\omega t}, \tag{2.6}$$

and

$$\overline{E}_r = Ee^{j(\omega t + \frac{2\pi d}{\lambda})}$$

$$= Ee^{j(\omega t + \frac{2\pi}{\lambda} x \sin\theta)} \tag{2.7}$$

The total field at the Point X is therefore:

$$\overline{E}_t = \overline{E}_d + \overline{E}_r = Ee^{j\omega t}\left(1 + e^{j\frac{2\pi x}{\lambda}\sin\theta}\right). \tag{2.8}$$

Suppressing the time dependence of this quantity and normalizing to 2E, we get:

$$|\overline{E}_N| = \tfrac{1}{2}\left[\left(1 + e^{j\frac{2\pi}{\lambda}\sin\theta}\right)\left(1 + e^{-j\frac{2\pi x}{\lambda}\sin\theta}\right)\right]^{\frac{1}{2}}$$

$$= \frac{\sqrt{2}}{2}\left(1 + \cos\frac{2\pi x}{\lambda}\sin\theta\right)^{\frac{1}{2}}$$

$$= \cos\left(\frac{\pi x}{\lambda}\sin\theta\right). \tag{2.9}$$

But from typical geometries, $\sin\theta \doteq \frac{2h_t}{R_o}$. Therefore:

$$|\overline{E}_N| = \cos\frac{2\pi x h_t}{\lambda R_o} \tag{2.10}$$

Combining equations (2.5) and (2.10), we get:

$$|\overline{E}_N| = \cos\frac{\pi x}{2h_r} \tag{2.11}$$

This equation represents the smoothly varying cosinusoidal interference pattern which peaks at height h_r, where the test antenna is commonly placed, and whose closest nulls are at the ground level and at a distance h_r above the test aperture.

The anechoic chamber under consideration here is a truncated rectangular cone with an apex angle of 20.54 degrees which terminates in a right parallelopiped as seen in Figure 3. The angle of incidence as measured from the plane of the absorber for the primary specular reflection is 15.6°. At the lowest operating frequency of 230 MHz and at this angle of incidence, this absorber represents a fairly smooth surface and at that frequency it is reasonable to assume that a significant amount of energy is reflected into the quiet zone.

To further examine the reflections from this region, suppose we wish to calculate the amplitude distribution as a function of position in the quiet zone of the chamber. We will consider only first bounce reflections in this examination for the sake of simplicity. However, the one bounce approximation is probably a good one since higher order bounces have much nearer normal incidence reflections which should attenuate the waves significantly. For example, a 2-bounce reflection has incidence angles of 40.3° and 19.7°, a 3-bounce reflection has incidence angles of 63.1°, 42.6°, and 22°, etc. It is also worth noting that the Fresnel zones present on the tapered surfaces decrease rapidly with higher order bounces. Figure 4 represents a top view of a simplified chamber geometry. The source antenna is positioned at point S and we wish to determine the amplitude of the incident wave at the field point P along a horizontal cut through the center of the quiet zone, represented by point O.

From the geometry of Figure 4,

$$R_D = (R_A^2 + x^2)^{\frac{1}{2}} . \tag{2.12}$$

Also

$$R_{R_1} = \left[R_D^2 + (2h_t)^2 - 2R_D(2h_t)\cos\{180-(90-\alpha)-\beta\}\right]^{\frac{1}{2}},$$

which reduces to:

$$R_{R_1} = \left[R_D^2 + 4h_t^2 + 4h_t\,(R_A \sin\alpha - x\cos\alpha)\right]^{\frac{1}{2}}. \tag{2.13}$$

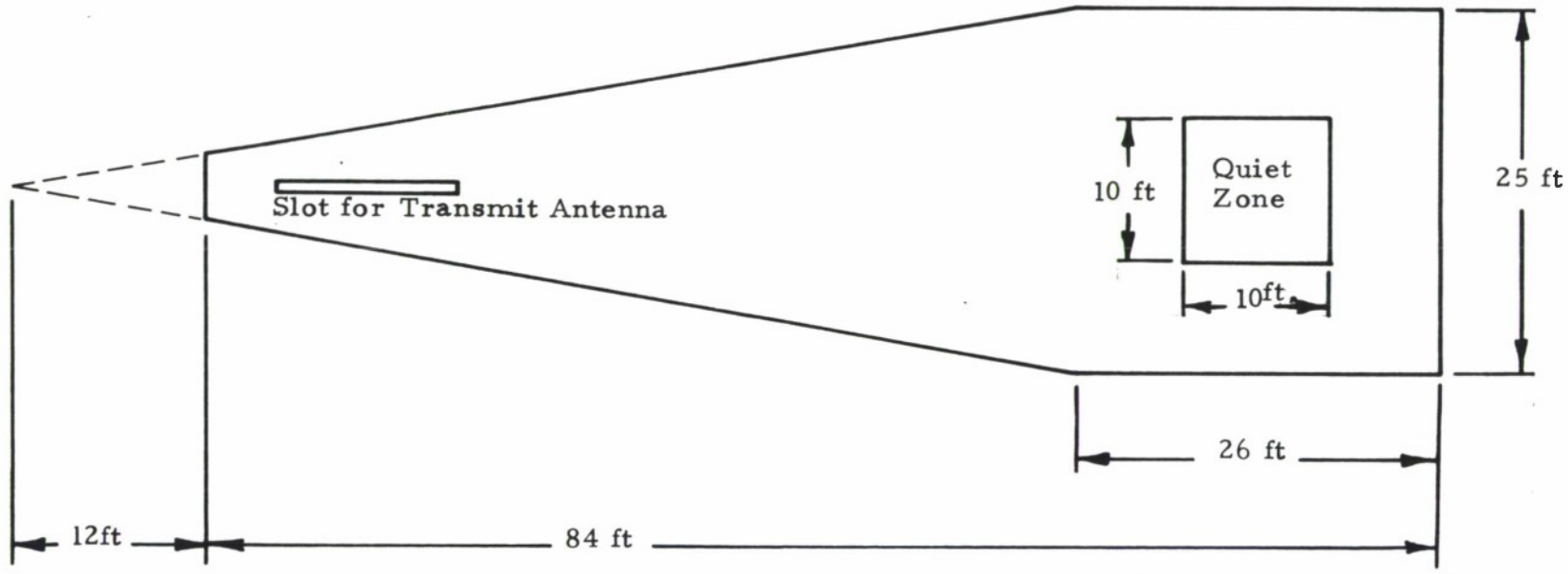

Figure 3. Plan View of Anechoic Chamber

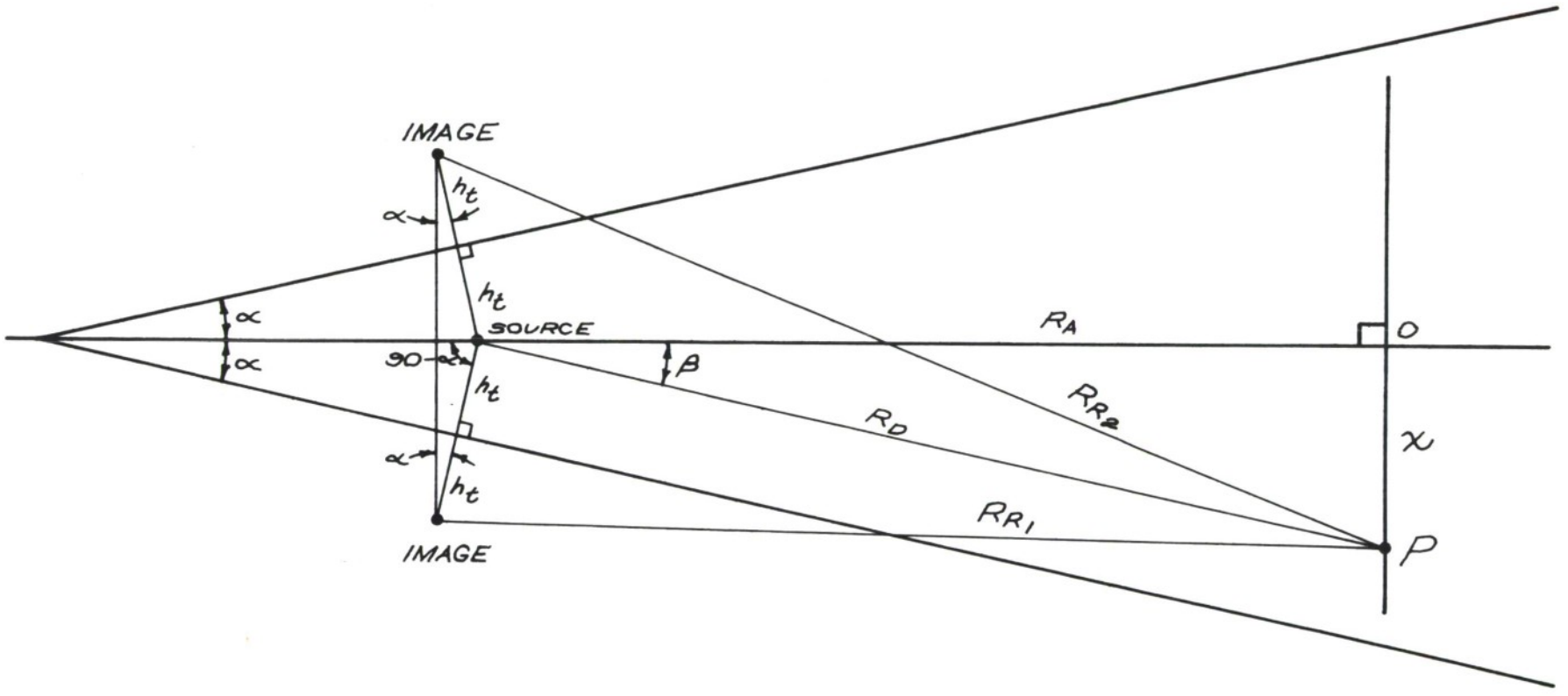

Figure 4. Simplified Plan Geometry of the Tapered Section of the Chamber Showing Quantities used in Calculation.

Likewise

$$R_{R_2} = \left[R_D^2 + 4h_t^2 + 4h_t(R_A \sin \alpha + x \cos \alpha) \right]^{\frac{1}{2}}. \qquad (2.14)$$

The quantities R_{R_1} and R_{R_2} represent the path lengths of the reflected waves shown in Figure 4 as the distance from the field Point P to the respective images. There are, however, two other reflecting surfaces to be considered. The path lengths from these reflections are equal and are represented by the length R_o in Figure 5.

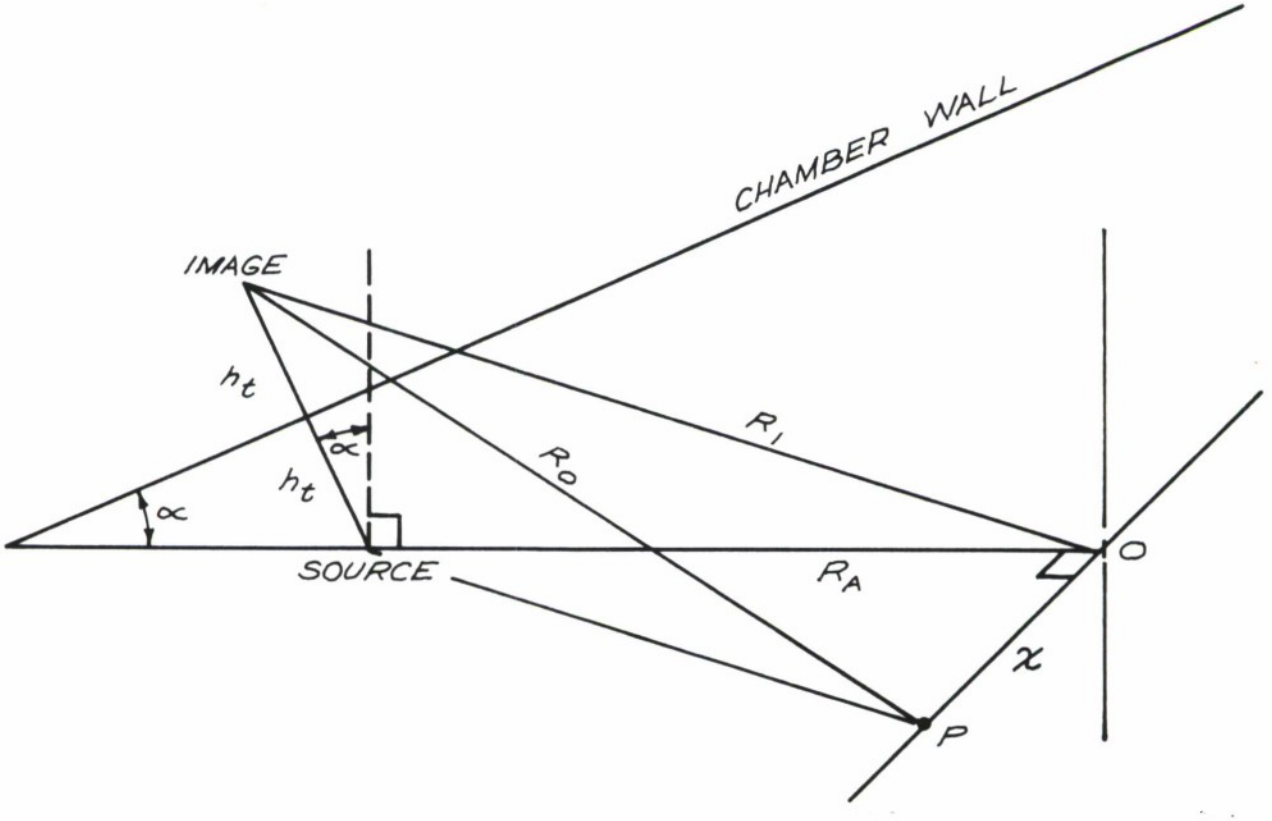

Figure 5. Three Dimensional Sketch of Chamber Geometry Showing Image of Reflection from Upper Wall to Field Point on Horizontal Plane.

As can be seen in Figure 5,

$$R_o = (R_1^2 + x^2)^{\frac{1}{2}}, \qquad (2.15)$$

where

$$R_1 = \left[R_A^2 + (2h_t)^2 - 2R_A(2h_t) \cos (90 + \alpha) \right]^{\frac{1}{2}}$$

$$= \left[R_A^2 + 4h_t^2 + 4R_A h_t \sin \alpha \right]^{\frac{1}{2}} \qquad (2.16)$$

Substituting equations (2.16) and (2.12) into equation (2.15), we get:

$$R_o = \left[R_D^2 + 4h_t^2 + 4R_A h_t \sin\alpha\right]^{\frac{1}{2}} \qquad (2.17)$$

Therefore in terms of the quantities R_D, R_{R_1}, R_{R_2} and R_o given in equations (2.12), (2.13), (2.14), and (2.17) respectively, the field at the Point P can be expressed in terms of the direct - path field amplitude E_D as:

$$E(P)=E_D\left[e^{-j2\pi R_D/\lambda} + C1\left(\frac{R_D}{R_{R_1}} e^{-j2\pi R_{R_1}/\lambda} + \frac{R_D}{R_{R_2}} e^{-j2\pi R_{R_2}/\lambda}\right) + 2C_2\frac{R_D}{R_O} e^{-j2\pi R_o/\lambda}\right] \qquad (2.18)$$

In equation (2.18), C_1 represents the reflection coefficient (both phase and amplitude) from the side walls of the chamber. It was assumed that the angles of incidence were similar enough for the two reflections over the quiet zone to assign equal reflection coefficients to these reflections. C_2 represents the reflection coefficient for the reflections from the top and bottom surfaces in the taper. The constants C_1 and C_2 depend upon the polarization of the incident wave, the effective dielectric constant of the reflecting medium, and the effective conductivity of the medium. It is difficult to obtain numerical quantities for the constants C_1 and C_2 because of the lack of experimental information available at angles of incidence other than those close to normal incidence. The difficult problem of assigning values to the material properties is complicated by the fact that the absorber is an anisotropic medium. A value $\epsilon_r = 1.1 - j\,0.12$ was used for an 8 inch pyramidal absorber manufactured by Secoa for the sake of comparing experimental and calculated results in a program evaluating microwave absorbing materials.* This corresponds to a conductivity of $\sigma \doteq 0.1$ mhos/m. The measurements described in the previous report however, were performed at 94 GHz and reflections were measured off the back of the material which represented an isotropic material. It was assumed that an effective value of conductivity would be somewhat lower for the anistropic case of the pyramidal absorber. An order of magnitude value of $\sigma = 0.1$ mhos/m was assumed and reflection coefficients calculated at values there about. Conductivities of .01 to .2 mhos/m all gave very similar results and for the sake of calculation, these representative values were used. Figure 6

*King, H. E., F. I. Shimabukuro, and J. L. Wong. 94Gc Measurements of Microwave Absorbing Materials, March, 1966, Air Force Report #SSD-TR-66-71.

shows curves with the calculated reflection coefficients plotted as a function of the angle of incidence as measured from the plane of the material. These calculations were based upon equations given by Jordan.* While the value of the calculated reflection coefficients do seem quite large, it must be remembered that this absorber was not designed for optimum performance at 250 MHz. Larger values of conductivity give larger reflection coefficients.

It should be noted that the Brewster angle lies considerably above the incident angle region of about 15°. A 180° phase shift can always be assigned to the reflection coefficient whose polarization is perpendicular to the plane of incidence. We will call this polarization the transverse electric or TE polarization. We will refer to the polarization in the plane of incidence as the transverse magnetic or TM polarization since its magnetic vector is transverse to the plane of incidence. Care should be taken in assigning a phase term to the TM reflection because this phase term must reflect how it will add in phase to the direct path signal and not how it conforms to the standard definition of phase shift. A near 0° phase is commonly attached to reflection coefficients considerably below the Brewster angle since this phase shift is commonly defined such that both polarizations exhibit 180° shift in phase at normal incidence. A 180° shift must be attached to it in this case, however, since it is the direct path signal with which the phase must be compared and the change in direction of the E-vector upon reflection must be interpreted as a phase shift. Therefore, the phases associated with both C_1 and C_2 in equation (2.18) are π radians. The signs in this case for both C_1 and C_2 reduce to -1. From the curves in Figure 6, the magnitudes of C_1 and C_2 are approximately .8 and .4, the order of which depends on the polarization of the transmit antenna.

Equation (2.18) was programmed for the computer and the above values of reflection coefficients were used. It should be noted at this time that beamwidth considerations were made for the transmit antenna used in the chamber. That is, the correct directivities in the direction of the reflections were used to modify the reflected signal strengths. The transmit antenna was a Taco yagi.

Figure 7 presents calculated curves in decibels for the amplitude of the field in the quiet zone as a function of distance from its center. Two curves are

*Jordan, E. C., Electromagnetic Waves and Radiating Systems, Prentice Hall, Inc., New York (1950), p. 611.

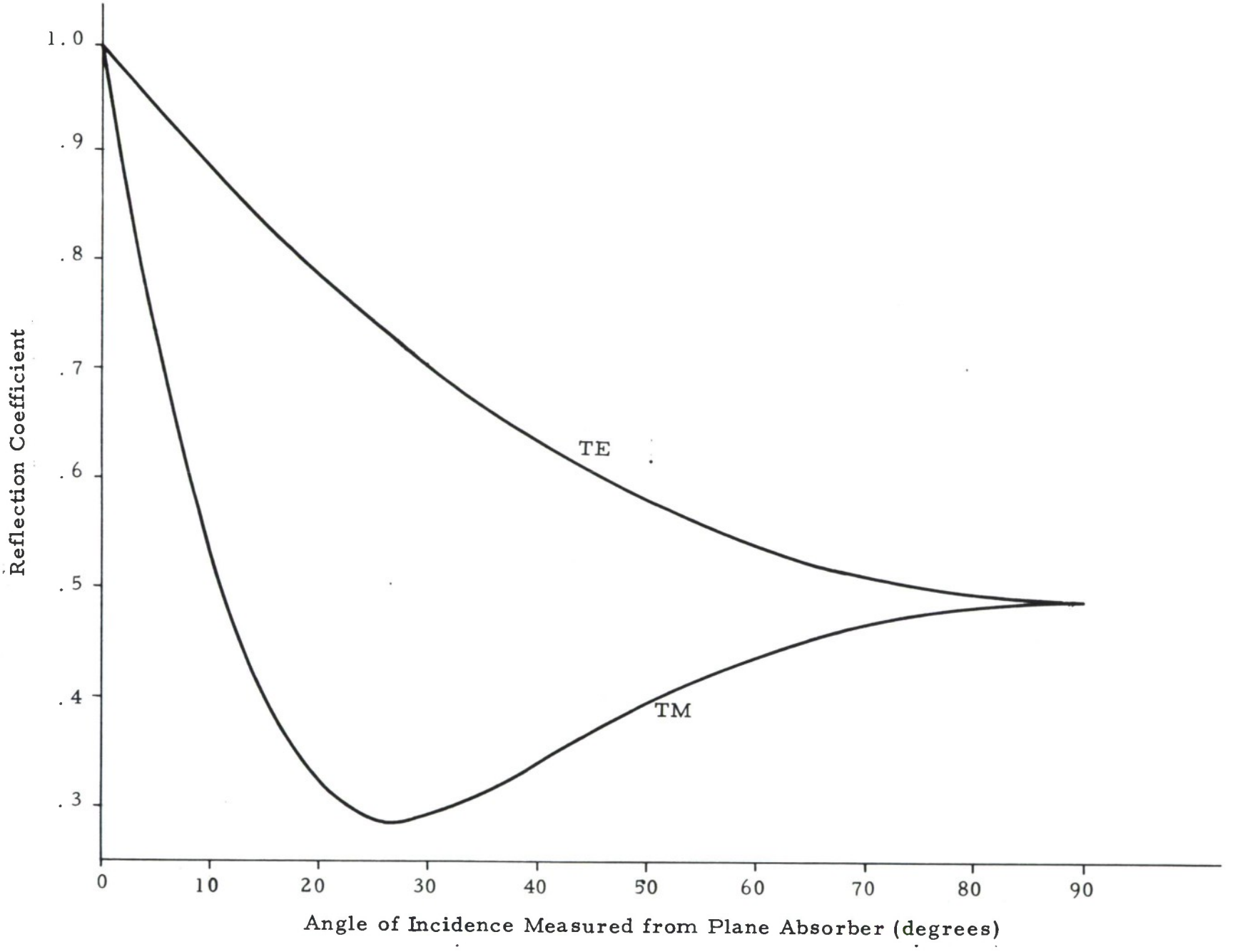

Figure 6. Calculated Reflection Coefficients as a Function of Angle of Incidence as Measured from the Tangent to the Reflector.

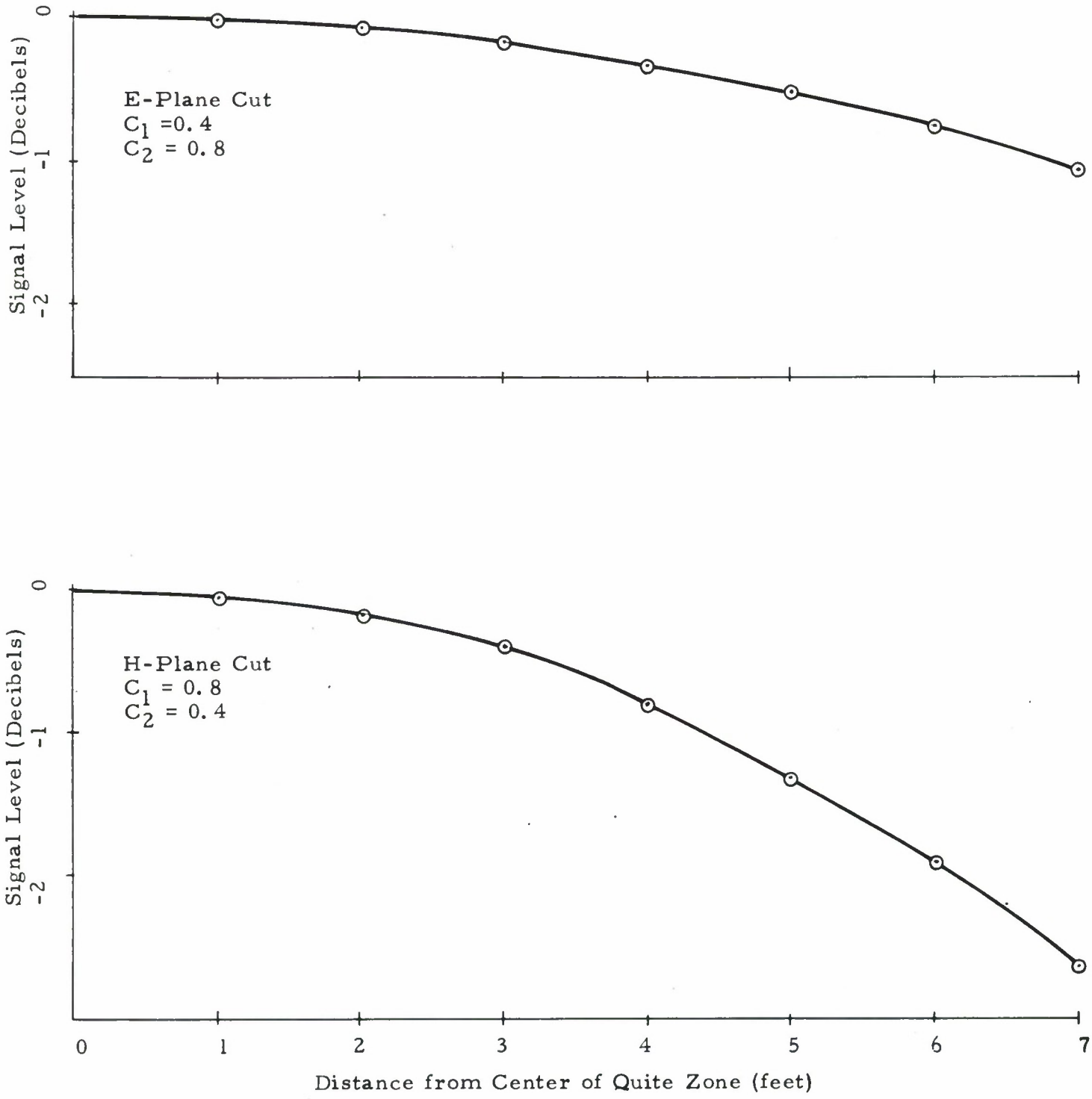

Figure 7. Calculated Amplitude Taper Across the Quite Zone in both E and H-Planes of the Transmit Antenna as a Function of Distance from the Center

presented which represent planes parallel to the E-plane and the H-plane of the antenna and are labeled as such. A sampling of the field in these planes was taken during the course of the evaluation and the data are presented in Figure 8. These data were recorded with the amplitude field probe device shown in Figures 9 and 10. The probe is basically a 9-foot beam along which a carriage supporting a probe antenna is driven by remote control to measure the incident field strength as a function of position. The field probe data shown in Figure 8 represent an excursion ±4. 5 feet from the center of the quite zone. Figure 7 predicts a roll off of about 0. 6 dB in the E-plane and about 1. 6 dB in the H-plane. Figure 8 shows experimental rolloffs of about 0. 7 dB in the E-plane and 0. 8 dB in the H-plane, which is a favorable comparison considering the means available for the selection of parameters from which the reflection coefficients were calculated. It should be noted that the rolloff predicted due to the directivities of the yagi and the probe antenna is on the order of 0. 1 dB. Much work remains to be done in the measurement of reflections from absorbing materials at off normal incidence before an entirely rigorous analysis of anechoic chambers can be carried out.

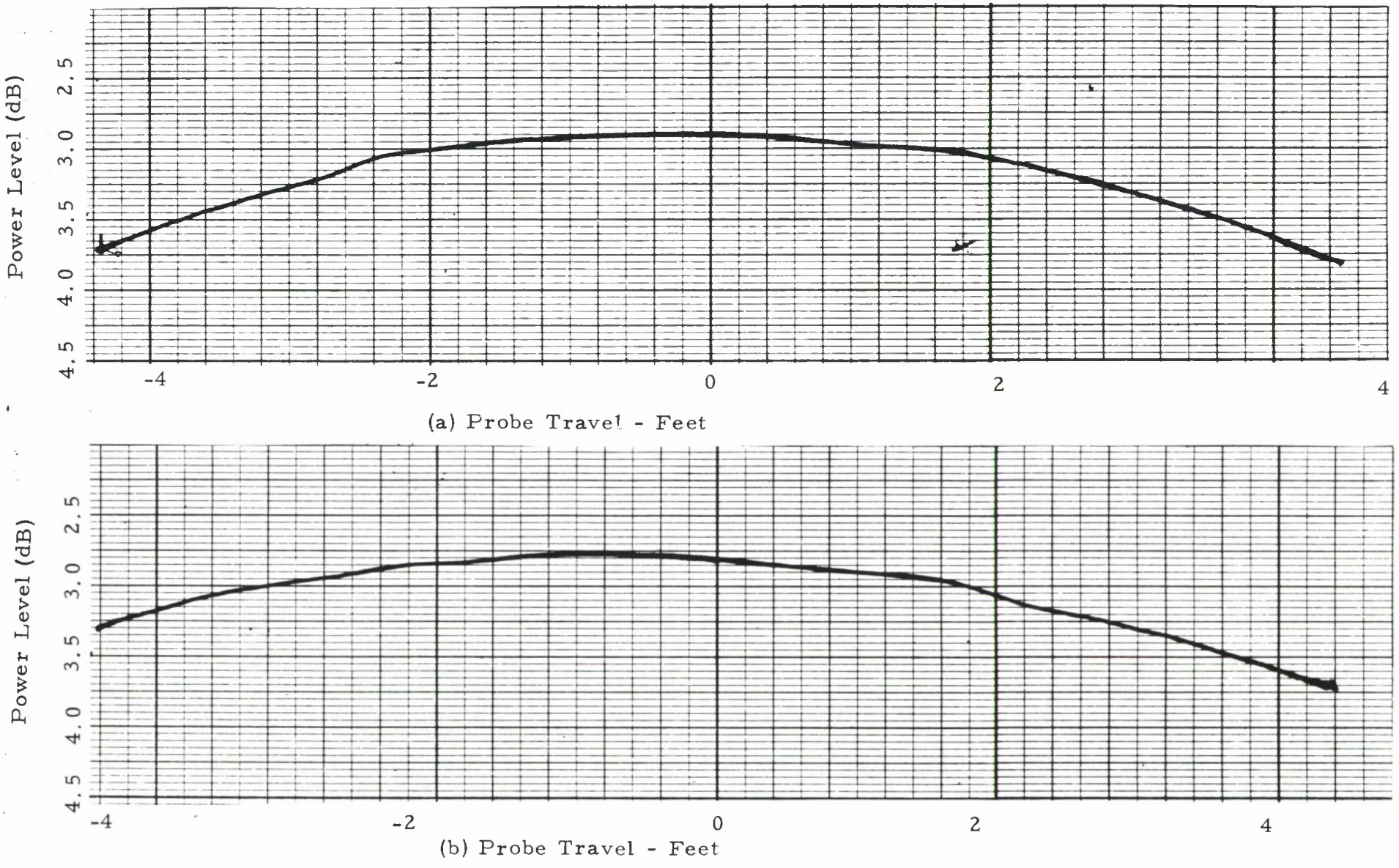

Figure 8. Transverse Field Probe Cuts Representing Excurison of ± 4.5 feet Across the Quiet Zone. (a) E-Plane Cut (b) H-Plane Cut.

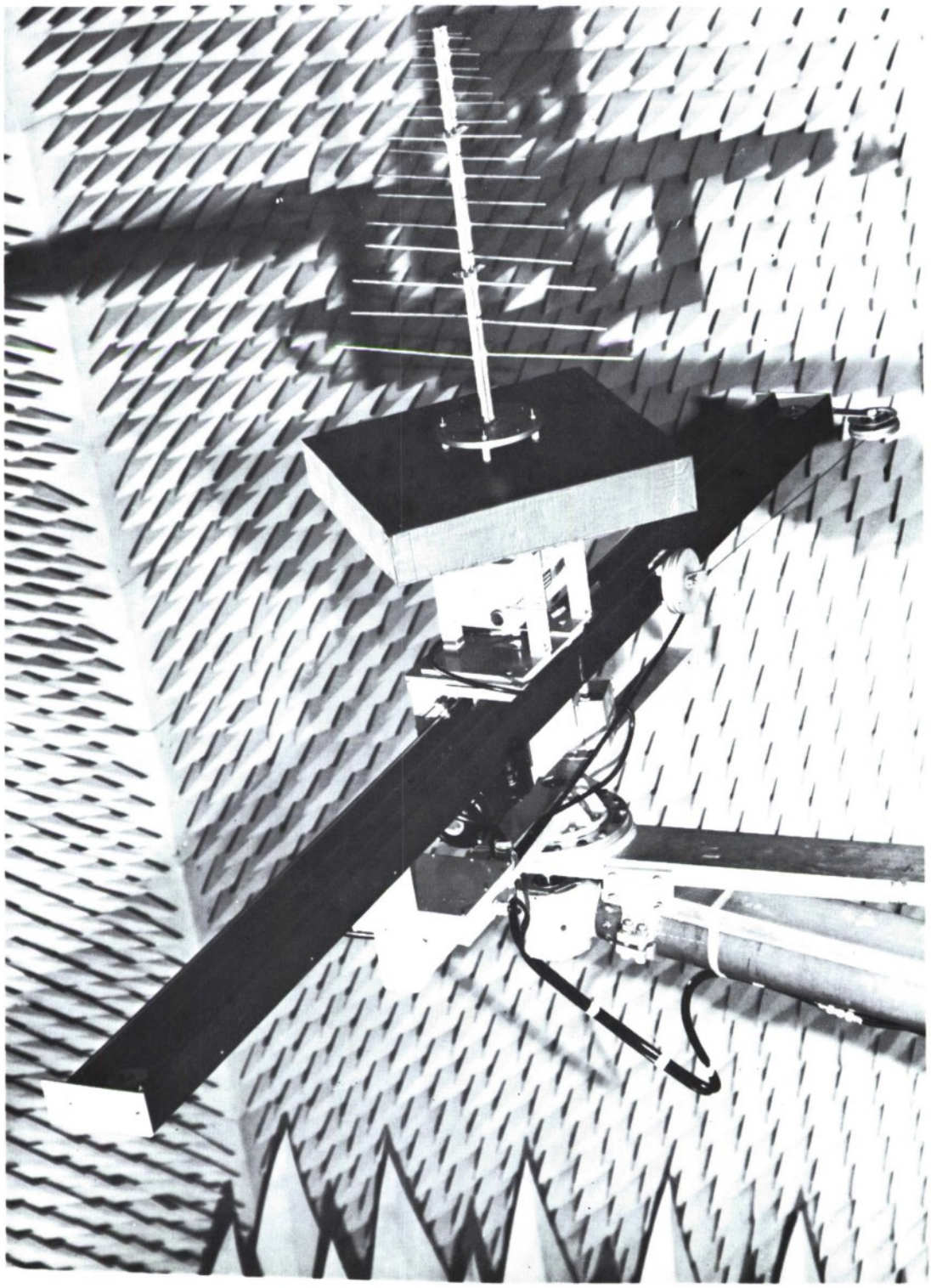

Figure 9. Aperture Field Probe Used in Making Probe Measurements

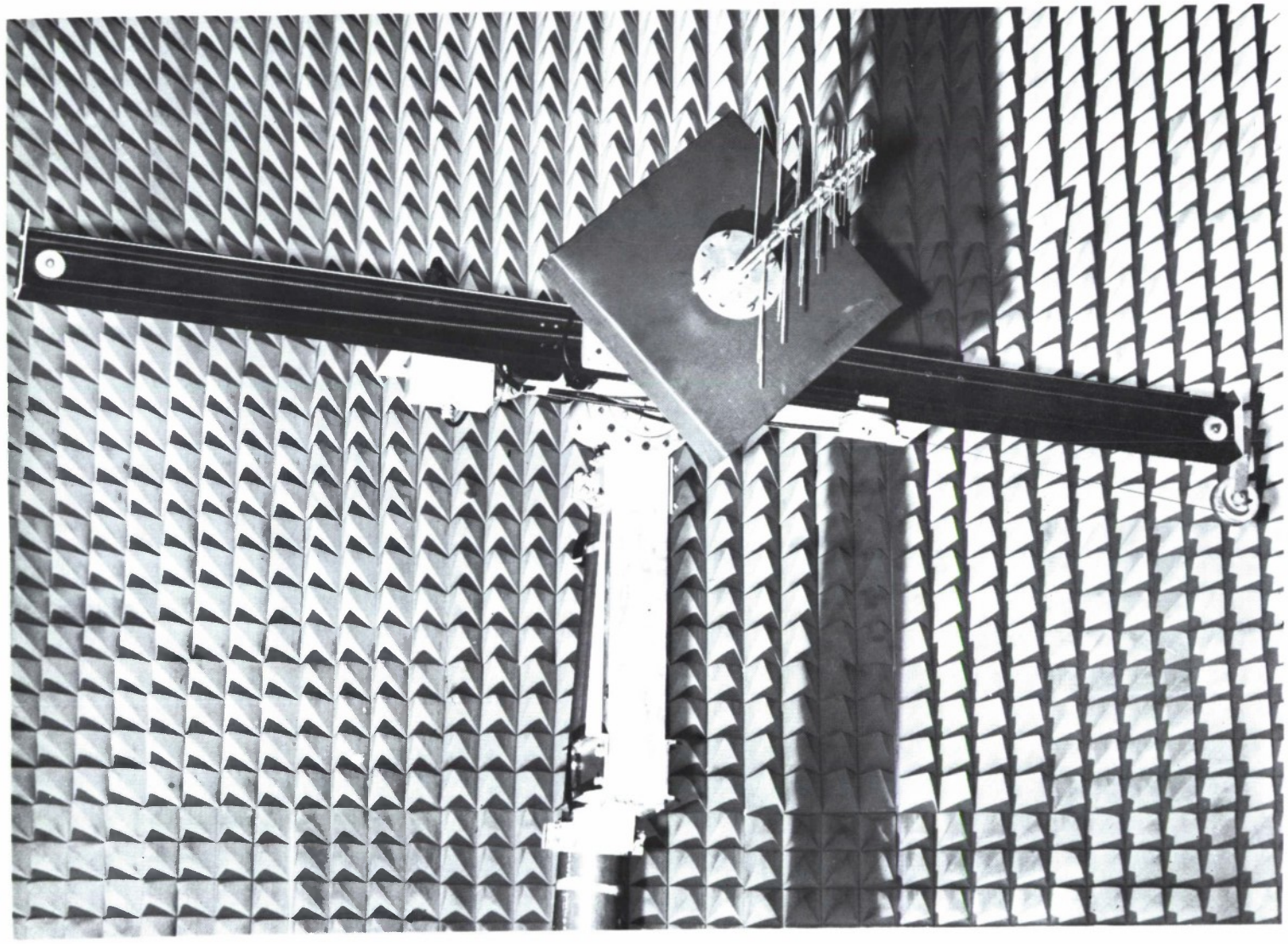

Figure 10. Aperture Field Probe Used in Making Probe Measurements

3.0 EXTRANEOUS SIGNAL LEVEL DETERMINATION

3.1 Distortion of the Incident Field

Consider the case of a direct-path plane wave of amplitude E_d which is normally incident on the test aperture[1] as shown in Figure 11(a). Let an extraneous plane wave of amplitude E_r enter the aperture at an angle θ from the normal. At any given time, t, the phase of the direct wave is constant across the aperture and the direct-path field magnitude may be expressed in phasor notation as

$$\overline{E_d} = E_d e^{j(\phi + \omega t)} \tag{3.1}$$

The phase of the postulated extraneous plane wave will vary across the aperture, so that the extraneous field magnitude is given by

$$\overline{E_r} = E_r e^{j(2\pi x \sin\theta/\lambda + \phi' + \omega t)} \tag{3.2}$$

In (1) and (2), ϕ and ϕ' are constants, λ is the wavelength, and x is distance measured across the aperture parallel to the plane containing the directions of propagation of $\overline{E_d}$ and $\overline{E_r}$. The total field in the aperture is then given by[2]

$$\overline{E_t} = \overline{E_d} + \overline{E_r} = \left[E_d e^{j\phi} + E_r e^{j(2\pi x \sin\theta/\lambda + \phi')}\right] e^{j\omega t} \tag{3.3}$$

Equation (3) describes a field with a sinusoidal variation in one dimension as sketched in Figure 11(b). In this figure, E_{r_1} and E_{r_2} represent two successive

---

[1] The discussion here assumes a separation, R, between source and receiving antennas equal to or greater than $2D^2/\lambda$, where D is the maximum dimension of the receiving aperture. It is further assumed that the ratio D/R is small in comparison with the half-power beamwidth of the source antenna's pattern, so that plane wave approximations are meaningful.

[2] This simplified example assumes that the polarizations of the reflected and direct-path waves are identical. While this is not strictly true, often the reflected wave will contain a large component with polarization identical to that of the direct-path wave.

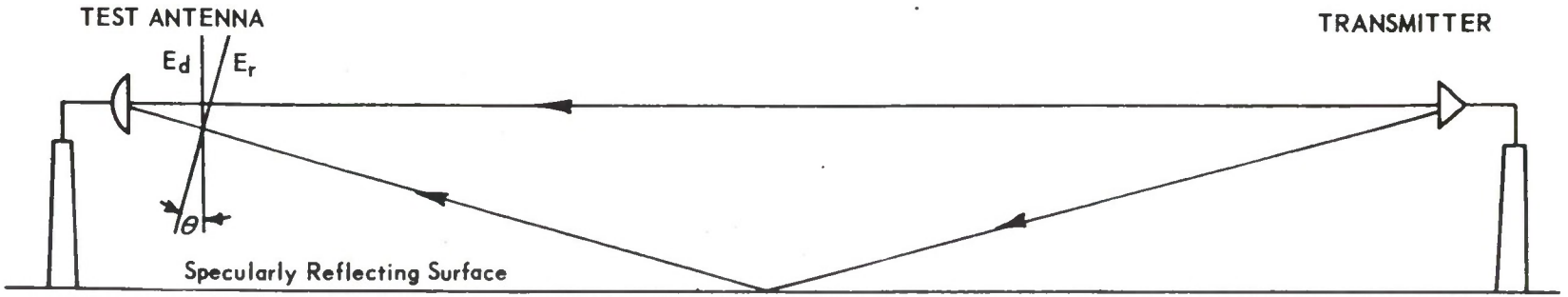

(a) Reflected Wave Incident on a Test Aperture at an Angle θ from the Direction of Propagation of the Direct Wave

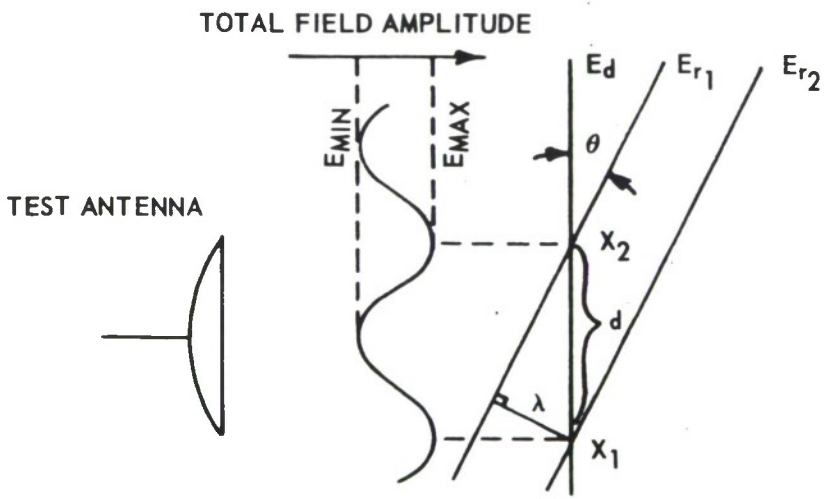

(b) Details of Wave Interference

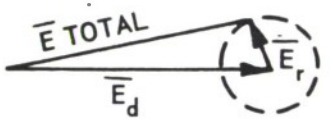

(c) Equivalent Phasor Representation

Figure 11. Simplified Sketch Illustrating Total Aperture Field Variation Caused by a Single Specularly Reflected Wave.

wavefronts of the reflected wave separated by λ, and E_d is a wavefront of the direct wave of identical phase. At points x_1 and x_2 the resultant amplitude is

$$E_{max} = E_d + E_r \quad . \tag{4}$$

Halfway between these two points the waves are in phase opposition, and the resultant amplitude is

$$E_{min} = E_d - E_r \quad . \tag{5}$$

The maximum amplitude variation within the aperture is thus given by

$$\Delta E = E_{max} - E_{min} = 2E_r \quad . \tag{6}$$

Figure 12 is a graph of the magnitude of the resultant field amplitude ripple as a function of the ratio E_r/E_d.

The angle θ can be determined by

$$\theta = \sin^{-1}(\lambda/d) \quad , \tag{7}$$

where d is seen in Figure 11(b) to be the spatial period of the resulting interference pattern across the aperture.

The field in the aperture may also be represented as the sum of two phasors, E_d^* and E_r^*, as illustrated in Figure 11(c), where E_r^* rotates relative to E_d^*. The phase of the field across the aperture will vary as the phase of the resultant of the direct-path and reflected phasors. The maximum phase variation for this plane-wave case is then

$$2 \sin^{-1}(E_r/E_d) \quad , \tag{8}$$

when E_r is less than E_d.

The preceding example, although representing an idealized reflection, demonstrates the manner in which extraneous signals distort an otherwise planar wavefront. In a general test situation, neither the direct nor the extraneous waves would be strictly planar, and there would be many extraneous signal

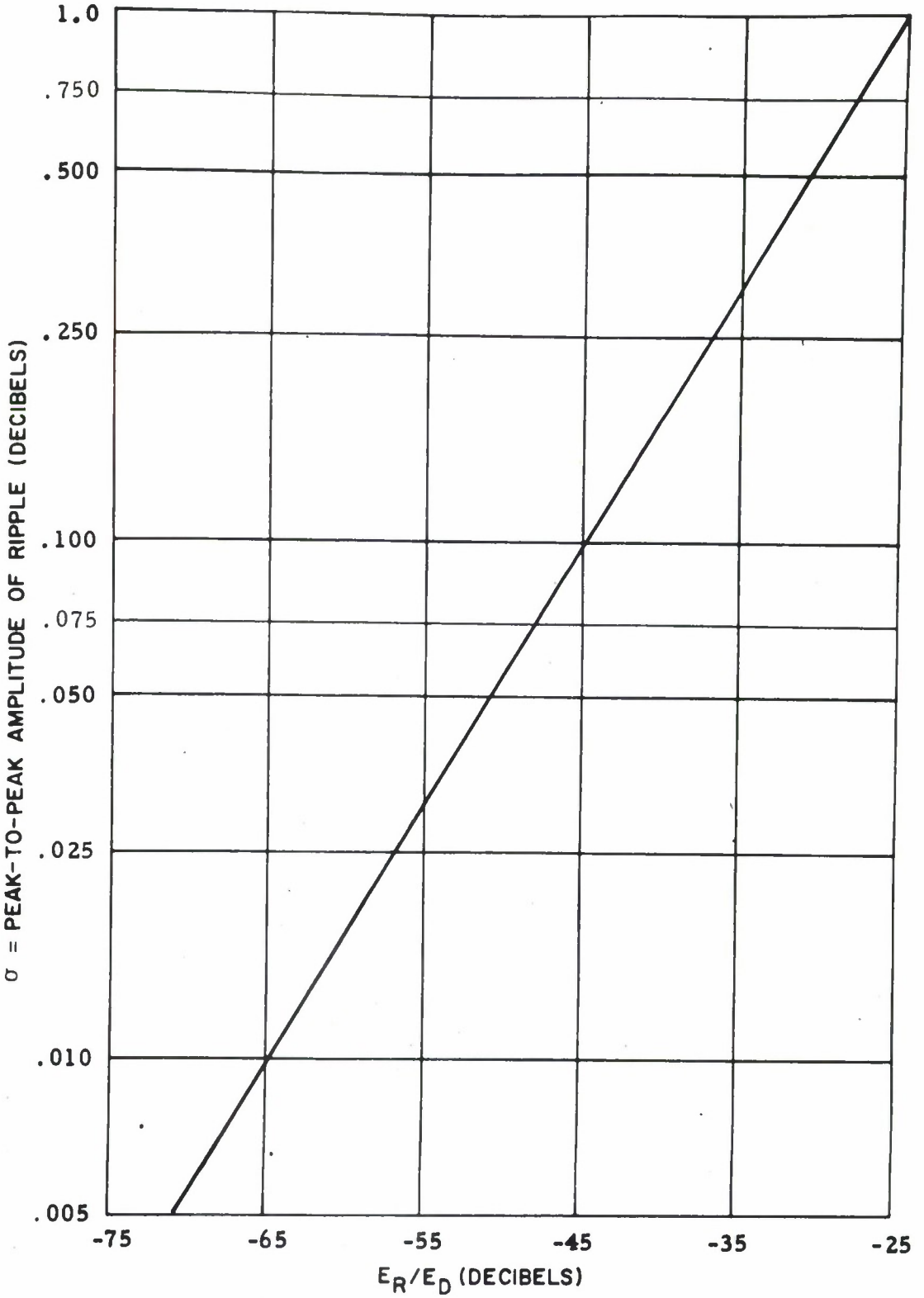

Figure 12. Magnitude of the Maximum Field Perturbation as a Function of the Relative Magnitude of the Reflected Signal.

sources which could contribute to distortion of the incident field. For the case of tapered anechoic chambers, however, for which the region around the chamber axis is clear of reflecting objects, the potential sources of extraneous energy are dissimilarities in the absorber on the walls and reflections from cables, the positioner, positioner pit, and other objects placed in the chamber.

3.2 Polarization Measurements

Linearly polarized antennas were used to evaluate the polarization properties of the chamber. In this case the received signal of interest is expressed by

$$E_r = K\cos(\alpha - \tau_T)$$

where α is the angle of rotation of the test antenna and τ_T is the tilt angle of the degenerate polarization ellipse of the received wave. In the absence of reflections, rotation of either the source antenna or the receiving antenna should produce the classic cosine polarization pattern of linearly polarized antennas. The degree and nature of the deviation of the measured polarization pattern are indicative of the polarization error introduced by the chamber.

For these measurements, the receive antenna was mounted on the model tower head axis and patterns were taken by rotating the probe antenna through 360 degrees for systematically stepped rotational displacements of the source antenna about the line of sight. These polarization measurements were made for different placements of the transmit antenna along the axis of the chamber and for different receive antenna positions in the quiet zone.

3.3 Field Probe Amplitude and Phase Measurements

Field probe measurements usually pertain to the measurement of the amplitude only, but since the Series 1750 Phase-Amplitude receiver was on site, phase measurements were made as well for some though not all probes at 250 MHz. At this low frequency, it was felt that the flexing of the coaxial cable would contribute negligible error to the measurement of phase.

These measurements were made with the field probe shown schematically in Figure 13 and whose photograph was shown previously in Figures 9 and 10. The probe mechanism is basically a 9-foot beam along which a carriage supporting a probe antenna is driven by remote control to measure the incident

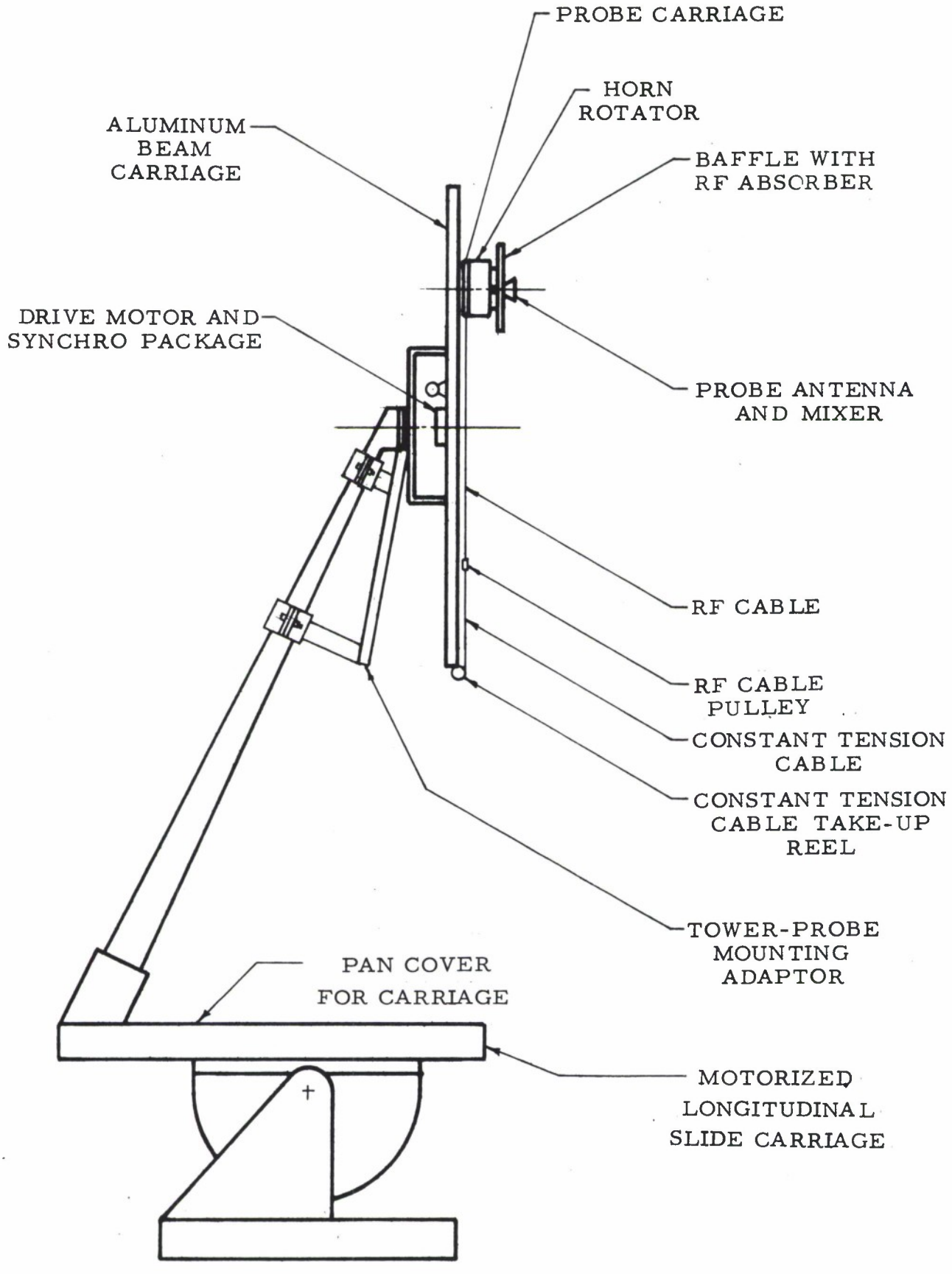

Figure 13. Field Probe Mechanism Mounted on the Model Tower.

field strength as a function of position. A synchro signal indicating the position of the probe drives a position indicator and the angular coordinate of the rectangular recorder chart in the receiving console, permitting plots of the received field versus aperture position to be obtained. Another probe technique was available in the chamber evaluation, namely a longitudinal field probe. The model tower is positioned on a slide carriage which facilitates loading and unloading of models on the head and which also allows one to position the center of phase of a test aperture coincident with the azimuth axis of rotation. This slide carriage can be seen in Figure 13. It had 52 inches of automated travel which allowed one to sample the incident field as a function of longitudinal position in the quiet zone. Synchro information was not available from this carriage but it could be driven at a constant rate. Thus, by so driving and running the recorder on a time base, meaningful probe measurements could be made.

3.4 Pattern Comparison Measurements

Pattern comparison measurements are based on the fact that any two patterns recorded with the same geometrical relationship between the incident field and the receiving antenna will be identical if no extraneous signals are present. When an extraneous signal is present, a pair of patterns which are measured with identical transmitter-receiver geometry but with differing scatter-receiver geometry, or vice versa, will differ due to the effects of the extraneous signal. Primary interest in this technique is directed toward the wide-angle structure of the pattern lobes, as opposed to the field-probe technique in which the main lobe of the receiving antenna is consistently directed toward the source of radiation. Changes in the minor lobe structure of pattern pairs are indicative of error caused by sources of extraneous signal both along the transmission path and at wide angles; thus, an evaluation program which includes the pattern comparison method serves as a more complete indication of the pattern measuring capability of an antenna measurement facility than does the field probe method alone.

Usually, pattern comparison data are collected by recording several conical-cut patterns about a fixed center of rotation for the receiving antenna. Suppose, for example, a 360° azimuth pattern of the probe antenna is made. The probe antenna is rolled 180° in polarization, and the previously made 360° pattern is

repeated, this time in the opposite direction so that the same pattern is made as before. The direction of travel of the abscissa on the chart recorder is reversed between cuts and the synchros readjusted so that the patterns will correspond. If no extraneous energy is present, the patterns will be identical. If extraneous energy is present, on the other hand, it should evidence itself as a difference in signal level between the two cuts unless it is symmetric about the range axis. In that case, another measurement would be necessary to detect its presence.

Another possibility for a pattern is to take identical conical cuts at symmetric azimuth pointing directions with respect to the chamber axis. For example, one could turn the azimuth axis to a given position, which we will call θ, and make a 360° pattern with the head axis of the model tower. He could then turn the azimuth axis to a setting of $-\theta$, roll the head axis 180° to achieve the same starting position, reset the synchros so the pattern will correspond, and repeat the 360° head axis pattern.

Both the pattern techniques were utilized in the present evaluation program to give useful information pertaining to the performance of the chamber. This by no means limits the possibilities of pattern comparison measurements since essentially an infinite number are available. A very good technique which could be used by chamber personnel before a new series of critical tests, for example, would be to place a probe antenna on the model tower head and drive the head axis through a vertical arc with the elevation axis on the positioner. The antenna could then be rotated and the arc reversed. At high frequencies, a short arc section would be, in essence, a field probe measurement and valuable information could be obtained about such things as the placement of the transmit antenna.

3.5 Boresight Measurements

Boresight determination was accomplished in the anechoic chamber at 250 MHz by sampling the phase of the incident field with a counterbalanced dielectric rotary probe device. This device is shown in Figures 14 and 15. A Scientific-Atlanta Model 26-0.1 log periodic antenna was modified to operate only in the frequency range above 250 MHz in order to reduce the weight and torqueing problem. This antenna was used as a probe antenna. It was mounted at one end

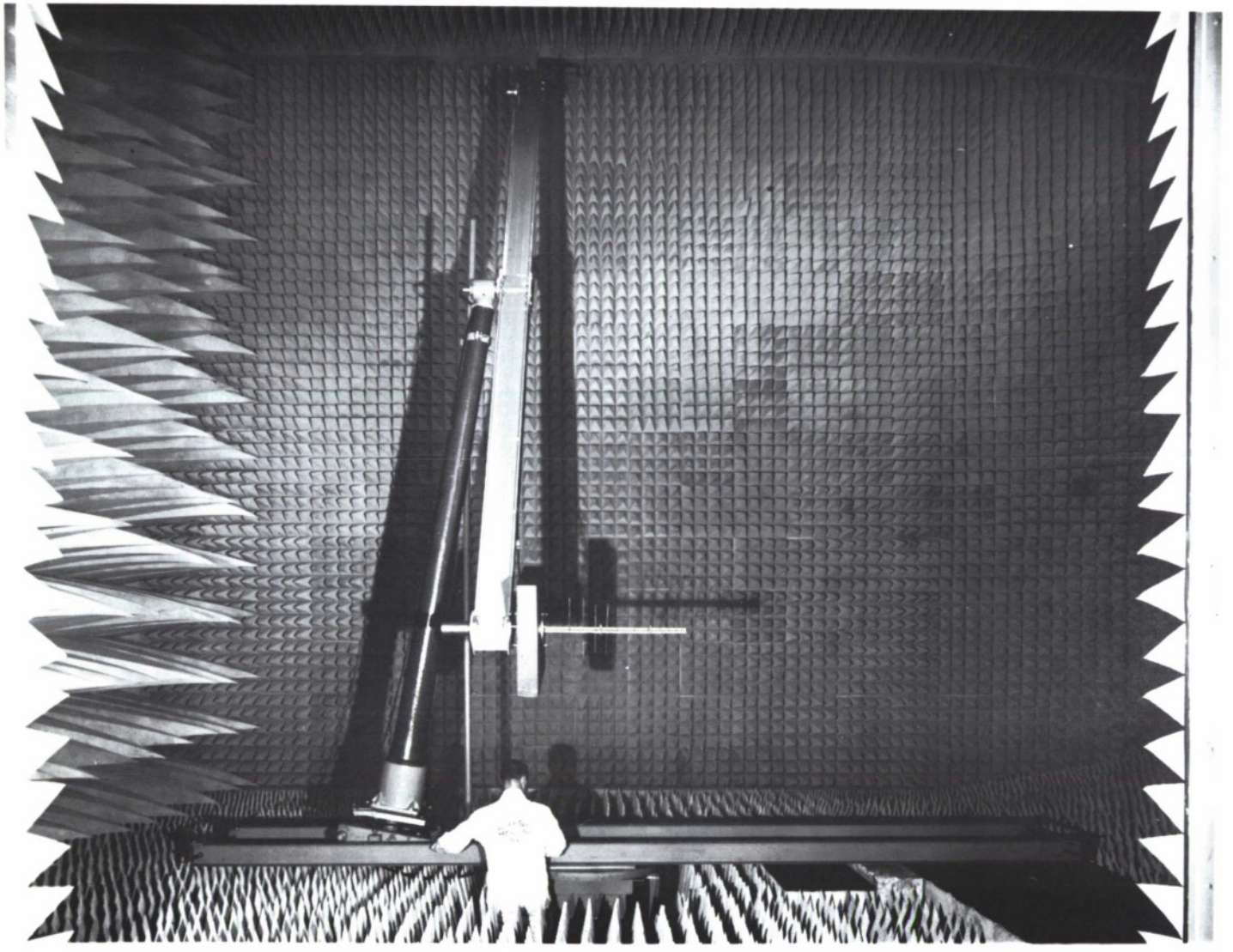

Figure 14. Dielectric Rotary Field Probe Used in Boresight Measurements

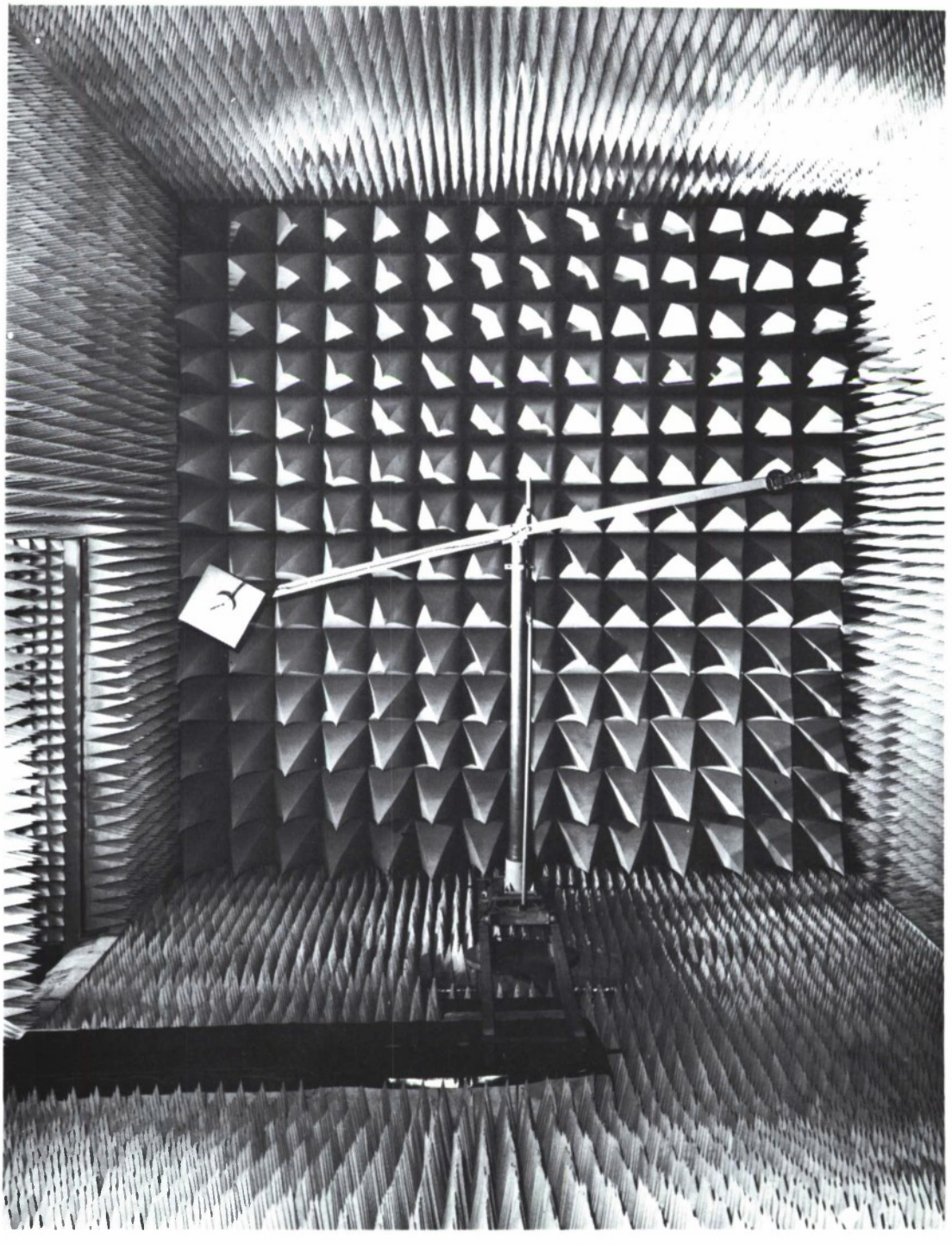

Figure 15. Dielectric Rotary Field Probe Used in Boresight Measurements

of the 18 foot dielectric I-beam shown in Figures 14 and 15. Counterweights were added on the back side of the beam to keep the beam from twisting and deflecting, and at the other end of the beam to reduce the torque on the model tower head axis. These counterweights are visible in the figures. The entire device was mounted on the head axis of the model tower so that it could be rotated from the remote console. The entire model tower was mounted on a carriage which ran along the 20 foot steel I-beams shown in the figures. These beams facilitated the measurement of boresight at different longitudinal positions in the test region.

Alignment of the configuration consisted of autoreflecting to a rifle telescope mounted on the transmit polarization positioner in the throat of the chamber and adjusting the azimuth axis of the model tower and elevation adjustment on the carriage until the head axis of rotation was aligned with the polarization axis of the transmit polarization positioner to within a specified tolerance. Alignment accuracy of approximately ± 0.1 inch was obtained. Having thus aligned the probe, the antenna would move through a circle all points of which were equidistant from the axis of rotation of the transmit antenna.

A coaxial cable passed from the antenna up the dielectric probe to a coaxial rotary joint in the head axis of the model tower. The detection system was a Scientific-Atlanta Model 1750 Phase Amplitude Receiver with a low frequency option unit. This receiver is shown in Figure 16. By examining the phase at diametrically opposite points in the test region and measuring the phase difference, one can calculate the location of the center of phase of the transmit array which consists of the transmit antenna and its images. The phase meter shown on the left side of Figure 16 was used as a null detector only and not used to make direct phase readings. The precision thumbwheels under this meter (which read 273.0 in the figure) were used to obtain the high resolution. Using this technique, measurements could be made to one tenth of an electrical degree. Each set of measurements was repeated many times to minimize any possible errors due to system drift or operator fault.

Figure 16. Scientific-Atlanta Model 1750 Phase Amplitude Receiver

4.0 EXPERIMENTAL RESULTS

4.1 250 MHz Measurements

The measurement procedures discussed in the previous chapter were utilized to assess the chamber's performance capability at the above stated frequency near the lower frequency design limit of the chamber. The polarization characteristics of the chamber were examined and the purity of the field in the quiet zone was measured. The phase center of the transmitted wave was accurately located to facilitate boresight measurements.

It should be noted at this time that the chart paper used to make the patterns in most of this report is graduated such that the standard 20 inch cycle is divided into 10 degrees, or 5 degrees on either side of center. This is convenient to use with the field probe since the synchro ratio is such that one foot of travel on the probe corresponds to one inch of travel for the chart paper and the one degree divisions on the paper represent two feet of travel for the field probe.

For 360° patterns such as polarization, however, the scale is less convenient. In that case, the one degree intervals represent 36° and each small division represents 3.6°.

To avoid confusion with regard to direction in this report, all references to right and left are as seen by one standing at the center of the quiet zone and facing the transmit antenna.

4.1.1 Polarization Measurements

The polarization properties of the chamber were evaluated by rotating a linearly polarized log periodic array through 360° for systematically stepped rotational displacement of the transmit antenna. The transmit antenna was a Taco yagi and was small enough to be positioned almost at the rear limit of the slot shown in Figure 3.

The first set of polarization measurements were made with the transmit antenna positioned 4.25 inches from the rear stop. Complete polarization patterns were made for each of the transmit antenna settings of 45°, 90°,

135°, and 180°. These patterns are shown in Figure 17. Since the reduced patterns are difficult to read, the peak levels and null depths are listed numerically as decibels. It is emphasized that the numbers by the nulls are the actual depths with respect to the peaks and are not the pattern level on the chart. The maximum variations in the peak values appear to be less than 0.1 decibels. This is beyond the resolution of this chart since the width of the pen line itself is about 0.1 dB. It is interesting to note that the null depths for the 45° polarization are only 29 dB while they are in the high thirties for the other polarizations including the other diagonal polarization, 135°.

Figure 18 represents polarization cuts for the diagonal polarization, 45° and 135°, after the transmitter has been moved to 12.75 inches from the rear stop. The 45° polarization still has -29 decibel nulls while the 135° polarization null levels remain at about -37 decibels. Again the peak levels are still at the 4.0 decibel level on the chart.

With the transmit antenna positioned 21.5 inches from the rear limit of travel, all null depths seemed to increase though those for the 45° polarization increased only slightly. The peak values are all still essentially constant. These data are presented in Figure 19.

Figure 20 presents the 45° and 135° polarization patterns with the transmit antenna positioned 29.75 inches from the rear limit of travel on the slide. The null depths have increased significantly for the 135° polarization, but the 45° polarization continues to have relatively shallow nulls compared with the other polarizations.

At this point the transmit antenna was set at 90° or horizontal polarization and and polarization patterns were taken as a function of the distance of the transmit antenna from the rear limit of the slot. The Figures 21 - 30 represent cuts made at one foot intervals for transmitter position beginning 0.5 feet from the rear limit and ending 9.5 feet from the rear limit. Ten decibels of gain were switched in as the null was approached to give better resolution in that area. This accounts for the discontinuities observed in the patterns. Table I lists the position of the transmitter in each individual pattern, summarizes the signal levels on each of these patterns, and compares this level to the calculated free space value. The change in signal level is plotted in Figure 31 for both the

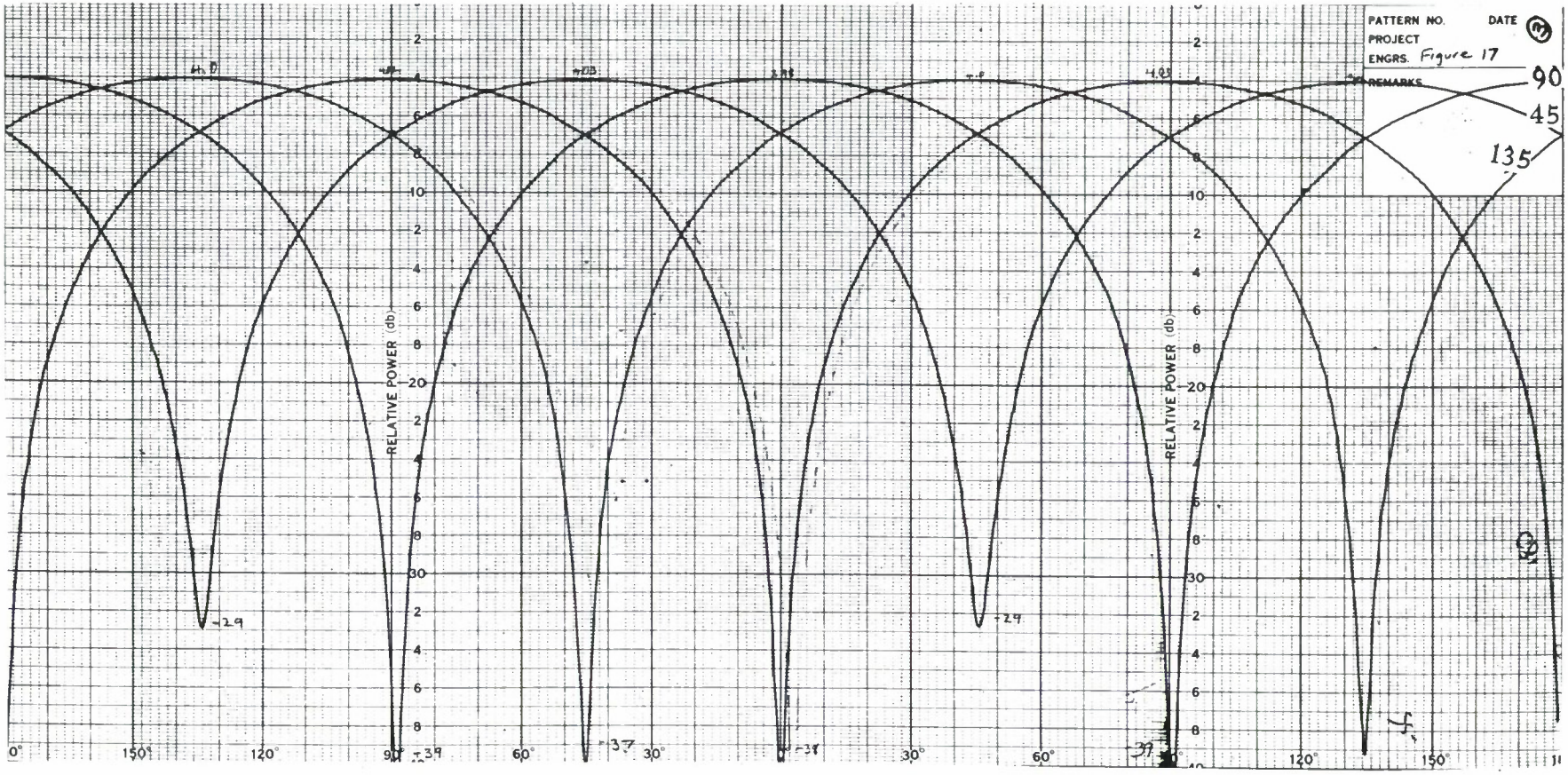

Figure 17. 360° Polarization Patterns for Transmit Antenna Polarizations of 45°, 90°, 135°, and 180°. Transmit Antenna was Positioned at 4.25 inches from the Rear Stop.

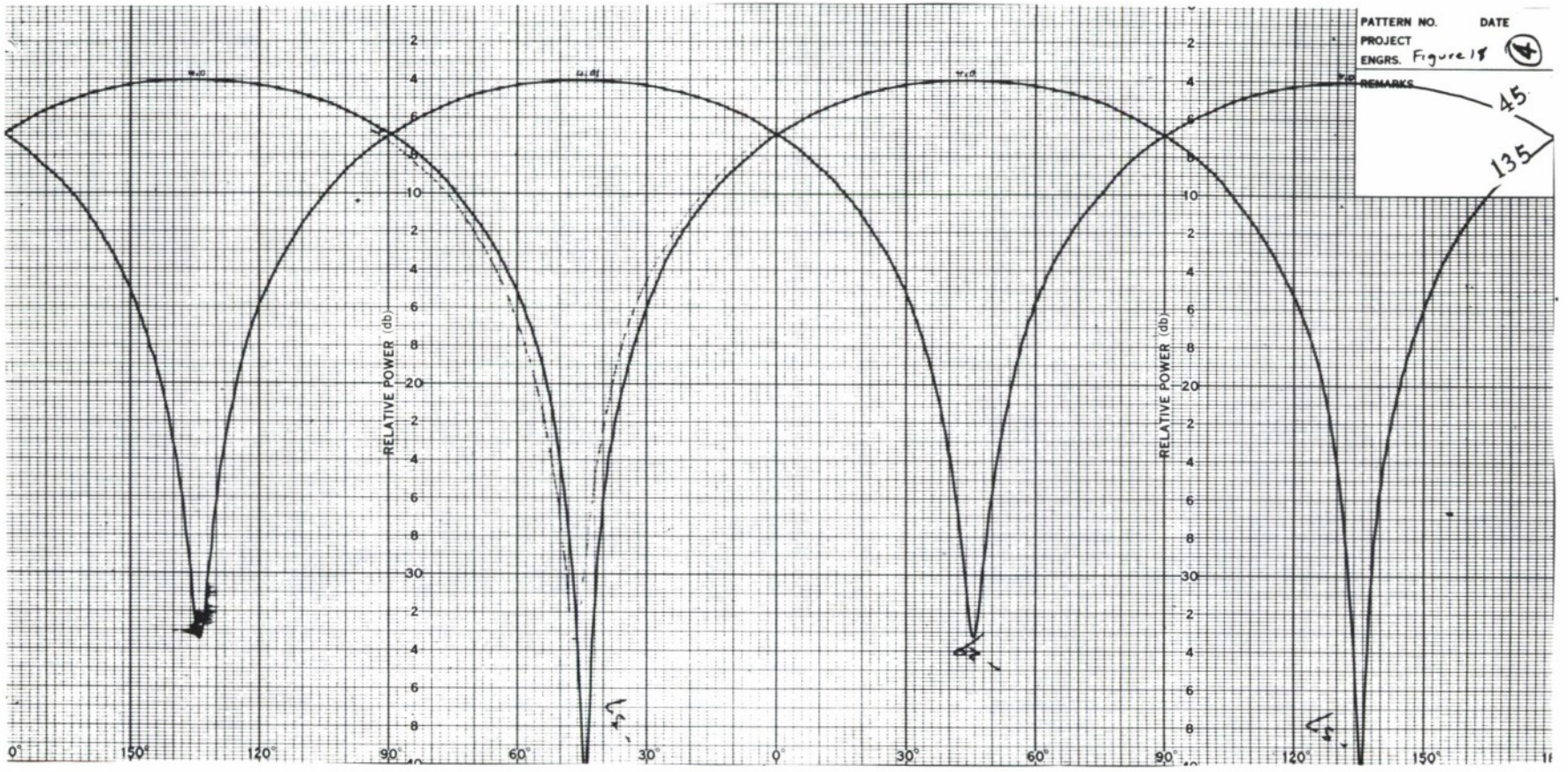

Figure 18. 360° Polarization Patterns for Transmit Antenna Polarizations of 45° and 135°. The Transmit Antenna was Positioned 12.75 inches from the Rear Stop.

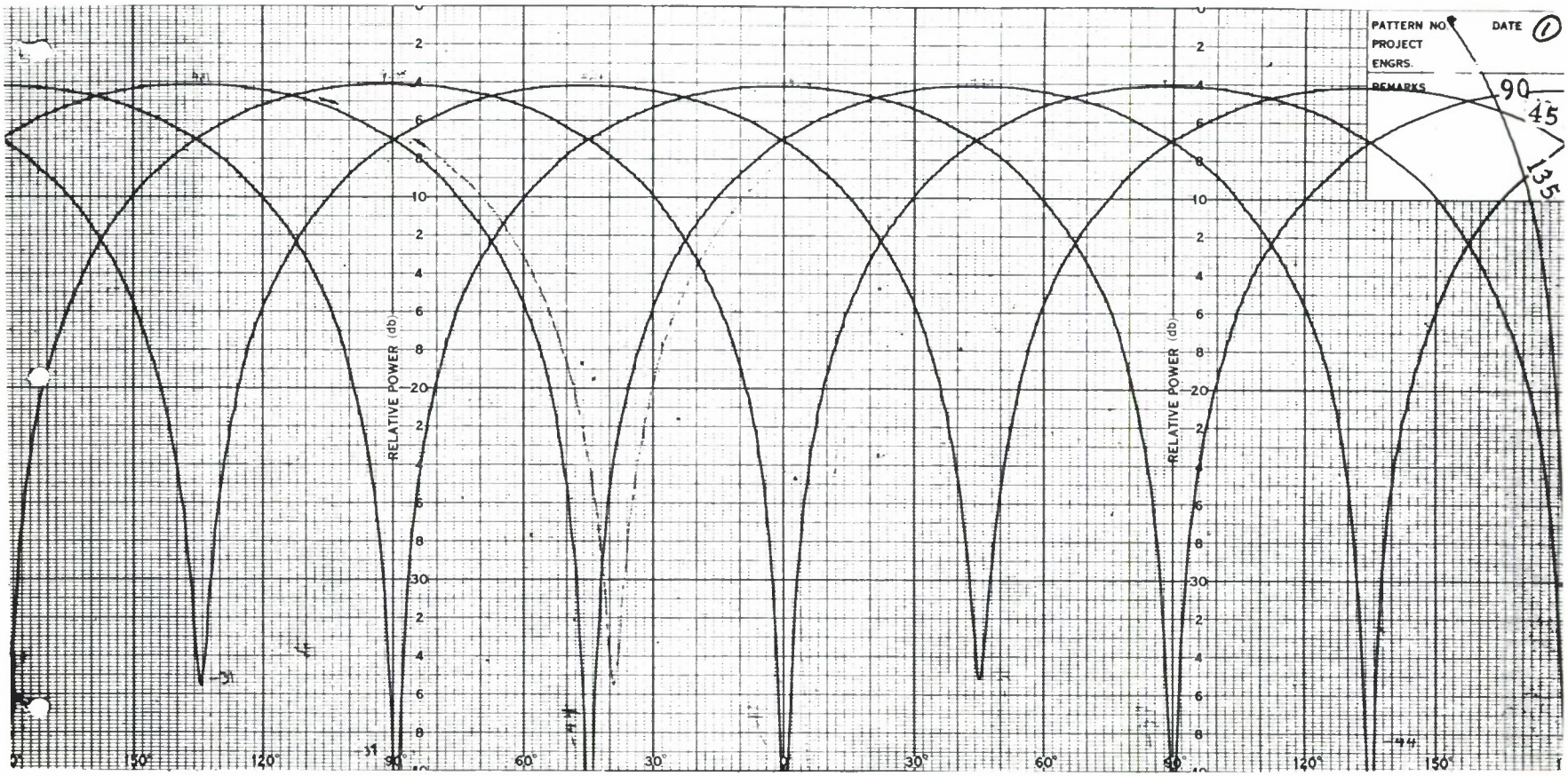

Figure 19. 360° Polarization Patterns for Transmitter Polarizations of 45° and 135°. The Transmit Antenna was Positioned 21.5 inches from the Rear Stop.

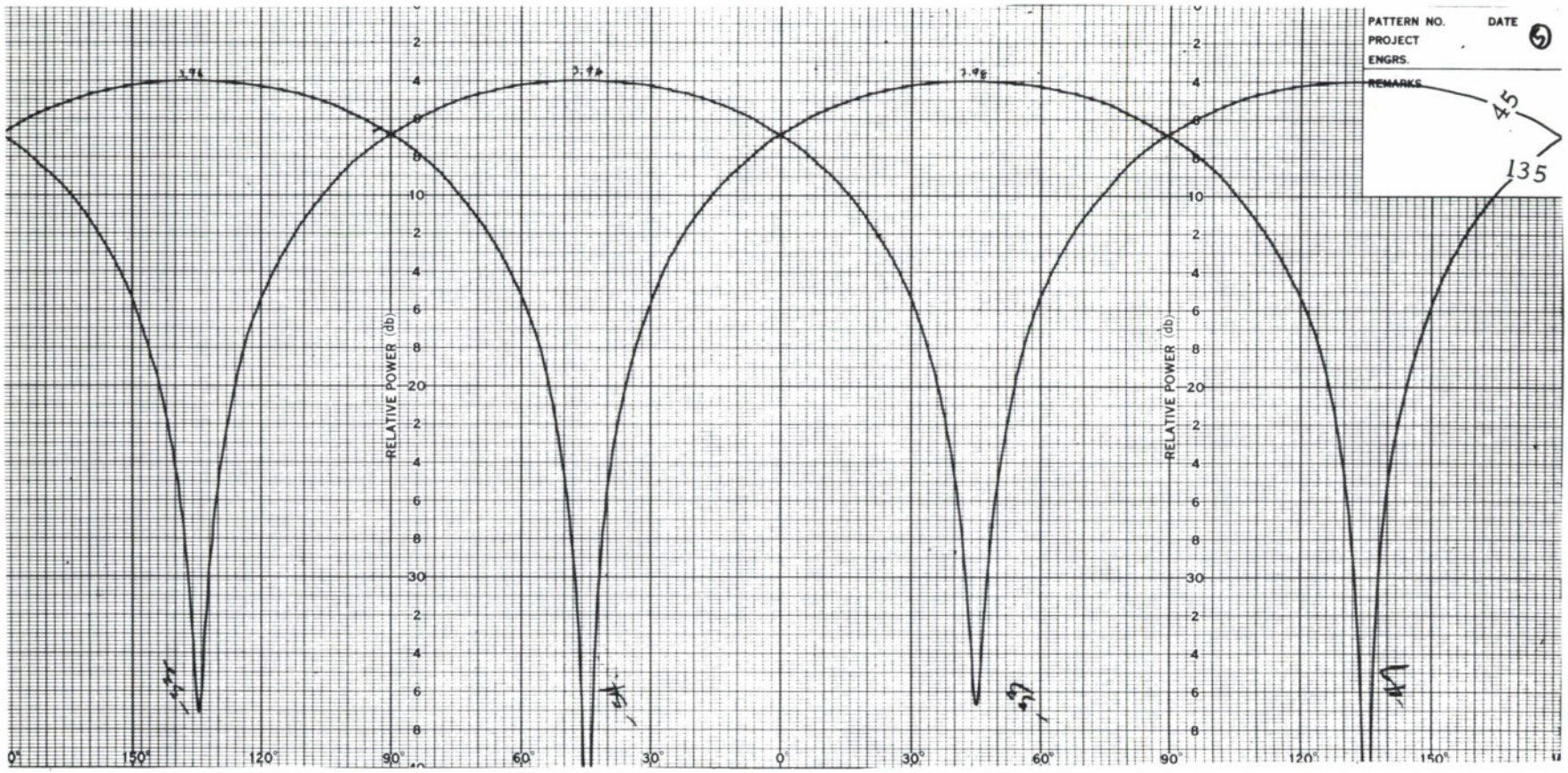

Figure 20. 360° Polarization Patterns for Transmit Antenna Polarizations of 45° and 135°. The Transmit Antenna was Positioned 29.75 inches from the Rear Stop.

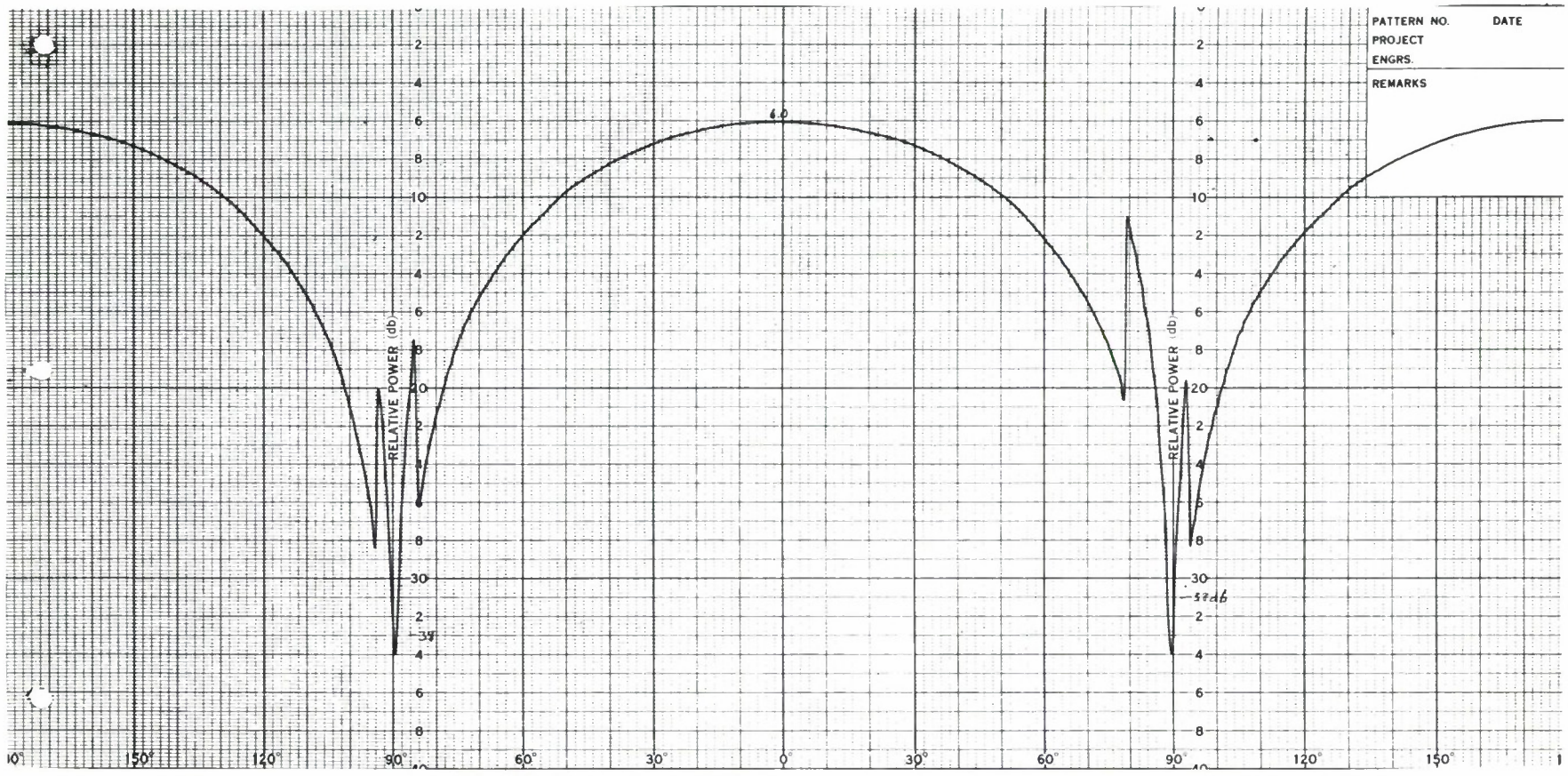

Figure 21. Polarization Pattern with Transmit Antenna Horizontally Polarized and Positioned 0.5 feet from the Rear Stop

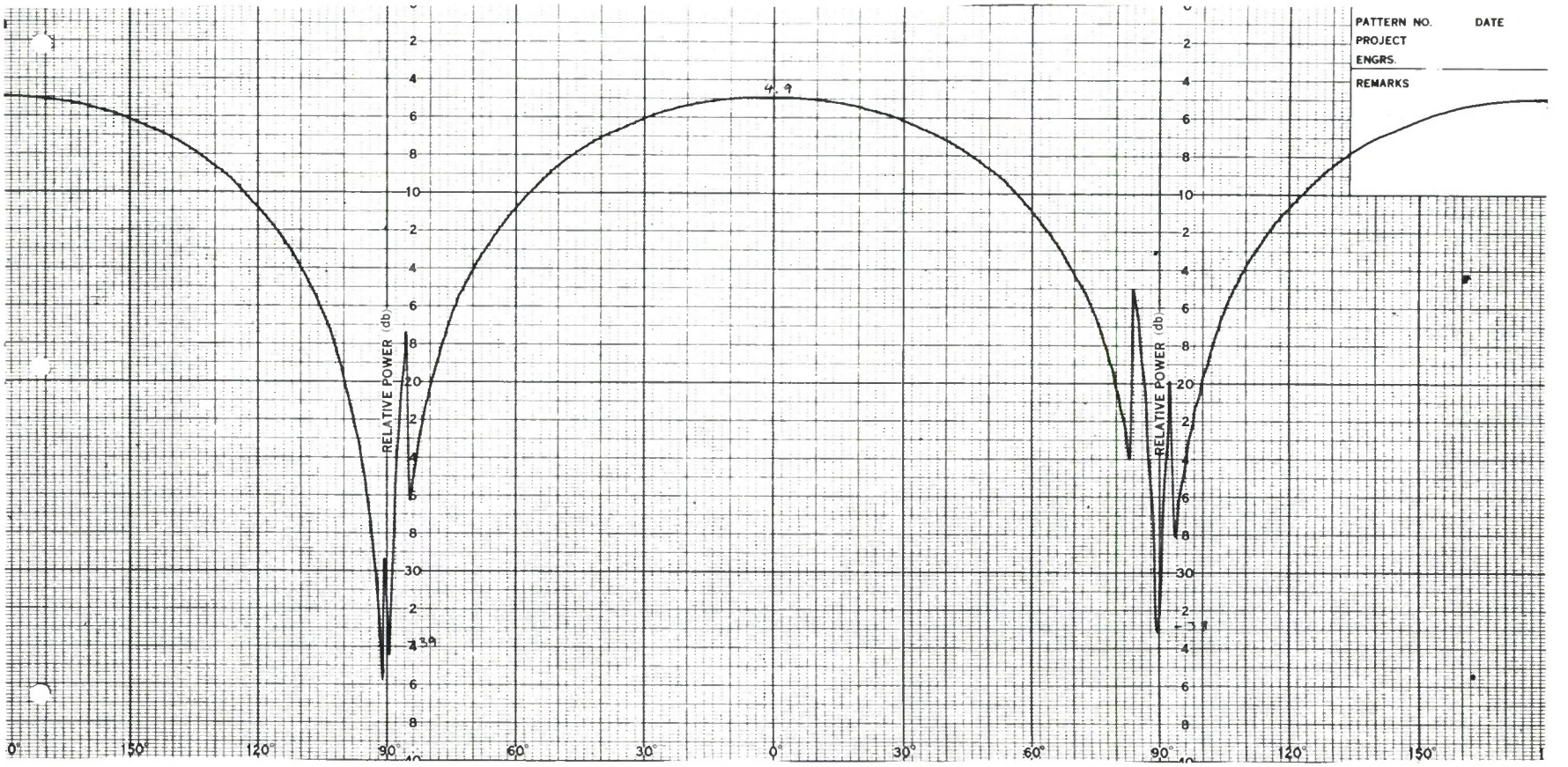

Figure 22. Polarization Pattern with Transmit Antenna Horizontally Polarized and Positioned 1.5 Feet from the Rear Stop.

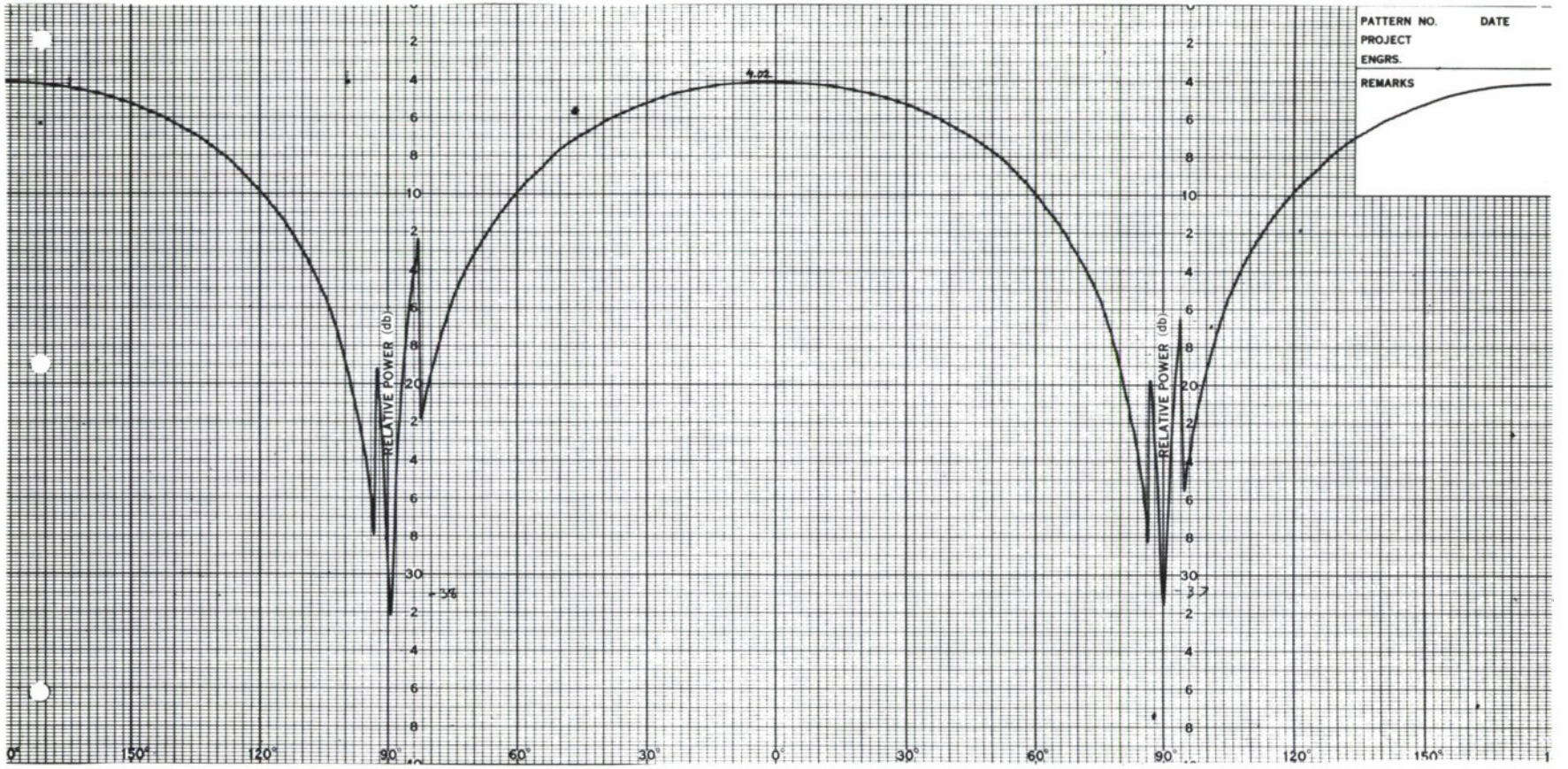

Figure 23. Polarization Pattern with Transmit Antenna Horizontally Polarized and Positioned 2.5 Feet from the Rear Stop.

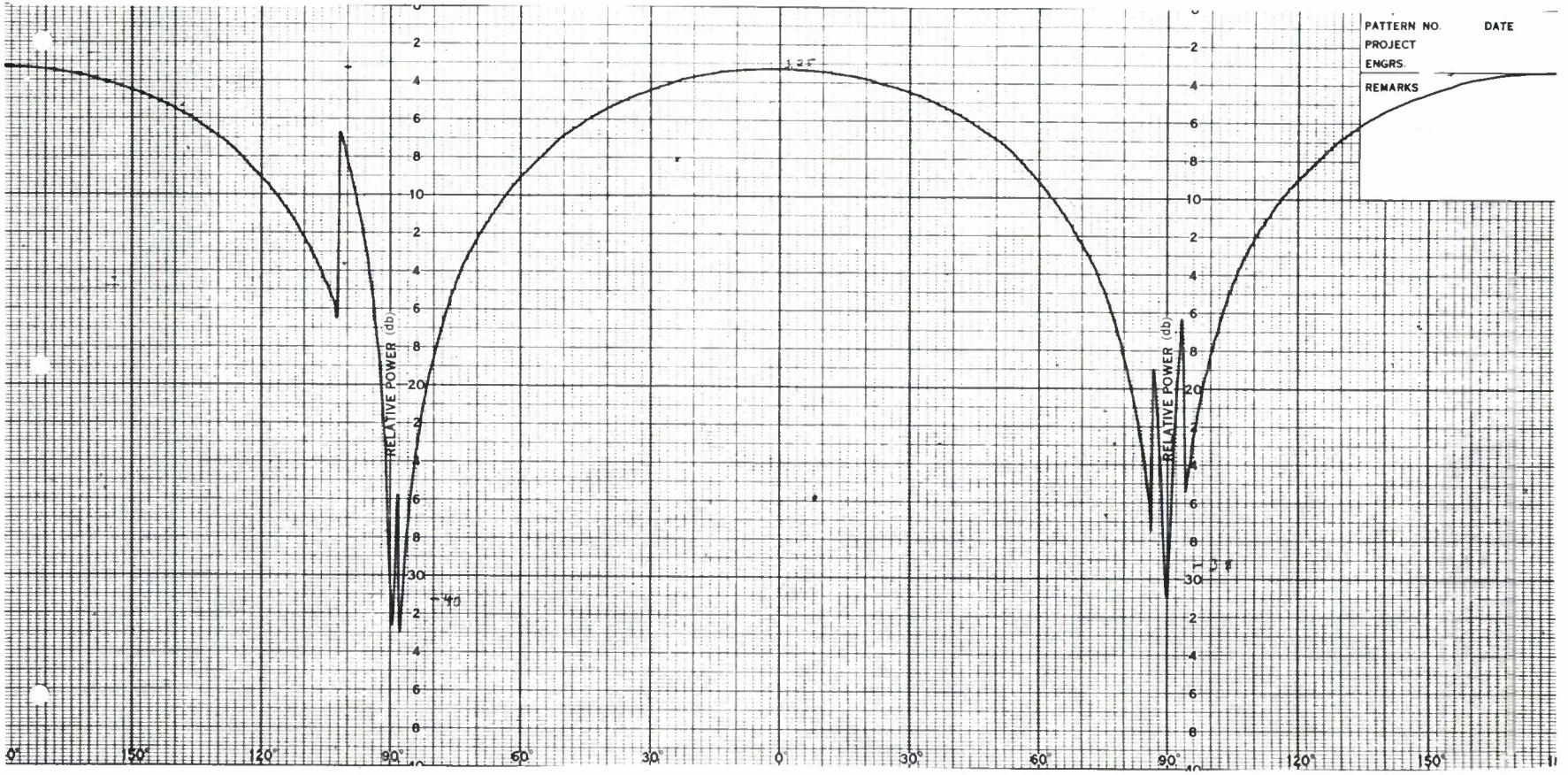

Figure 24. Polarization Pattern with Transmit Antenna Horizontally Polarized and Positioned 3.5 Feet from the Rear Stop.

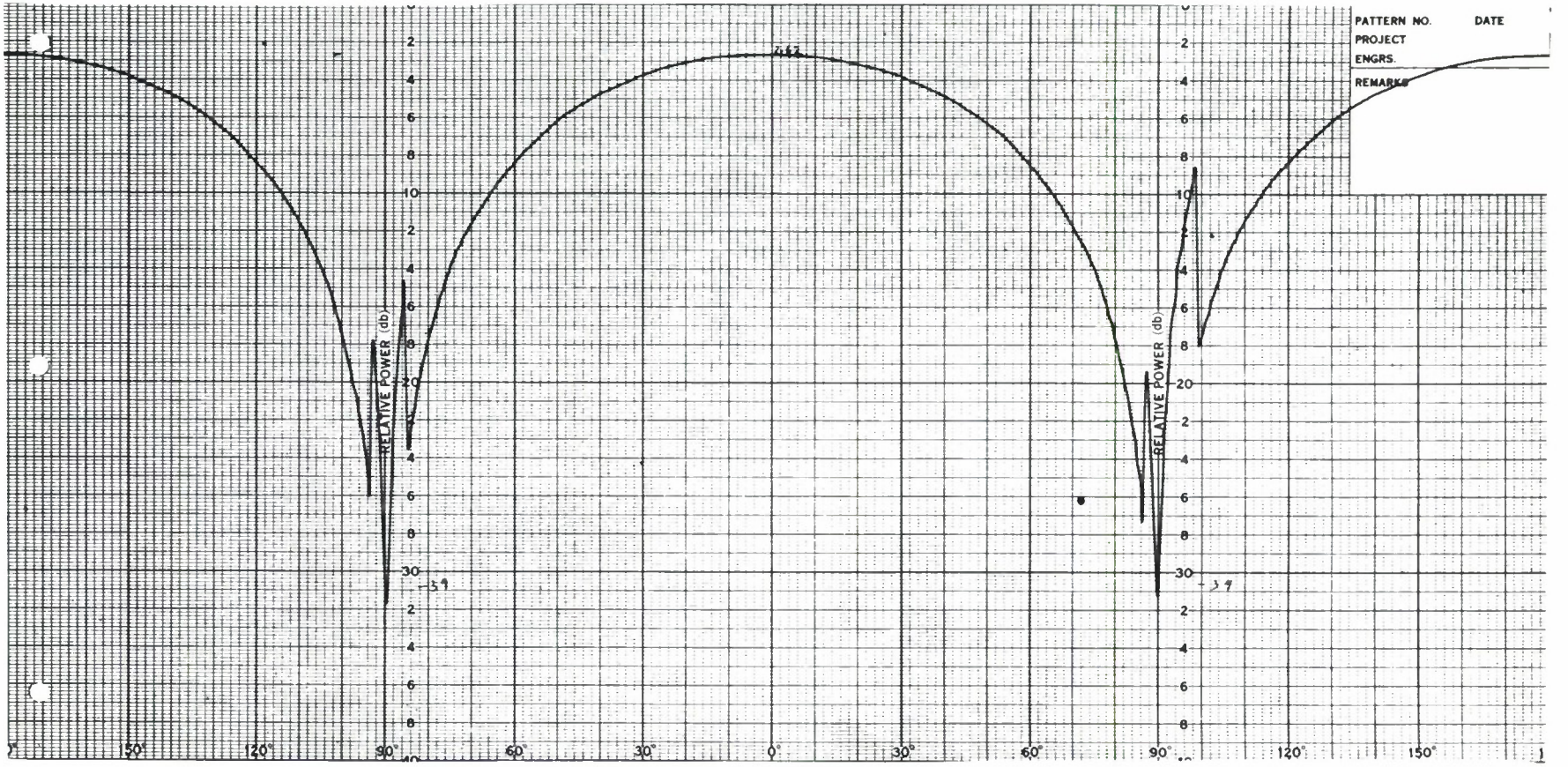

Figure 25. Polarization Pattern with Transmit Antenna Horizontally Polarized and Positioned 4.5 Feet from the Rear Stop.

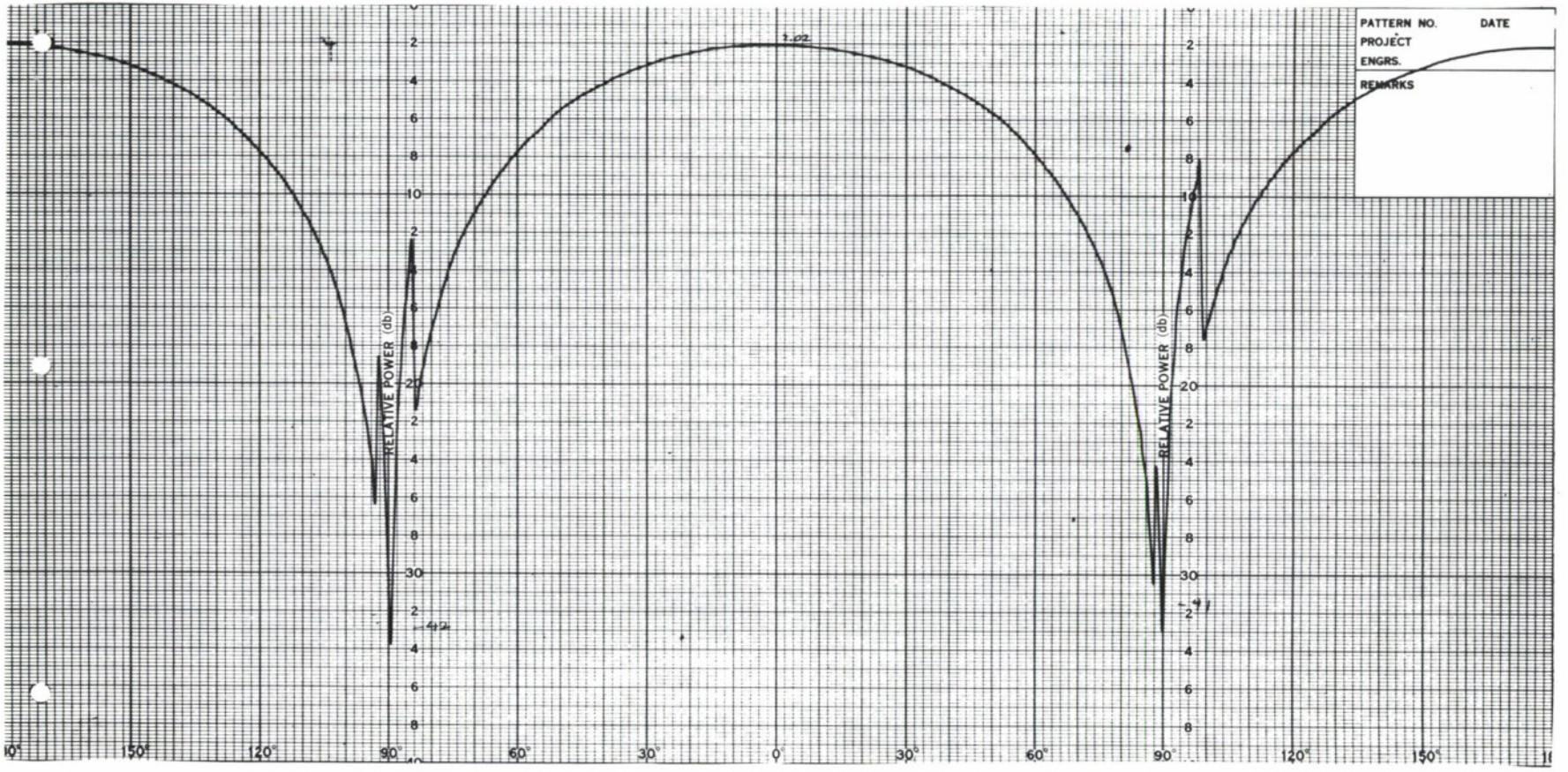

Figure 26. Polarization Pattern with Transmit Antenna Horizontally Polarized and Positioned 5.5 Feet from the Rear Stop.

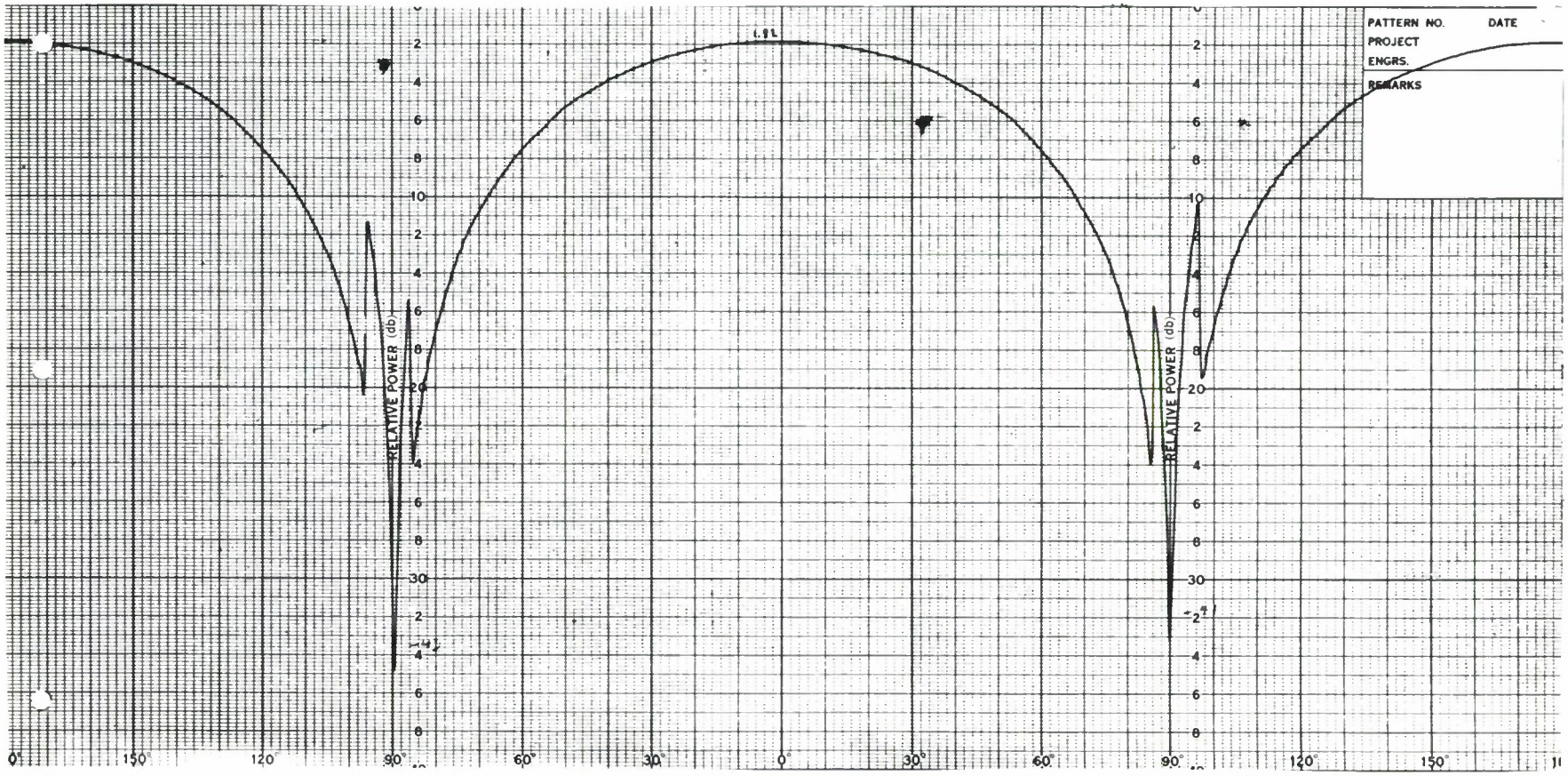

Figure 27. Polarization Pattern with Transmit Antenna Horizontally Polarized and Positioned 6.5 Feet from the Rear Stop.

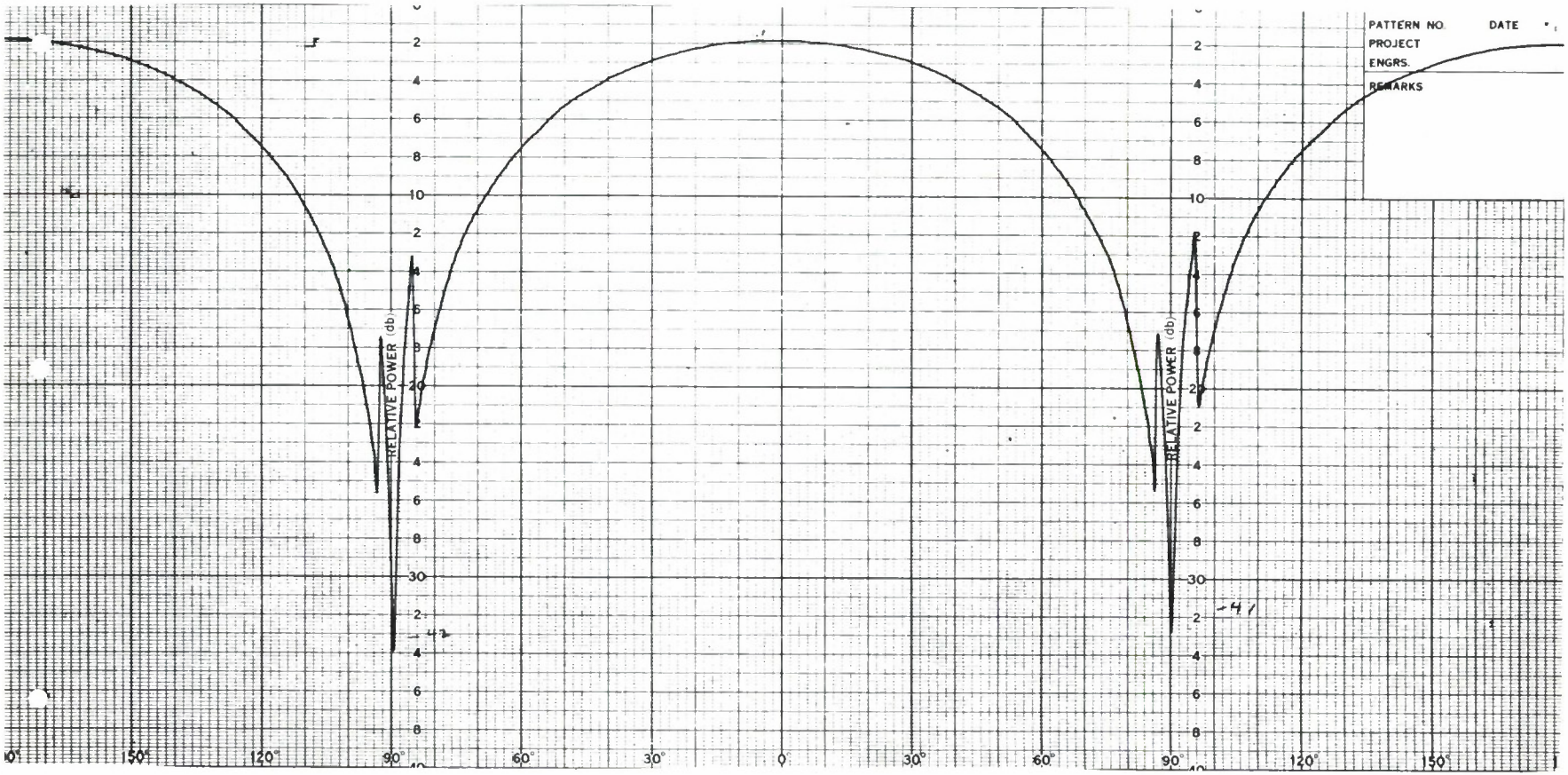

Figure 28. Polarization Pattern with Transmit Antenna Horizontally Polarized and Positioned 7.5 Feet from the Rear Stop.

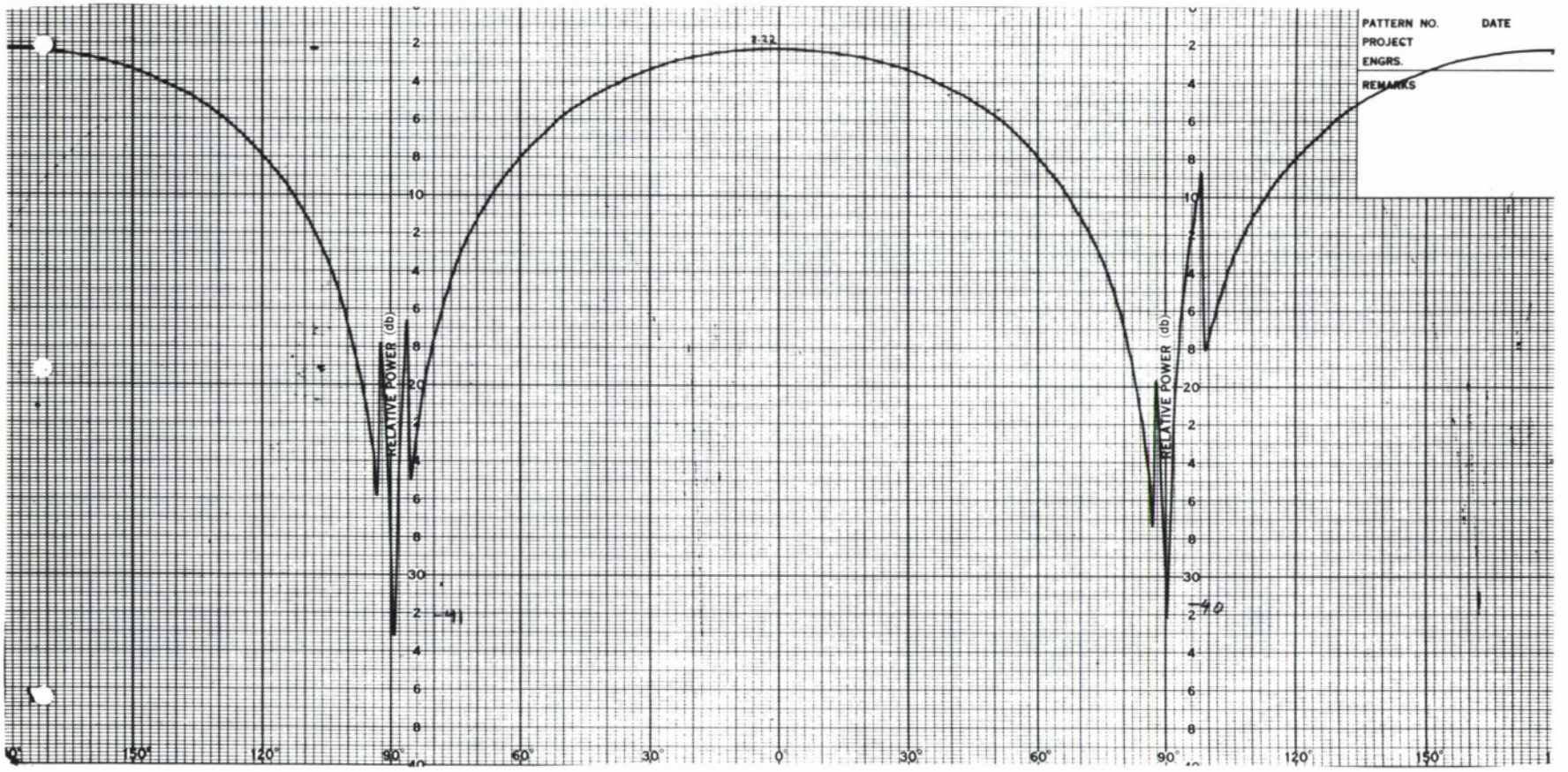

Figure 29. Polarization Pattern with Transmit Antenna Horizontally Polarized and Positioned 8.5 Feet from the Rear Stop.

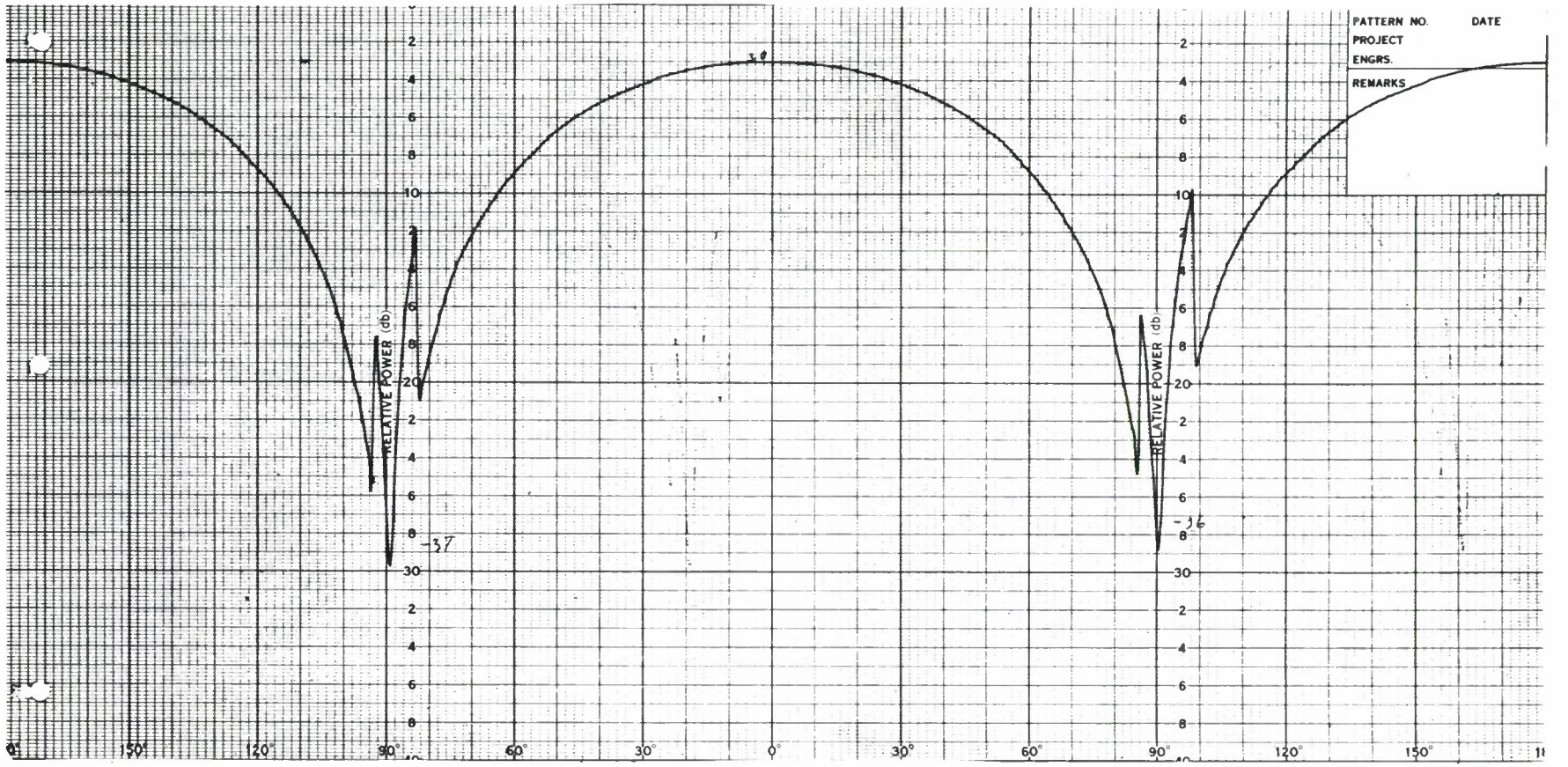

Figure 30. Polarization Pattern with Transmit Antenna Horizontally Polarized and Positioned 9.5 Feet from the Rear Stop.

TABLE I

Figure Number	Distance from Rear Stop (ft.)	Distance from Receive Antenna (ft.)	Theoretical Space Dispersion (dB)	Maximum Measured Pattern Level (dB)	Free Space Signal Increase (dB)	Measured Signal Increase (dB)
21	.5	62	45.95	6.0	0	0
22	1.5	61	45.81	4.9	0.14	1.1
23	2.5	60	45.66	4.02	0.29	1.98
24	3.5	59	45.52	3.25	0.43	2.75
25	4.5	58	45.36	2.62	0.59	3.38
26	5.5	57	45.20	2.02	0.75	3.98
27	6.5	56	45.06	1.82	0.87	4.18
28	7.5	55	44.90	1.80	1.05	4.20
29	8.5	54	44.76	2.22	1.19	3.78
30	9.5	53	45.58	3.0	1.37	3.0

measured values and the predicted free space value. This figure is perhaps misleading in that the actual received signal at a separation of 62 feet is not necessarily equal to the free space level but this point only serves as a reference point for both curves. The experimental curve does, however, peak at a separation of 55 to 56 feet and start back down again for closer separations which indicates that the received signal is in fact an interference pattern. It is interesting to note that equation (2.18) predicts an interference peak at approximately the same position as the one observed in Figure 31.

Measurements were made to determine whether any depolarization effects resulted from the presence of the model tower pan cover in the chamber. This pan cover can be seen in Figure 13. Polarization patterns were made with this cover exposed, and repeated with it covered with microwave absorber. No effect was observed when the transmit antenna was vertically polarized. Figure 32 shows the results at horizontal polarization. The nulls remain fixed and only insignificant changes in null depths were observed indicating little or no depolarization results from the presence of this pan. However, the difference in the peak levels indicate that extraneous energy does enter the aperture from this source. This extraneous energy level will be documented later under the field probe measurements.

4.1.2 Pattern Comparison Measurements

Pattern comparison measurements were used to help determine the level of extraneous energy in the quiet zone. The same log periodic antenna that was used in the polarization measurements discussed in the previous section was used in the pattern comparison measurements. This antenna had 3 dB beamwidths of 67° and 115° in the E and H-planes respectively.

Azimuth pattern comparisons were performed as described in Section 3. Figure 33 is a typical 360° comparison made at 250 MHz with the transmit antenna horizontally polarized. The change in phasing of the extraneous energy evidences itself as a change in pattern level. The patterns are slightly displaced in angluar position due to an error in resetting the synchros after rotating the antenna and reversing the chart direction. But a good comparison can be made on the sidelobes which is the principal region of interest. At the peak of the first sidelobe, levels differ by 1.3 dB. An extension of Figure 12 shows that an excursion of 1.3 dB represents an extraneous signal level 22 dB below the direct path signal. However, this excursion occurs at a point

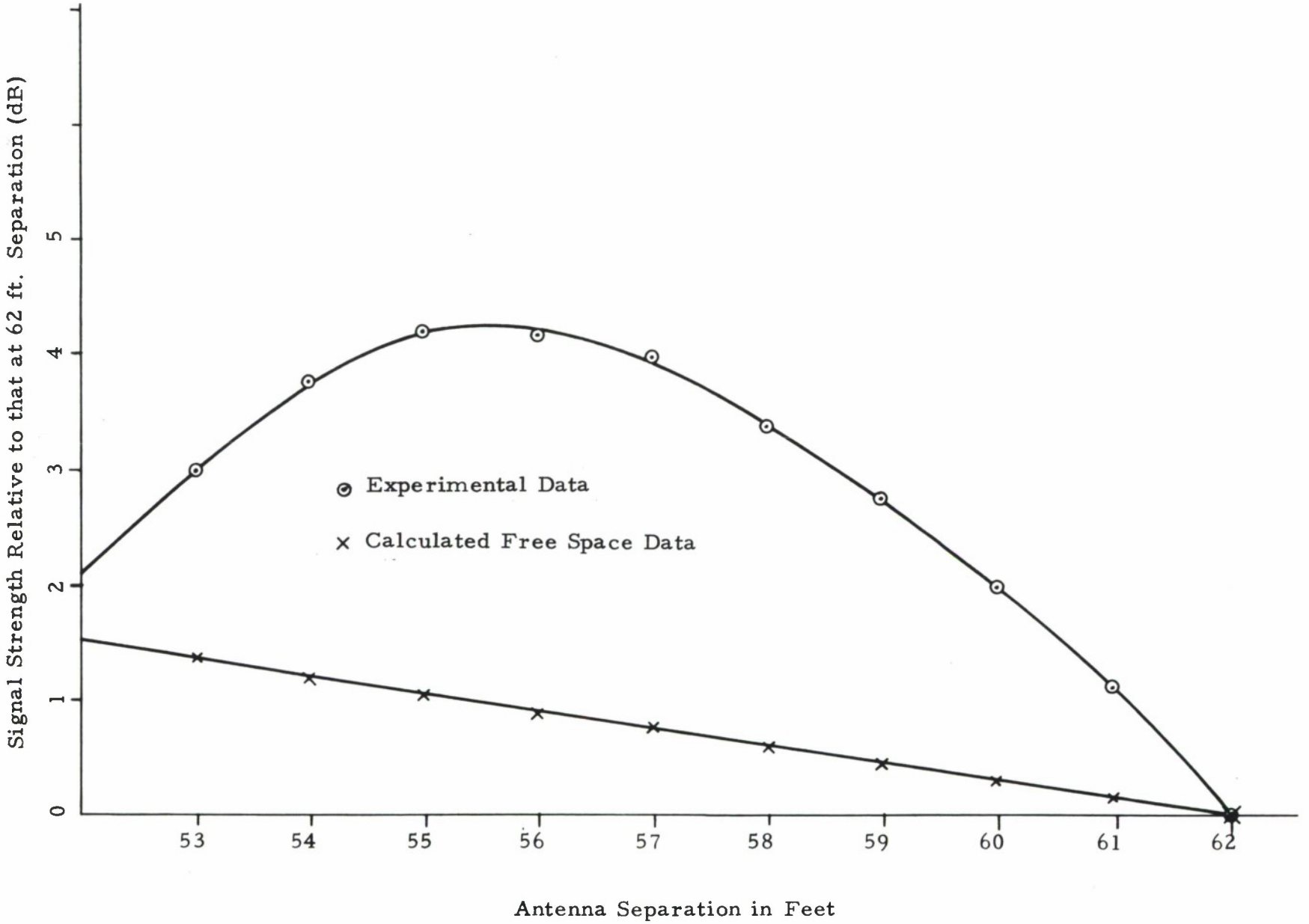

Figure 31. Calculated Field Level versus Antenna Separation

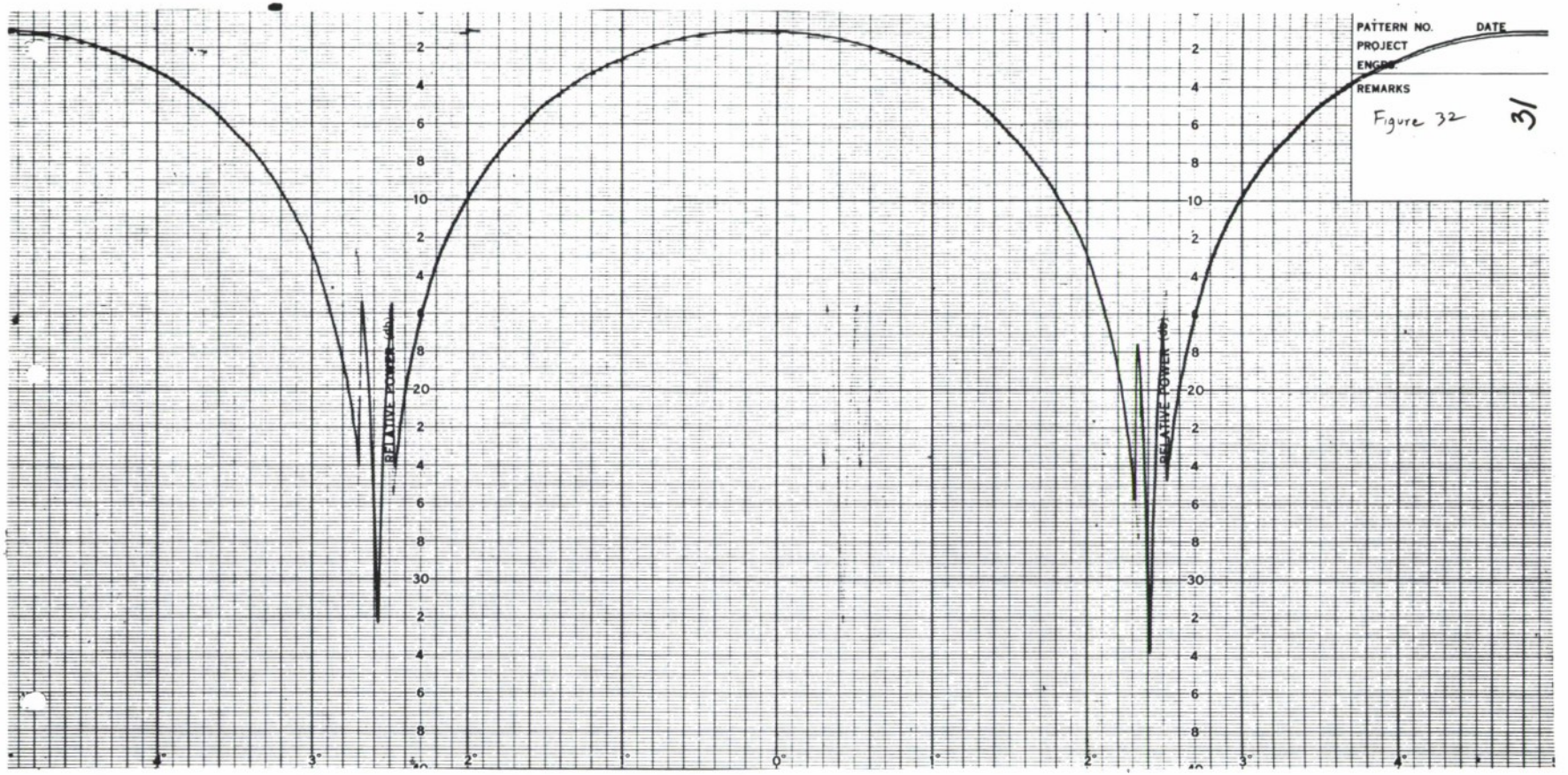

Figure 32. Polarization Cuts at Horizontal Polarization with and without Absorber on Model Tower Pan Cover.

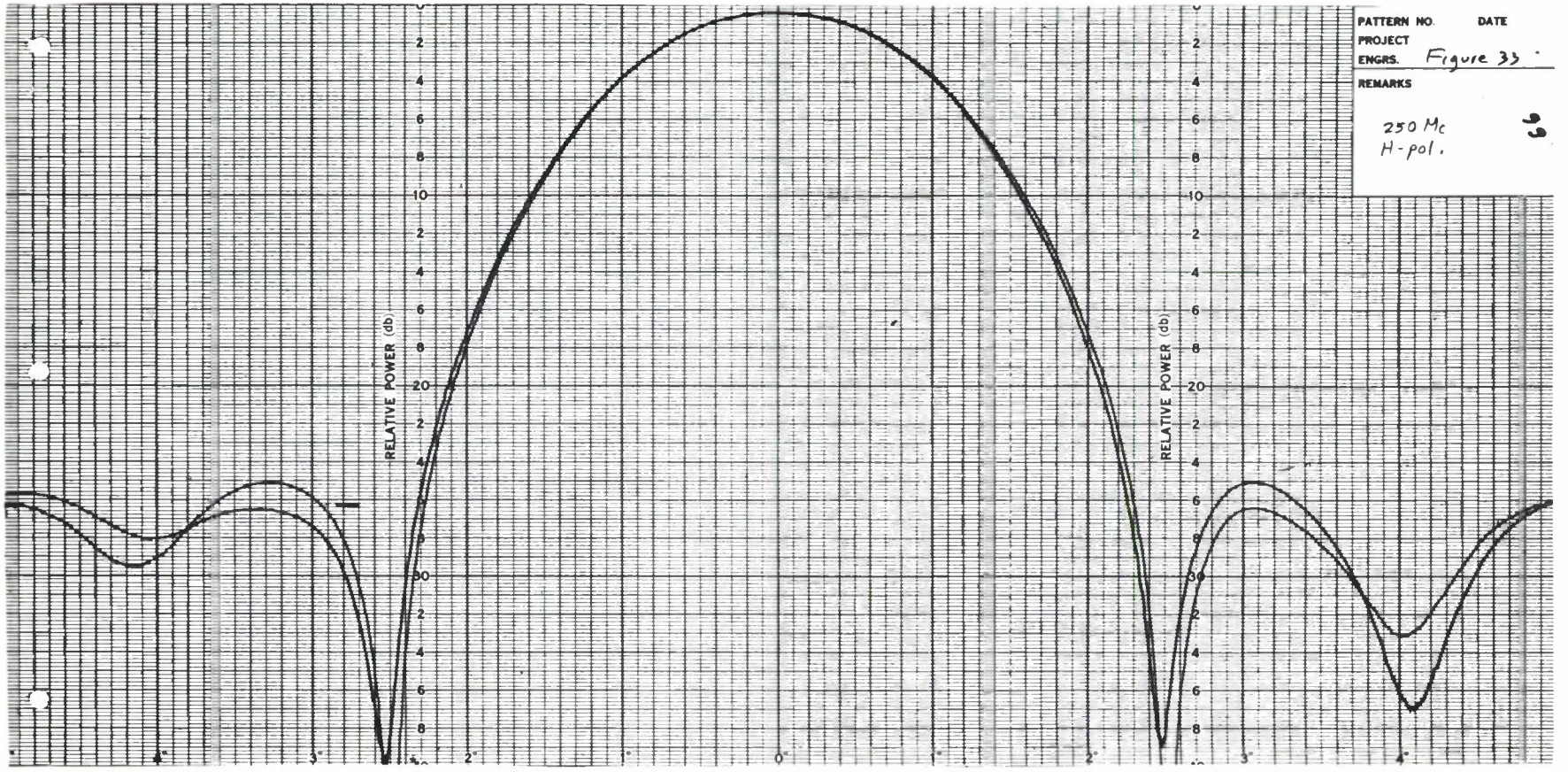

Figure 33. 360° Azimuth Pattern Comparison at 250 MHz with Transmitter Horizontally Polarized.

approximately 26 dB below the peak of the primary lobe so that extraneous energy could have been received with this 26 dB gain with respect to the direct path signal. The excursion seen in Figure 33 therefore, represents an extraneous signal 48 dB below the direct path signal or stronger.

Figure 34 is an H-plane pattern of the antenna which required that the transmit antenna be vertically polarized. The maximum extraneous signal level evidenced in this figure is -60 dB relative to the direct path signal or greater.

Figures 35 and 36 are repeats of Figures 33 and 34 respectively at 265 MHz. The sidelobe differences in Figure 35 show the extraneous signal to at least as great as -45 dB with respect to the direct path while Figure 36 shows about the same level as Figure 34.

4.1.3 Field Probe Measurements

The device used for probing the incident field in the chamber was the Scientific-Atlanta Model 5951-9 Aperture Field Probe which was previously shown in Figures 9 and 10. These photographs also show the log periodic array antenna used as a receiving antenna. The microwave absorbing material behind the antenna was used to retard reflections from the probe device itself.

It was determined in the polarization measurements section that energy was being reflected from the pan cover on the model tower base. Figure 37 is a vertical probe of the aperture field first with this pan cover covered with microwave absorber, which yielded the rather smooth curve; then with this absorber removed, which yielded the periodic ripple about this smooth curve. A high resolution potentiometer was used in the recording system so that a more accurate determination of extraneous signal level could be made. The smallest division on the ordinate scale represents 0.05 dB. The accentuated divisions on the abscissa corresponding to 0°, 1°, 2°, etc., were at 2 inch intervals on the original chart and correspond to 2 feet of travel for the field probe.

The magnitude of the ripple in Figure 37 is ± 0.2 dB or 0.4 dB peak to peak. This corresponds to an extraneous signal 33 dB below the received direct path signal. However, the extraneous signal was received from a point about 90° from boresight in the H-plane of the antenna and as can be seen in Figure 34,

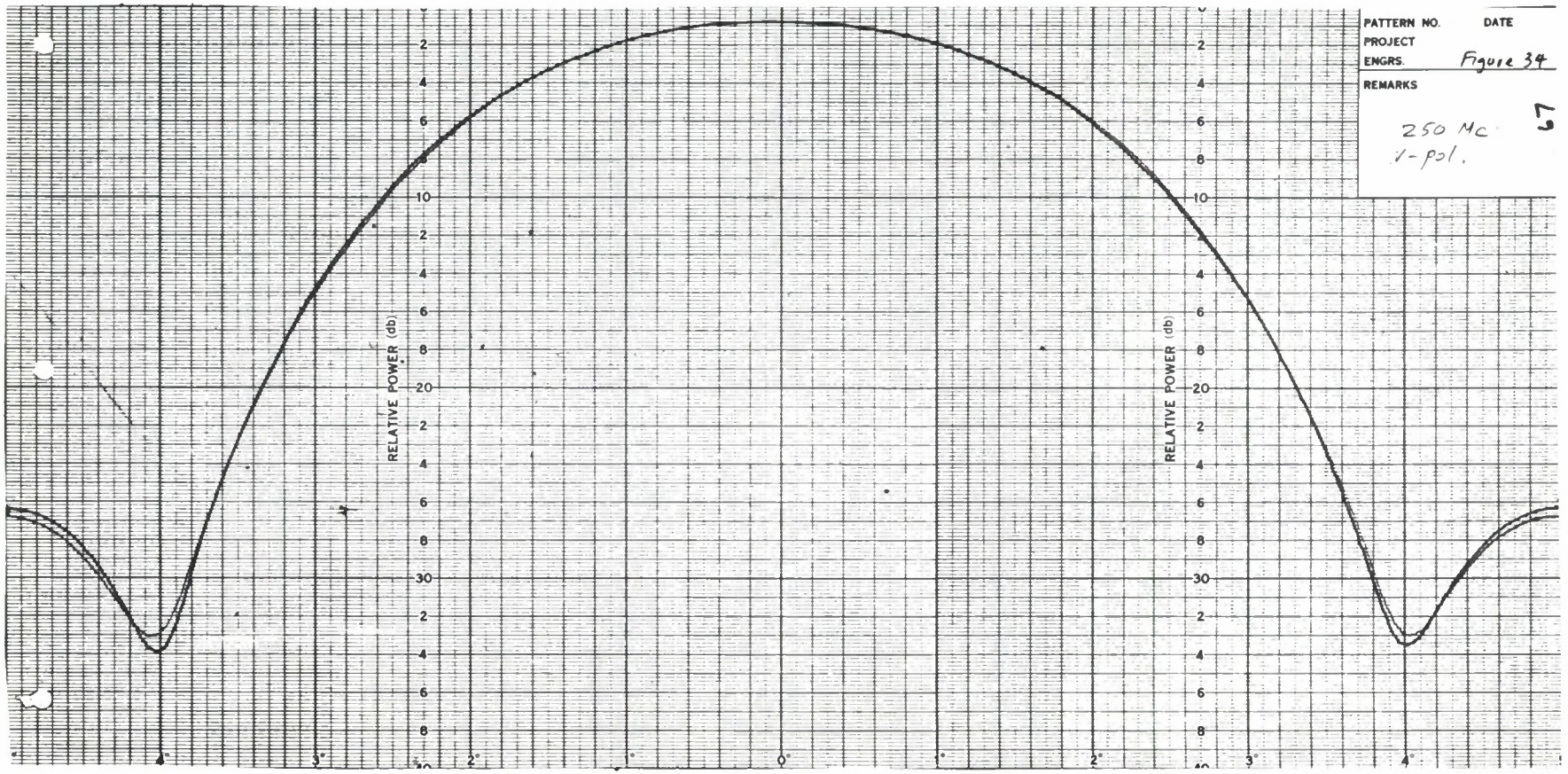

Figure 34. 360° Azimuth Pattern Comparison at 250 MHz with Transmitter Vertically Polarized.

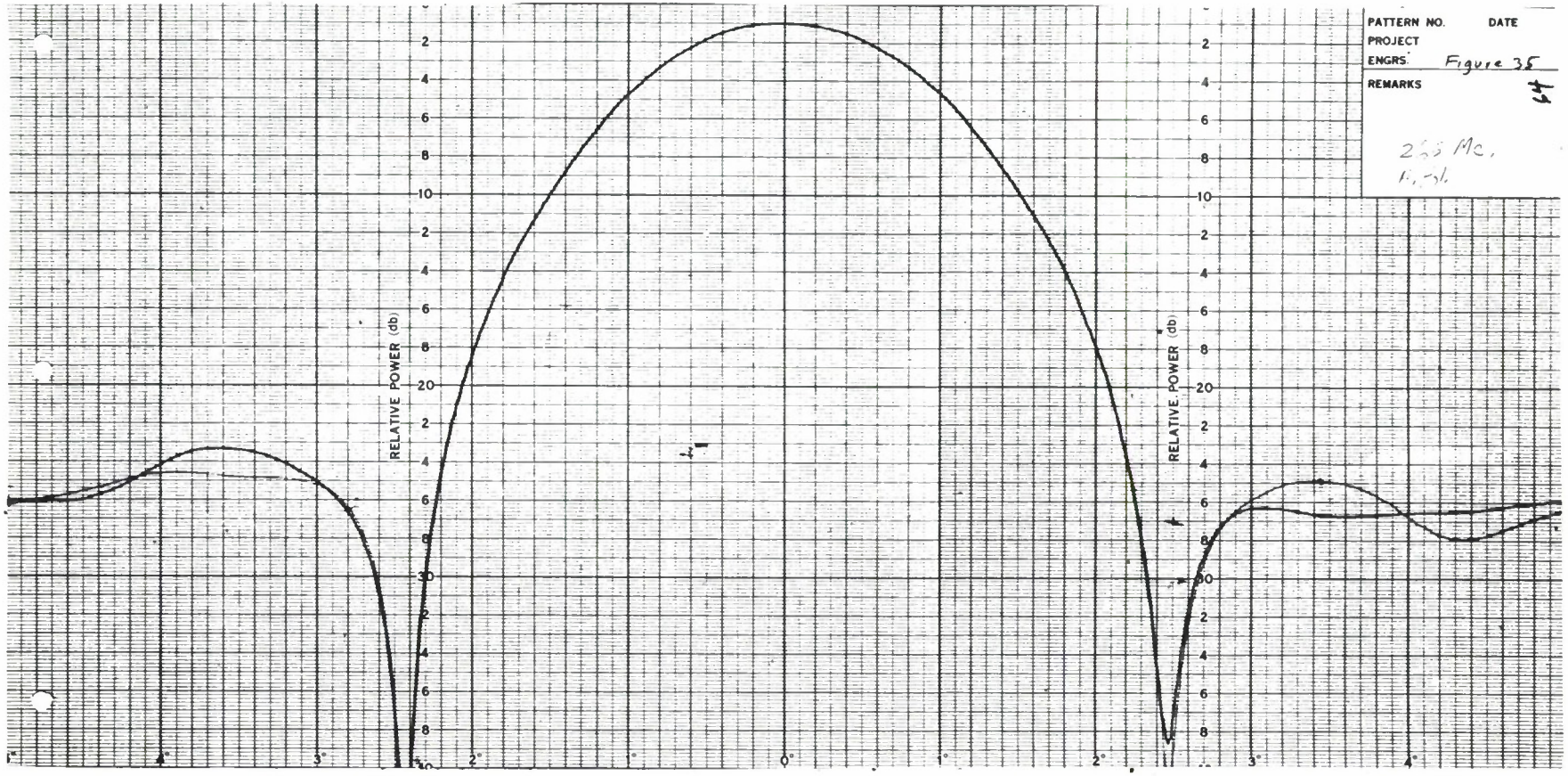

Figure 35. 360° Azimuth Pattern Comparison at 265 MHz with Transmitter Horizontally Polarized.

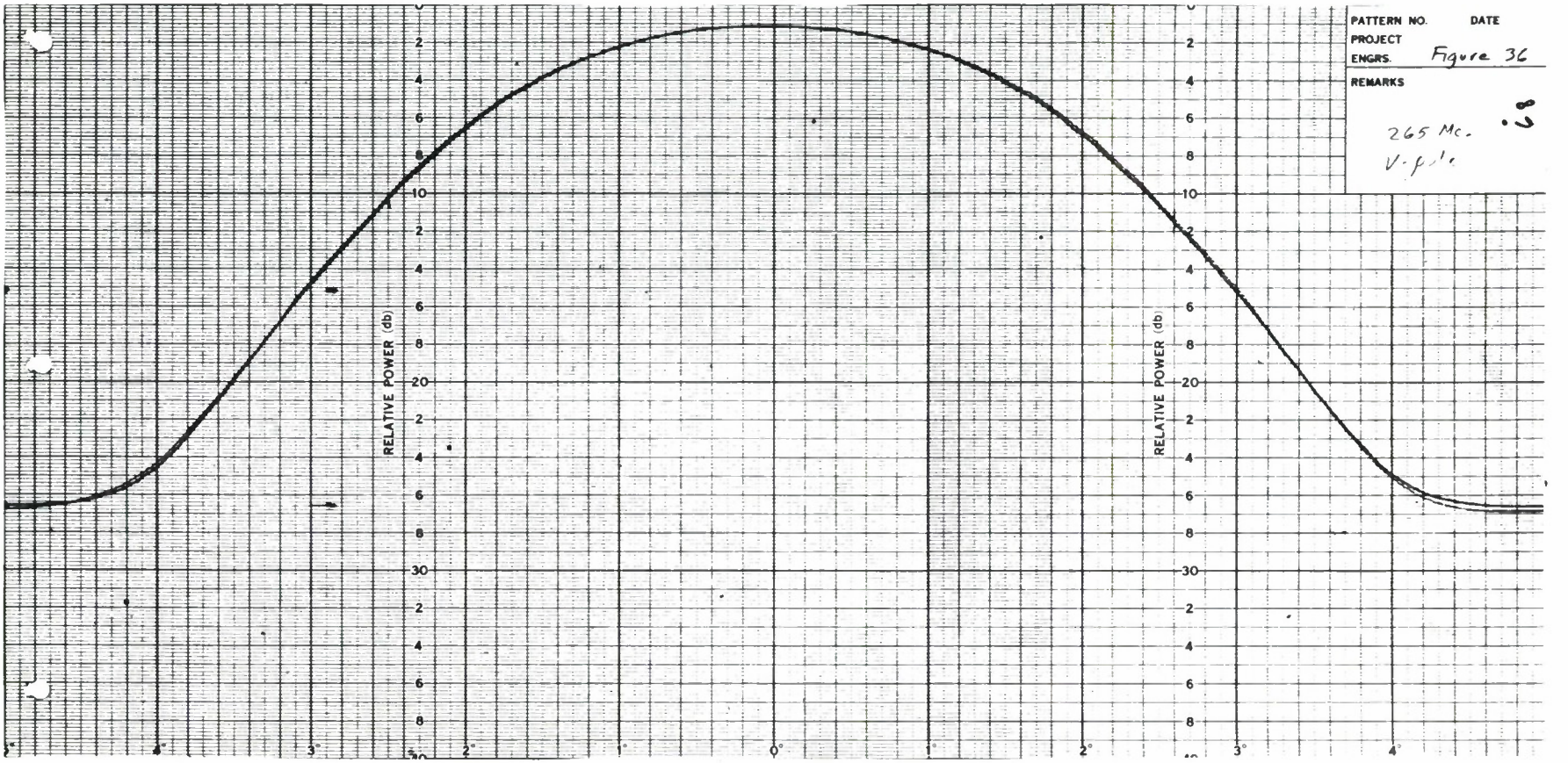

Figure 36. 360° Azimuth Pattern Comparison at 265 MHz with Transmitter Vertically Polarized.

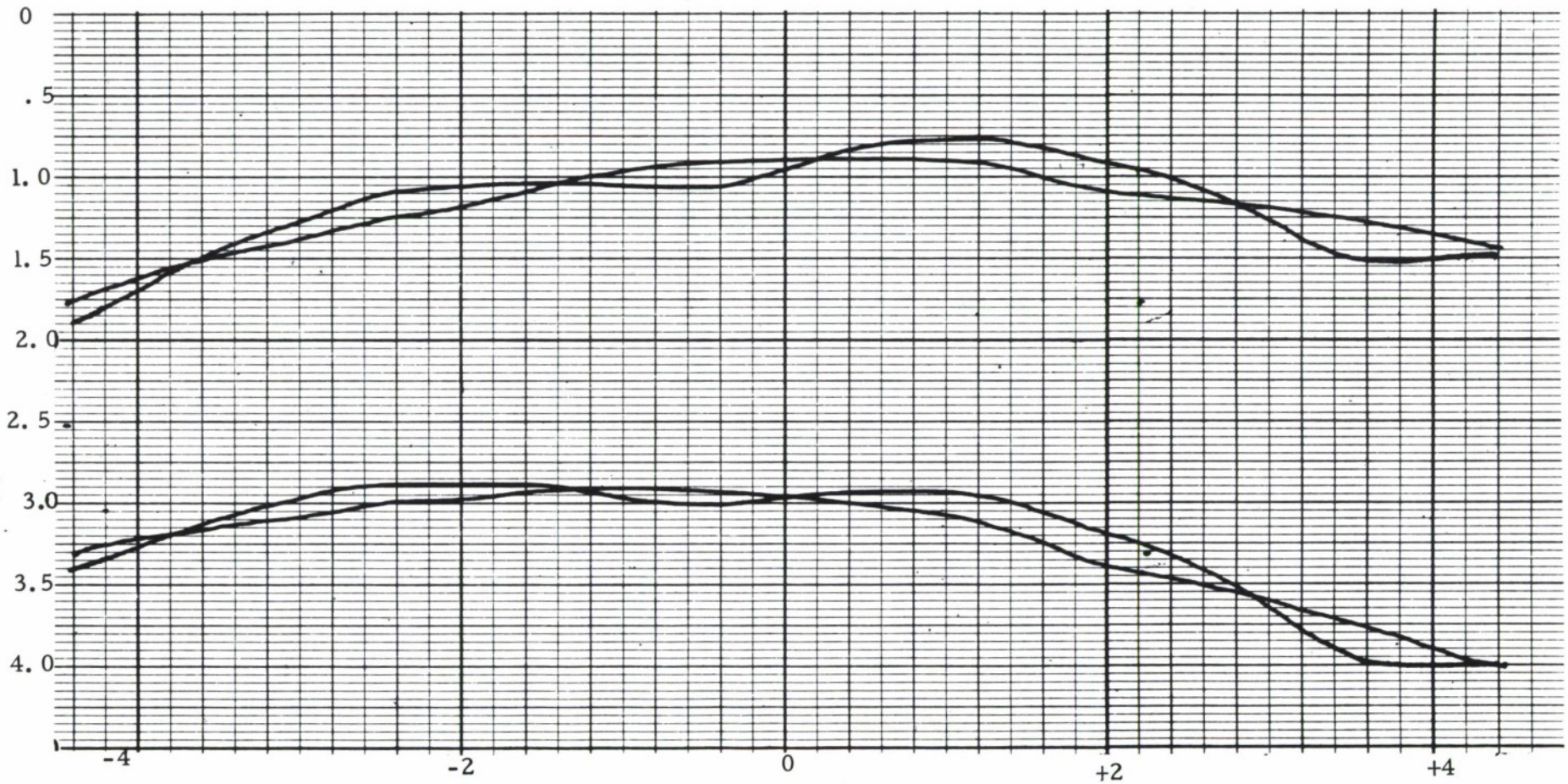

Figure 37. Vertical Field Probe Measurement at Horizontal Polarization with and without Microwave Absorber on Model Tower Pan Cover. Lower set is a Repeat Measurement. Absciassa in Probe Travel in Feet. Ordinate is Field Level in Decibels.

the antenna provides about 10 dB discrimination in that direction. Therefore, energy being reflected into the aperture at this frequency from the model tower is only about 23 dB below the direct path signal. The period of the ripple is about four feet which means that it is a reflection and not coupling between the pan and the probe antenna.

Figure 38 is a similar representation at vertical polarization. The smooth curves suggest that energy being reflected into the aperture is greatly suppressed. Figure 33, however, shows that there is a null in the E-plane at 90° so the reproducibility of the curves was really to be expected. What is meaningful, however, is that the curves do not show any evidence of reflections from elsewhere. The curves represent a smoothly varying amplitude taper across the quiet zone as is desired in a good test facility. In each of the Figures 37 and 38, the right end of the chart represents the downward direction, the left end upward.

Figure 39 represents horizontal probes of the quiet zone at horizontal polarization with the pan covered and uncovered as in Figures 37 and 38. Neither of the probes in Figure 39 alone would suggest reflections from the pan since they are at an almost constant phase with respect to the direct path signal throughout the probe. Since this energy is absent in one case, however, the curves are displaced with respect to each other though the gain on the recorder was not changed between probes. The phase associated with Figure 39 can be seen in Figure 40. Note the resultant phase change when the absorber was removed from the pan cover. The calibration of the phase chart is seen in the figure. The smoothly varying amplitudes associated with horizontal cuts at vertical polarization shown in Figure 41 again depict a clean aperture field as seen by the probe antenna indicating that any energy coming from the side walls is extremely low. The remaining patterns shown in this section were made with the model tower pan covered with absorber so that other sources of extraneous energy could be evaluated. A slight difference in amplitude distribution was observed upon changing the polarization of the transmit antenna by 180°. The effect is only 0.3 dB but is clearly visible in Figure 42, which represents vertical cuts at horizontal polarization. The curves in this figure cross each other at approximately the center of the quiet zone which strongly indicates that the pointing direction of the antenna is not coincident with the center of the quiet zone. Changes in the vertical pointing direction (vertical squint) of the antenna corrected this condition only slightly. Further change in the squint in the same direction

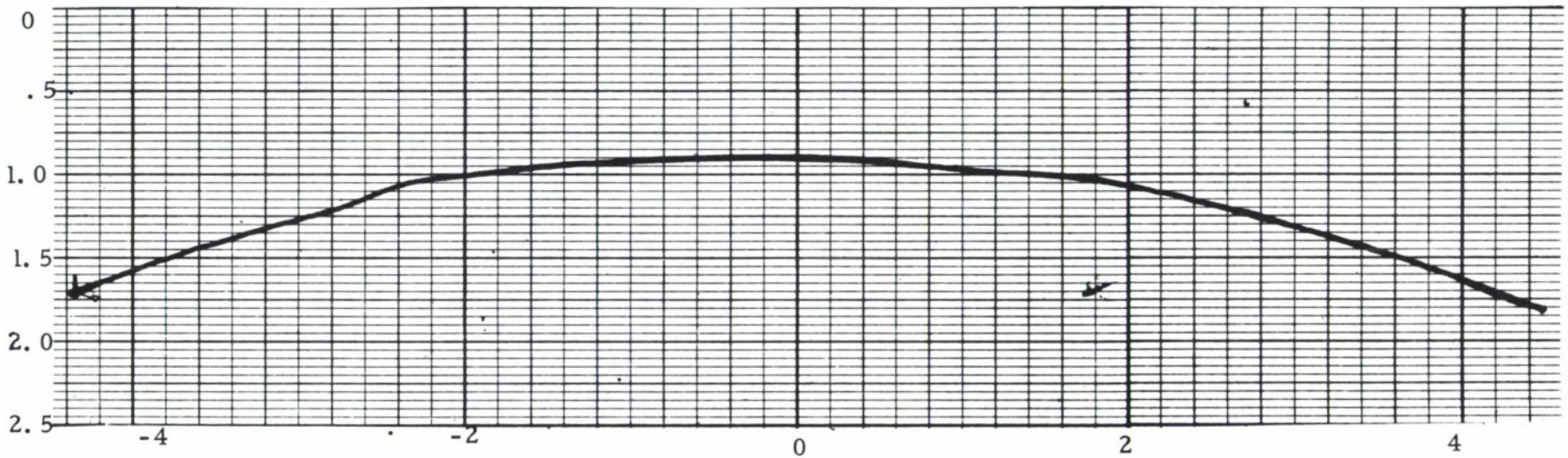

Figure 38. Vertical Field Probe Measurement at Vertical Polarization with and without Microwave Absorber on Model Tower Pan Cover. Abscissa is Probe Travel in Feet. Ordinate is Field Level in Decibels.

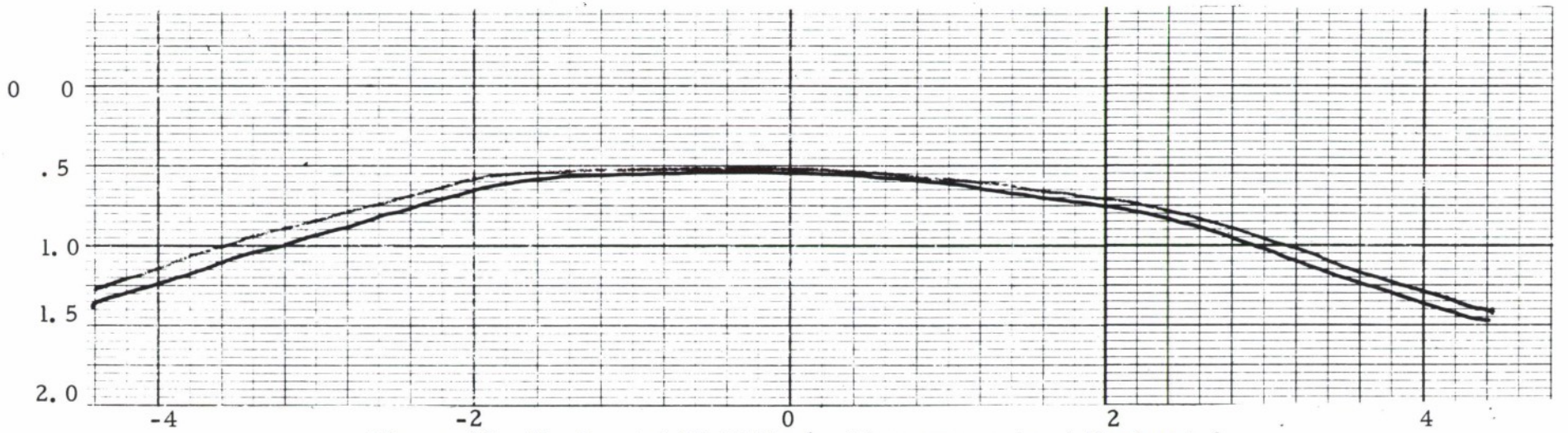

Figure 39. Horizontal Field Probe Measurements at Horizontal Polarization with and without Absorber on the Model Tower Pan Cover.

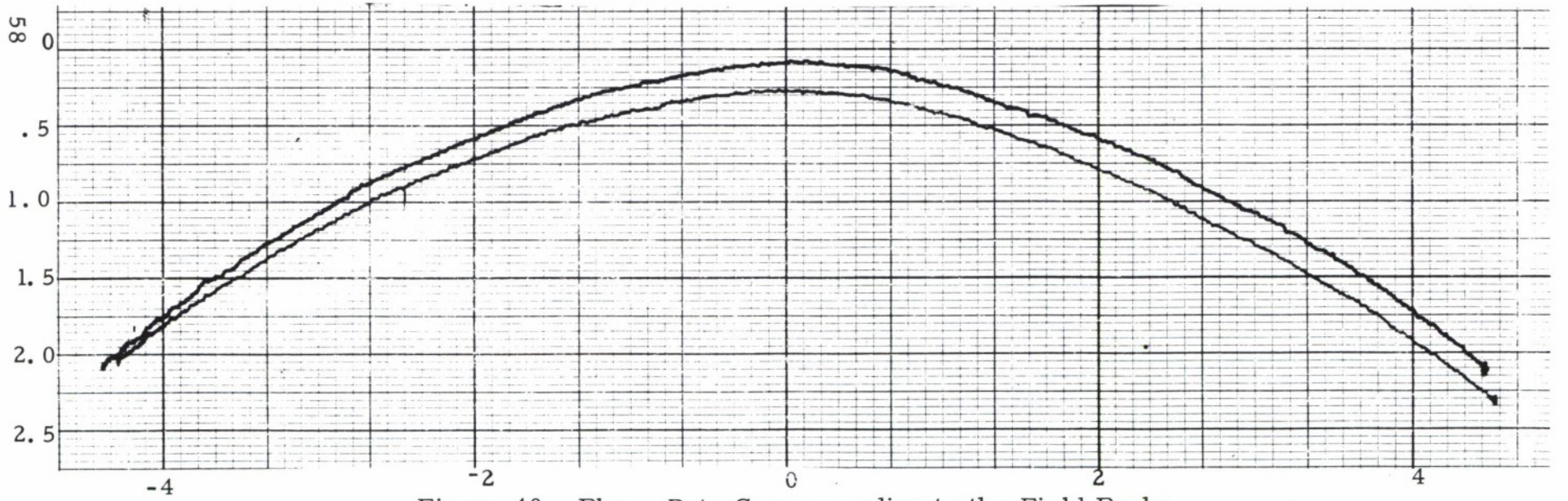

Figure 40. Phase Data Corresponding to the Field Probe Measurement in Figure 39. (Smallest Division is 0.4°) Abscissa is Probe Travel in Feet. Ordinate is Field Travel in Decibels.

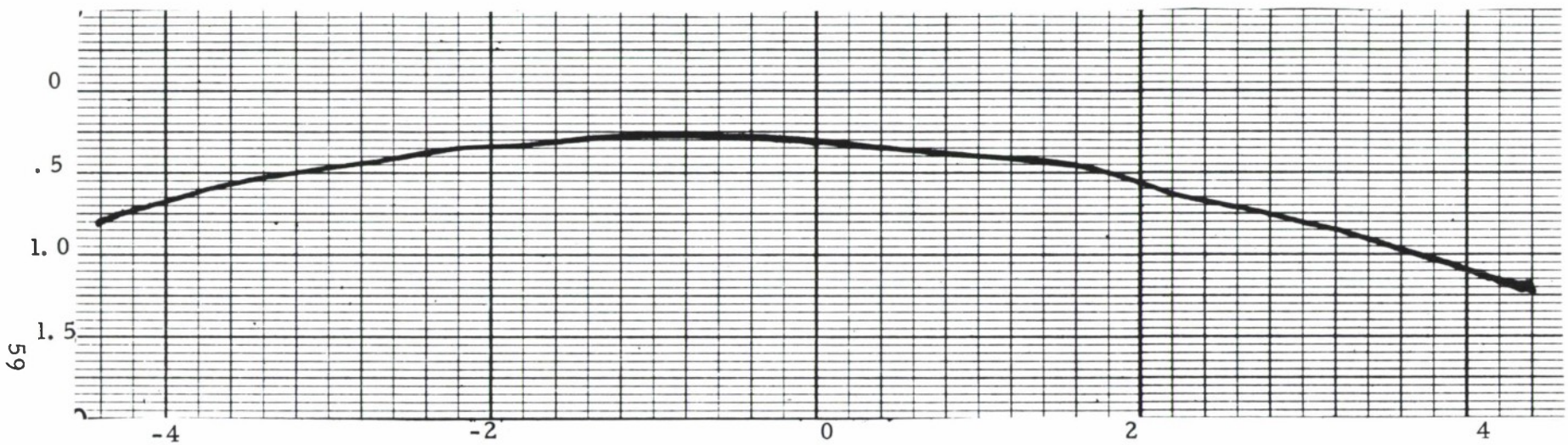

Figure 41. Horizontal Field Probe Measurement at Vertical Polarization. Abscissa is Probe Travel in Feet. Ordinate is Field Level in Decibels.

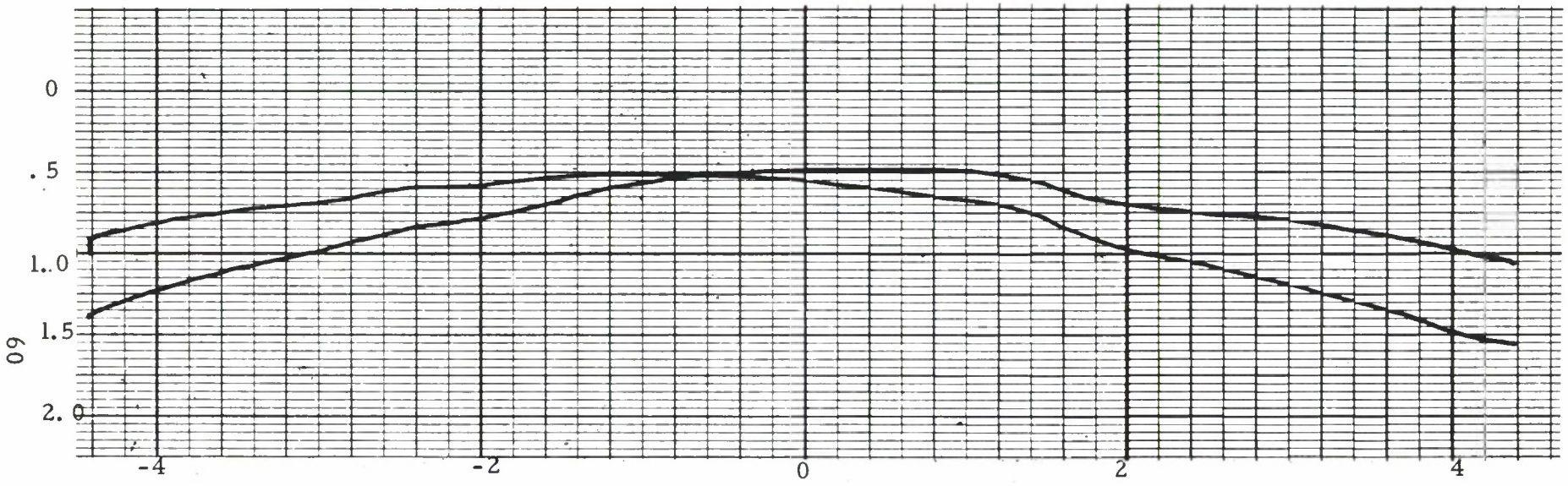

Figure 42. Vertical Field Probe Measurements at Horizontal Polarization with 180° Rotation of Transmit Antenna Between Cuts. Abscissa is Probe Travel in Feet. Ordinate is Field Level in Decibels

worsened the condition. A possible explanation is that the antenna transmits a stronger signal on one side of the H-plane than the other. Changing the pointing direction of the antenna helps correct the situation by moving the beam toward the center until its phase center moves enough off axis that the difference in reflection levels from the walls overrides the change in squint. This condition was also observed for horizontal cuts in the H-plane of the transmit antenna thereby ruling out chamber asymmetry as a cause. Similar cuts in the E-plane of the antenna, that is vertical cuts at vertical polarization, are seen in Figure 43. Rotation of the receiving antenna by 180° between two otherwise identical cuts yielded identical patterns. The difference in pattern levels in Figure 43 again indicates that the pattern maximum is not coincident with the axis of rotation.

The phase and amplitude plots in Figures 44 and 45 show the effect of removing the absorbing material from the slot for the transmit antenna polarization positioner. In each of the figures, the transmit antenna was stationed at its rearmost position and the cuts were vertical. The polarizations are horizontal and vertical for Figures 44 and 45 respectively.

Longitudinal field probes performed by driving the antenna along the chamber axis with the motorized slide on the model tower produced no additional information and are not included here. However, previously observed effects were substantiated.

4.1.4 Boresight Measurements

The previously described measurements of boresight were performed with excellent repeatability. Alignment of the axis of rotation of the model tower to within 0.1 inch of the axis of rotation of the transmit polarization positioner was accomplished by autoreflecting from a mirror on the head axis of the model tower. Since the receive antenna was rigidly fixed to the dielectric probe antenna, phase measurements made at diametrically opposite points in the chamber should differ by 180°, if the points were actually at equal phase, due to the 180° rotation of the antenna. Depending upon whether the phase needs to advance or lag to attain the 180° phase difference position after moving to this diametrically opposite point, one can determine the location of the phase center. For the particular case given in Table II, the phase center was high.

Table II lists data for one such set of measurements and demonstrates the repeatability obtained. The diametrically opposite points sampled were 8.5

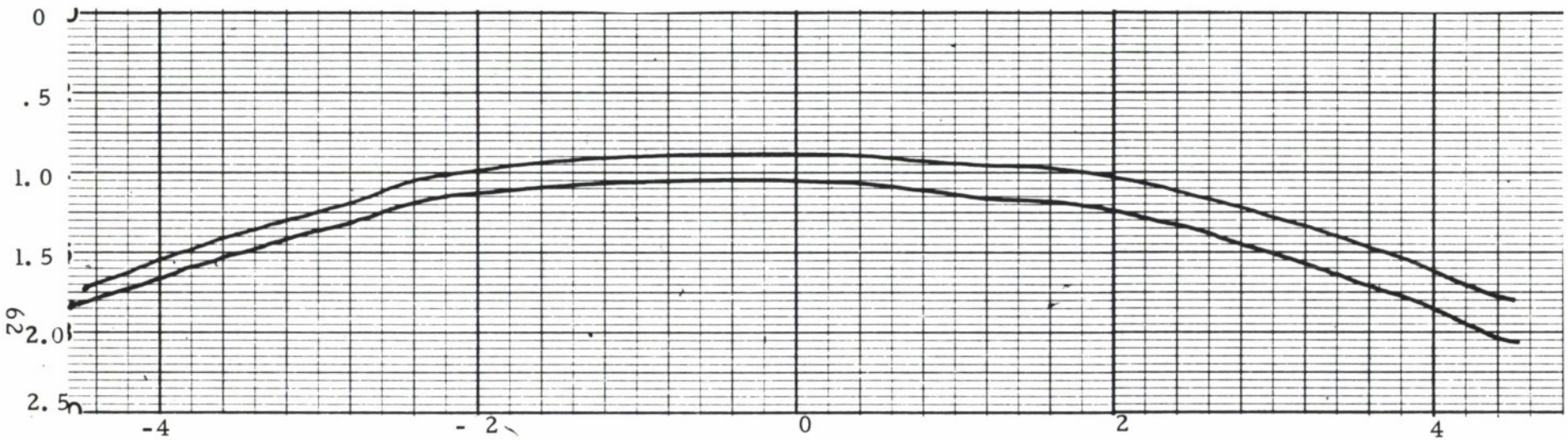

Figure 43. Vertical Field Probe Cut at Vertical Polarization. Transmit Antenna was Rolled 180° Between Cuts. Abscissa is Probe Travel in Feet. Ordinate is Field Level in Decibels.

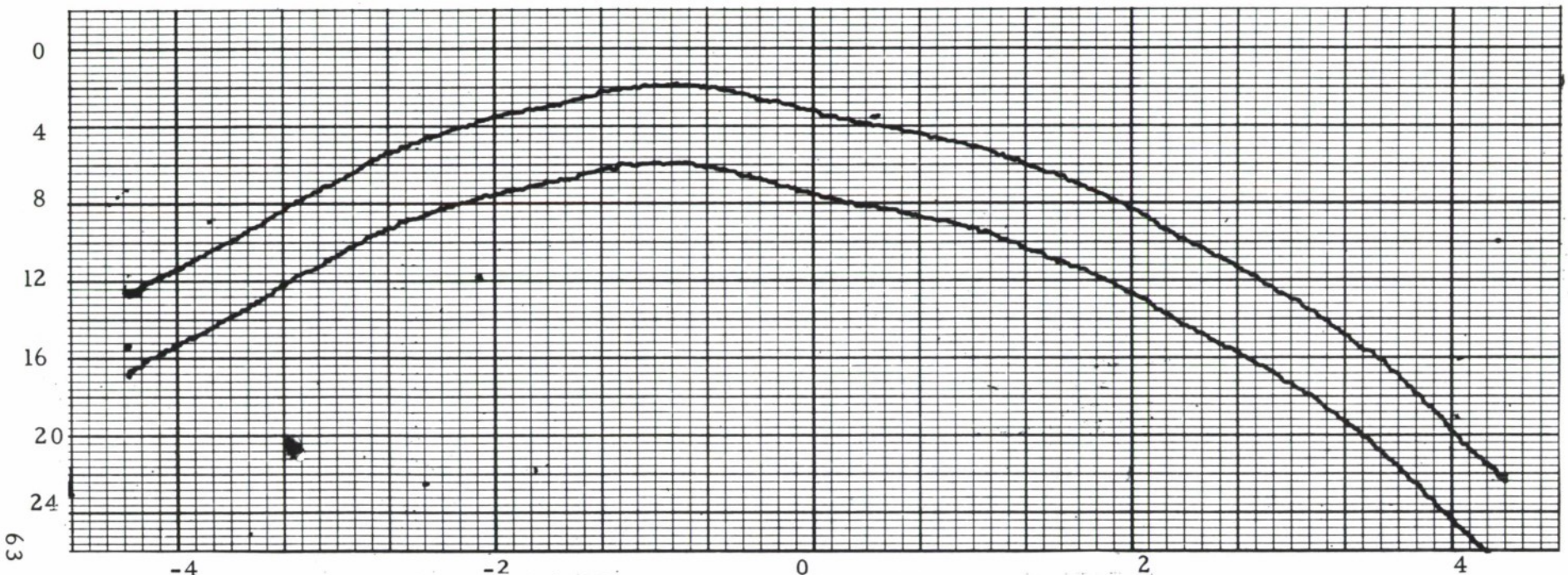

(a) Phase Plot. Smallest Division is 0.4°

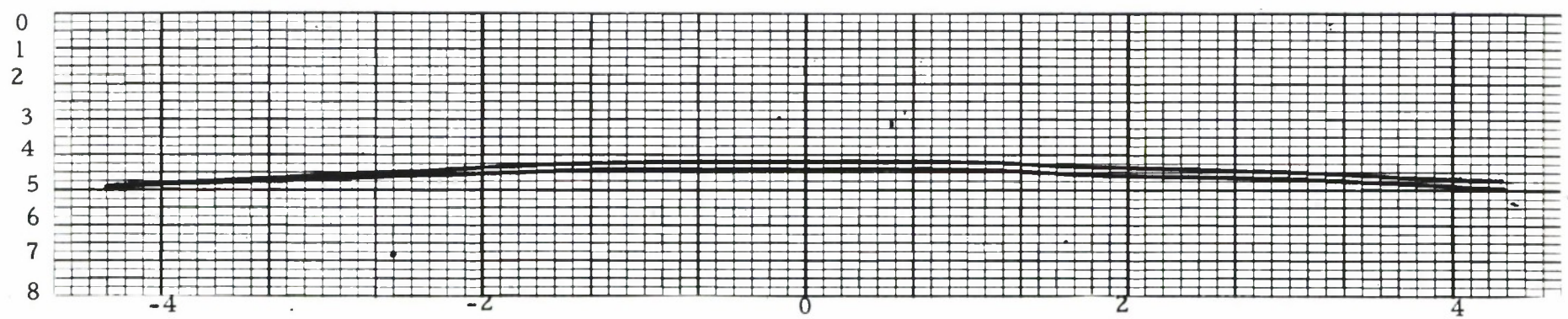

(b) Amplitude Plot. Smallest Division is 0.25dB.

Figure 44. Phase and Amplitude Field Probe Cuts Taken with the Transmitter Positioned at the Rear Limit and Horizontally Polarized. One Curve is with Absorber in the Transmit Slot, the Other without.

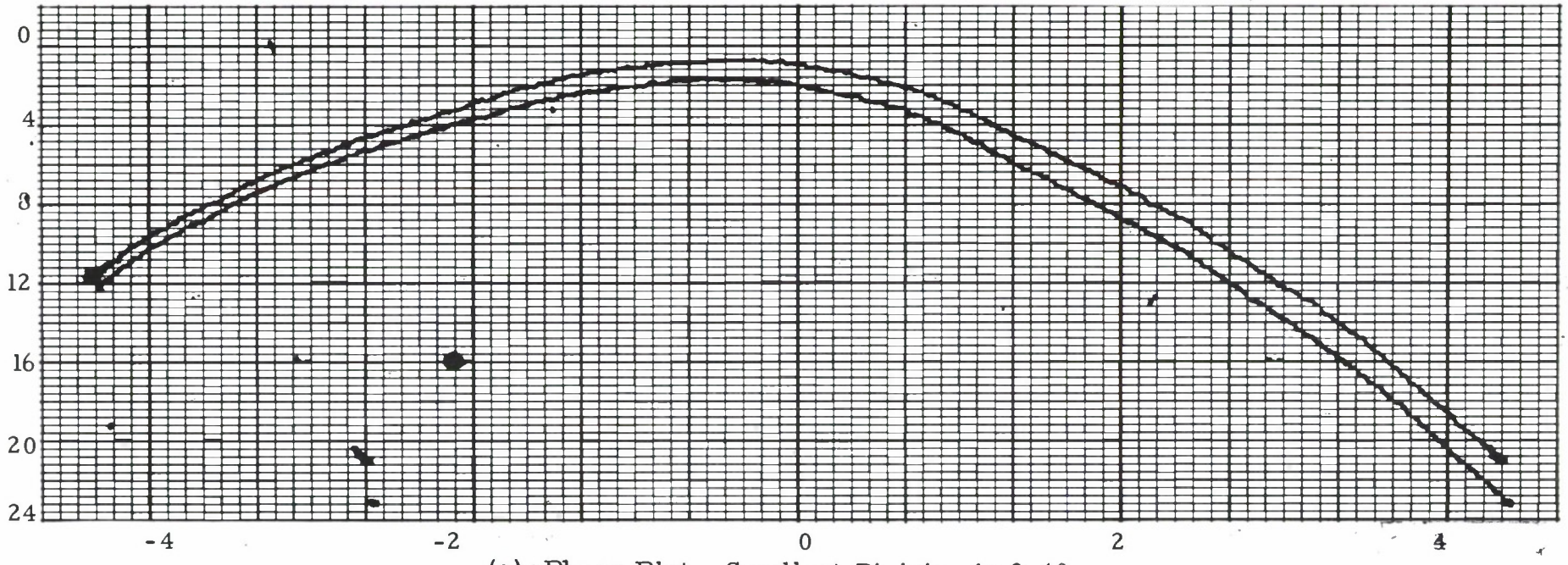

(a) Phase Plot. Smallest Division is 0.4°.

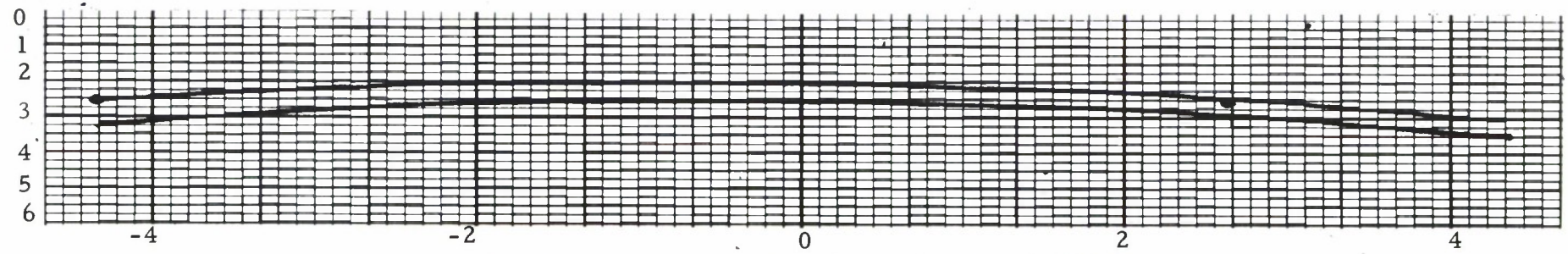

(b) Amplitude Plot. Smallest Division 0.25dB.

Figure 45. Phase and Amplitude Field Probe Cuts Taken with the Transmitter Positioned at the Rear Limit and Vertically Polarized. One Curve is with Absorber in the Transmit Slot, the Other without.

feet above and below the head axis of the model tower. The transmit antenna was horizontally polarized and positioned at the rearmost position.

TABLE II

ϕ Phase Reading (degrees)	$\Delta\phi$ Difference from Previous Reading (degrees)	$\lvert 180° - \Delta\phi \rvert$ (degrees)
502.3		
681.2	178.9	1.1
502.3	178.9	1.1
681.4	179.1	0.9
502.2	179.2	0.8
681.2	179.0	1.0
502.2	179.0	1.0
681.3	179.1	0.9
502.3	179.0	1.0
681.4	179.1	0.9
502.2	179.2	0.8
681.3	179.1	0.9
502.5	178.8	1.2
681.5	179.0	1.0
502.5	179.0	1.0
681.7	179.2	0.8
502.8	178.9	1.1
682.1	179.3	0.7

The average of the numbers in the last column in Table II is 0.93°. The geometry for calculating the position of the phase center is shown in Figure 46. In this figure, we see that

$$(8.5 - \delta)^2 + 60^2 = x^2 \tag{4.1}$$

and

$$(8.5 + \delta)^2 + 60^2 = y^2 \tag{4.2}$$

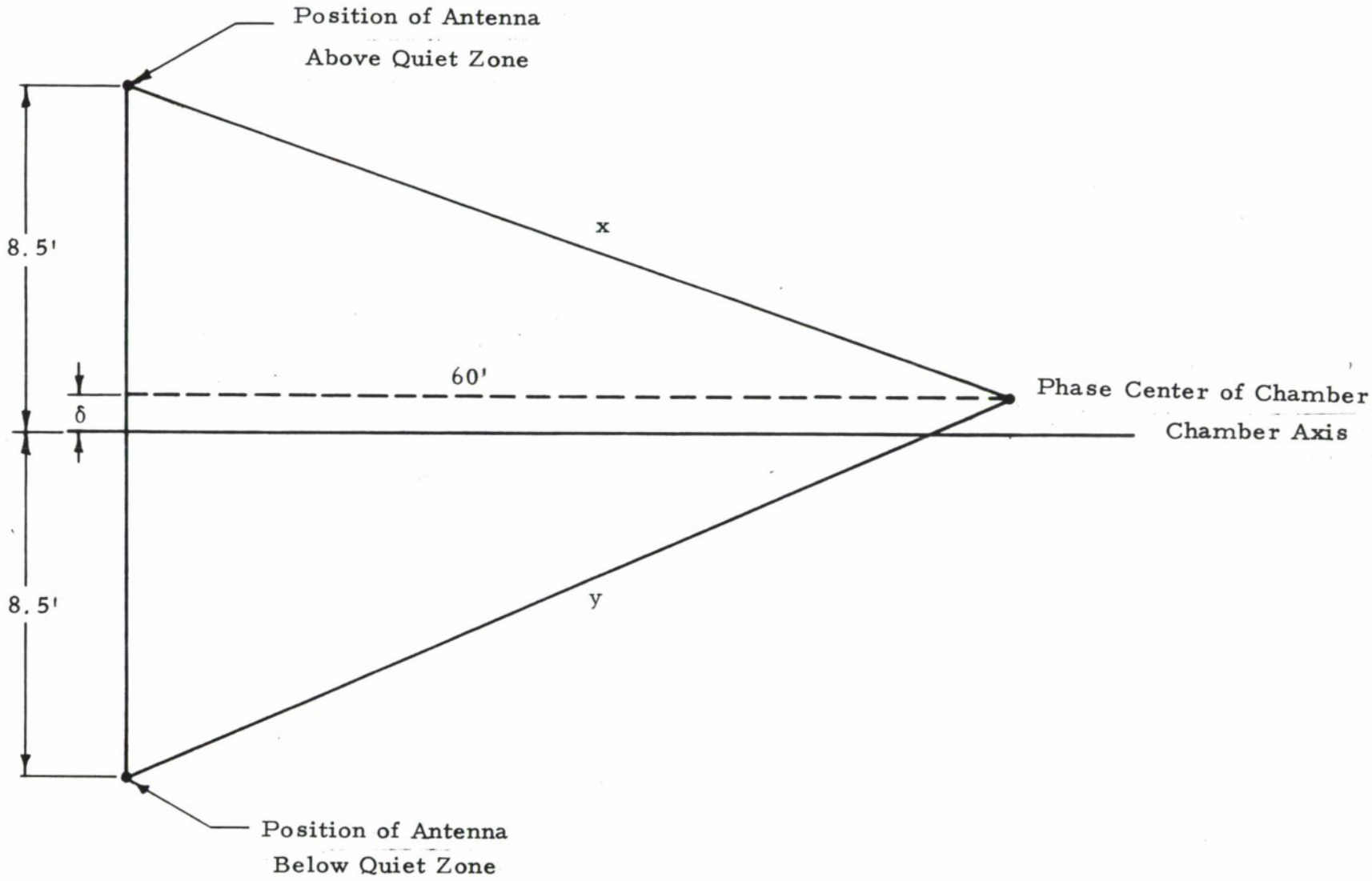

Figure 46. Geometry for Calculating Boresight Position in Chamber

But from the boresight measurement, we know that y - x yields 0.93 electrical degrees which at 250 MHz equals 0.122 inches. Converting equations (4.1) and (4.2) to inches, we now have the following three simultaneous equations from which δ can be determined.

$$(102 - \delta)^2 + 720^2 = x^2 \tag{4.3}$$

$$(102 + \delta)^2 + 720^2 = y^2 \tag{4.4}$$

and

$$y - x = .122 . \tag{4.5}$$

Solution of these equations for δ showed the location of the composite phase center to be 0.435 inches above the axis of rotation of the transmit antenna.

Horizontal phase comparisons at horizontal polarization revealed through similar calculations that the center of phase was 1.8 inches to the right of the source axis as seen from the quiet zone. Measurements at vertical polarization showed that the phase center was 0.6 inches to the right and 2.3 inches high relative to the center of the polarization positioner. The above results and those for measurements made with the antenna positioned at a 50 inch radius are presented in Table III. The column labeled "Average" is weighted slightly toward the 102 inch radius because better resolution was obtainable at that radius.

TABLE III

Boresight Directions with Transmit Antenna Positioned in Rear

Polarization	102 inch Radius (inches)	50 inch Radius (inches)	Average (inches)
Vertical	0.6 Rt.	0.3 Left	0.2 Rt.
	2.3 High	1.3 High	1.8 High
Horizontal	1.8 Rt.	1.3 Rt.	1.6 Rt.
	0.4 High	1.0 High	.7 High

As was stated previously, all directions are as seen by one standing at the center of the quiet zone and facing the transmit antenna.

The transmit antenna was moved to the end of the chamber nearest to the quiet zone to see if any significant shift in boresight occurred as a result of this movement. At this transmit position, measurements were once again observed to be extremely repeatable as a function of antenna radius position. Table IV presents the observed boresight directions at this transmit position.

TABLE IV

Boresight Directions for Transmit Antenna Positioned in Front.	
Polarization	Boresight Direction (inches)
Vertical	6.2 Rt.
	2.1 Low
Horizontal	3.8 Rt.
	2.6 Low

The boresight directions given in Table IV are farther off center than the ones given in Table III where the transmitter was positioned at the rear of the slot. This is, however, a reasonable trend since the image sources are more widely separated in the front positions and any asymmetry associated with reflections would be amplified as the individual source element separation increased.

After completing the measurements given in Table IV, the model tower and probe device were moved five feet to the edge of the quiet zone nearest the transmitter in order to obtain comparative data at another position in the quiet zone. These data are presented in Table V.

The worst observed deviation of the boresight direction from the chamber axis is recorded in Table IV and at 6.2 inches to the right of and 2.1 inches below the axis. This represents an angle of approximately 10 milliradians or 0.6 degrees.

Since any actual boresight determinations at this frequency would probably be done with the transmit antenna positioned at the rear of the chamber in order to reduce the distance between the images, the deviations recorded in Table III are more likely to be encountered in practice. These deviations range from 1.9 to 3.2 milliradians. These accuracies are more than adequate for most measurements made at this frequency.

TABLE V

Boresight Directions at Front of Quiet Zone	
Polarization	Boresight Direction (inches)
Vertical	4.8 Rt.
	2.0 Low
Horizontal	1.8 Rt.
	4.7 Low

4.2 3 GHz Measurements

The following sections describe the evaluation measurements at 3.0 GHz. This particular frequency was selected because it was a representative mid-frequency of operation for the chamber. The probe antenna used for all measurements at 3.0 GHz was a modified Scientific-Atlanta Model 12-2 Standard Gain Horn, with 3 dB beamwidths of 32° in the E-plane and 36° in the H-plane. The transmit antenna was a standard gain horn. Boresight measurements were made at vertical polarization in one plane only and the phase center was found to be only 0.1 inches high.

4.2.1 Polarization Measurements

Polarization characteristics of the chamber at 3 GHz are presented for transmitter polarization intervals of 10° in Figure 47. Ten decibels of gain were added in the region of the nulls which accounts for the jagged sections of the curves. The curves shown in the figure are very uniform, even down to the null depths.

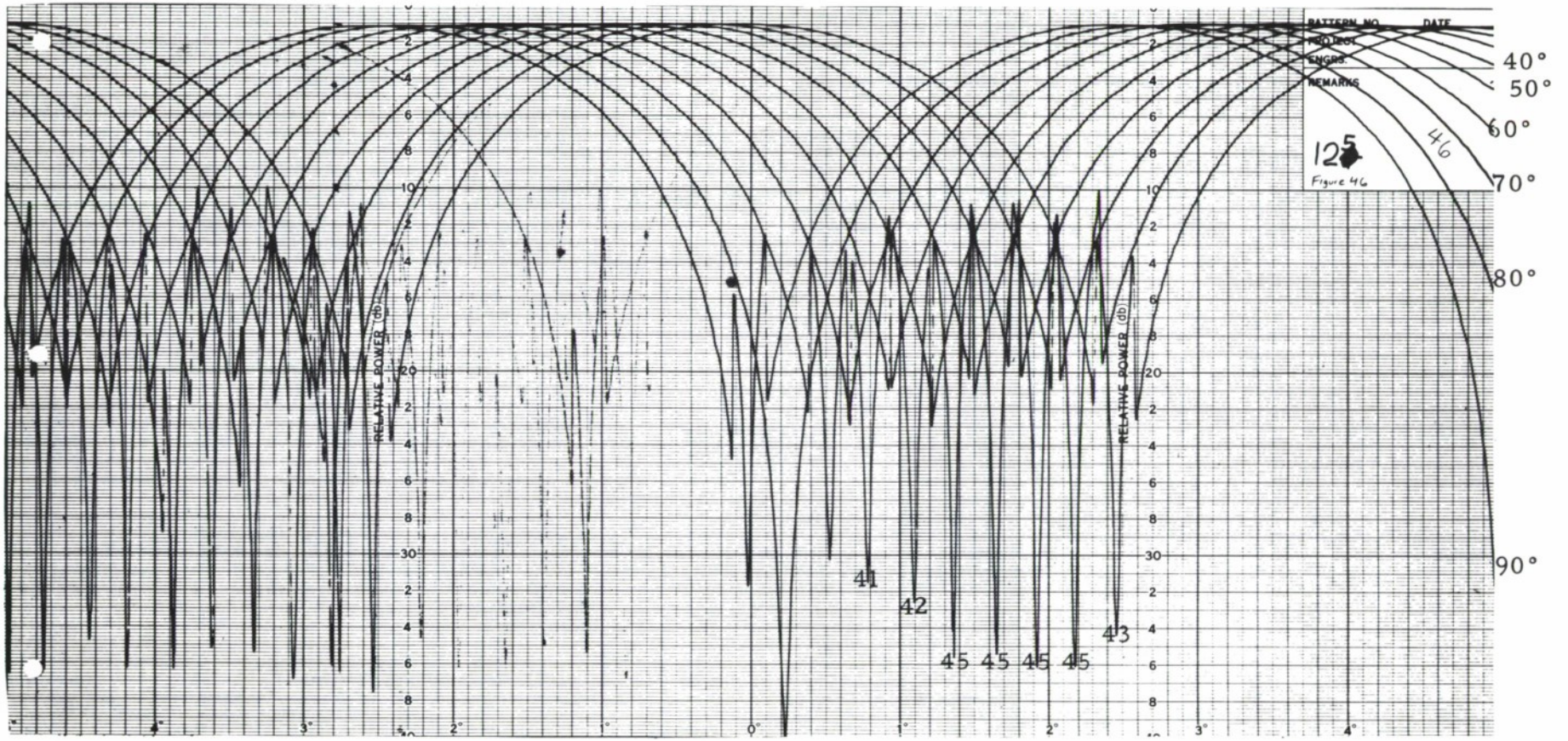

Figure 47. Polarization Patterns at 3 GHz for Transmitter in Rearmost Position. Patterns are taken at 10° Intervals from 90° to 180°.

Only about 0.2 dB change in the maximum recorded signal was observed for these curves. These curves represent transmitter polarizations from 90° to 180° with the transmit antenna positioned at the rearmost position. Those plots taken in the other quadrant from 0 to 90° are presented in Figure 48.

Polarization characteristics of the chamber are fairly independent of the position of the transmit antenna in the throat. Figures 49 and 50 are polarization patterns for transmitter polarizations of 0° to 90° and from 90° to 180° respectively in 10° increments with the source antenna at its most forward position. The patterns are almost identical with those taken with the source antenna in the rearmost position.

4.2.2 Pattern Comparison Measurements

Azimuth pattern comparison measurements for 360° rotations are presented in the following figures. Full scale deflection on the chart represents 40 dB. Figures 51 and 52 were taken at vertical and horizontal polarizations respectively. The pan was covered with absorber in one plot and uncovered in the other as was done at 250 MHz. The difference in sidelobes in Figure 51 indicate the energy from the pan cover was about 33 dB below the direct path signal. This is evidenced in the first sidelobe to the left which shows a 0.4 dB separation in the curves at a point 24 dB below the peak of the beam. It can be seen in Figure 52 that the energy coming in from the pan would also enter the horn at a point about 23 dB below the direct path signal. The 0.4 dB separation, therefore, corresponds to a suppression level of about 33 dB with respect to the direct path signal. At this frequency, essentially no reflected energy from the pan cover is in evidence for horizontal polarization.

Figures 53 and 54 represent 360° azimuth pattern comparisons for vertical and horizontal polarizations respectively with the model tower pan covered with absorber. Indicated reflection levels are as great as -43 dB and -38 dB with respect to the direct path signal level for vertical and horizontal polarizations respectively.

Figure 55 represents a 360° pattern comparison at horizontal polarization to test the effect of the absorber in the transmitter slot. The patterns were started on boresight instead of 180° to allow better examination of the back lobes.

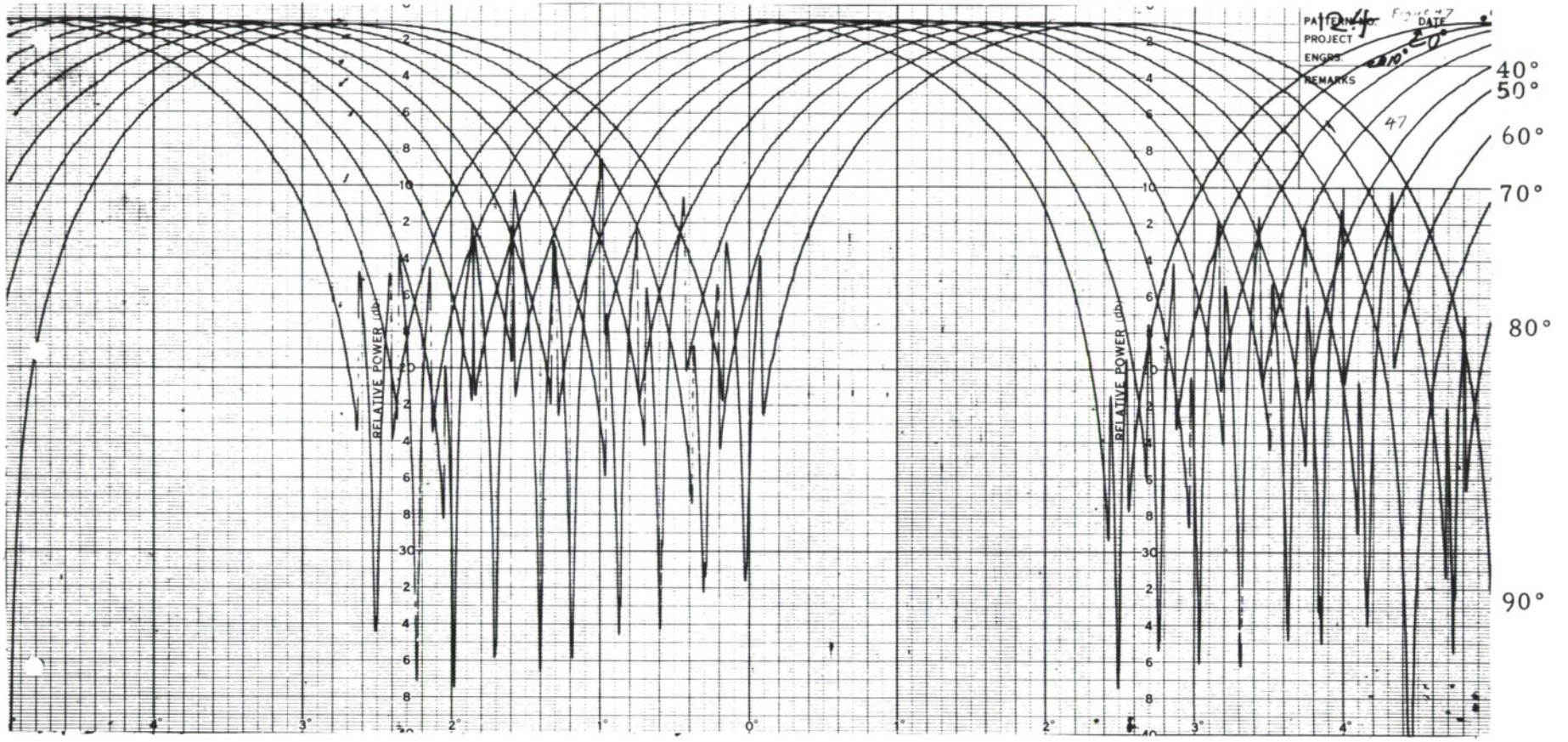

Figure 48. Polarization Patterns at 3 GHz for Transmitter in Rearmost Position, Patterns are taken at 10° Intervals from 0° to 90°.

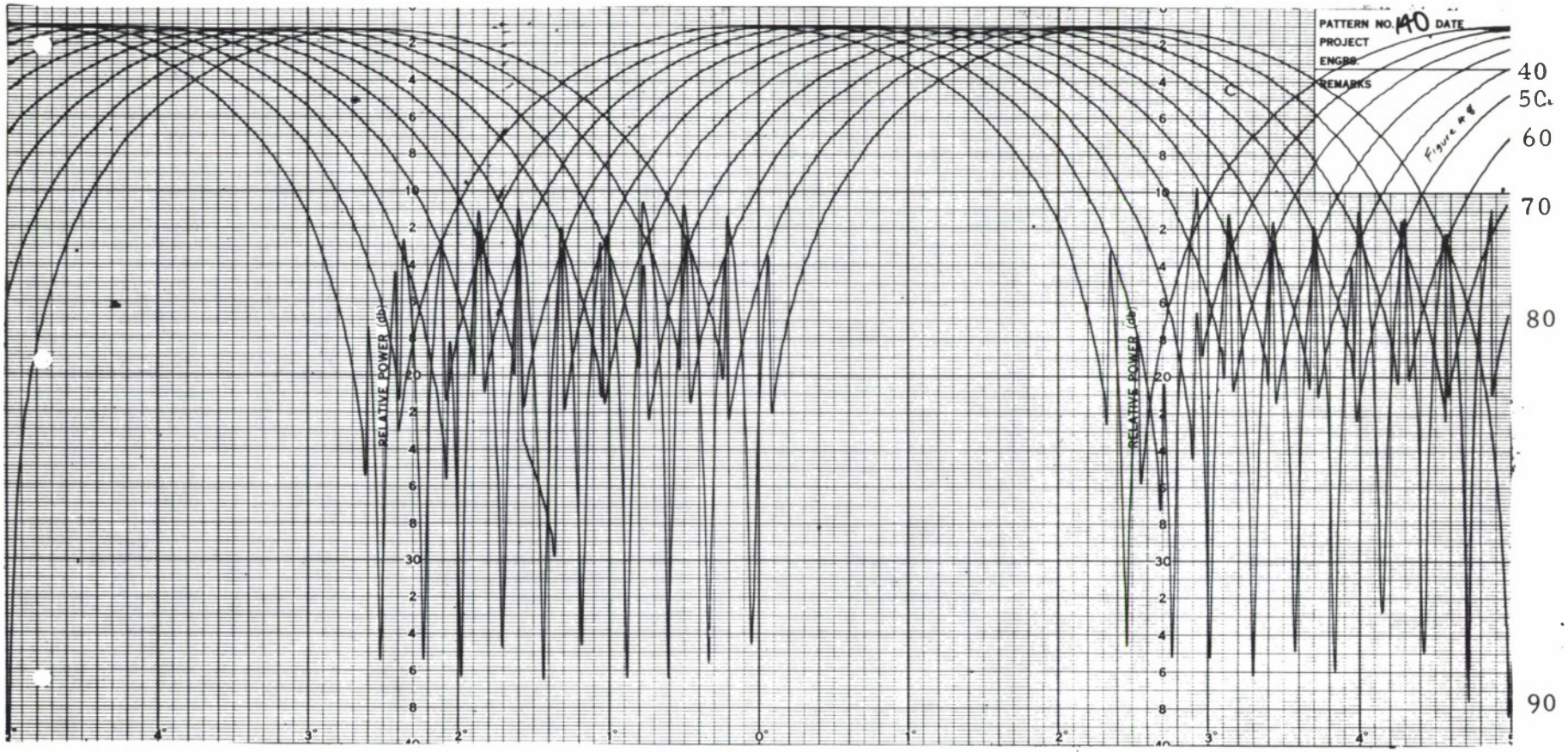

Figure 49. Polarization Patterns at 3 GHz for Transmitter in Forward Position. Patterns are taken at 10° Intervals from 0° to 90°.

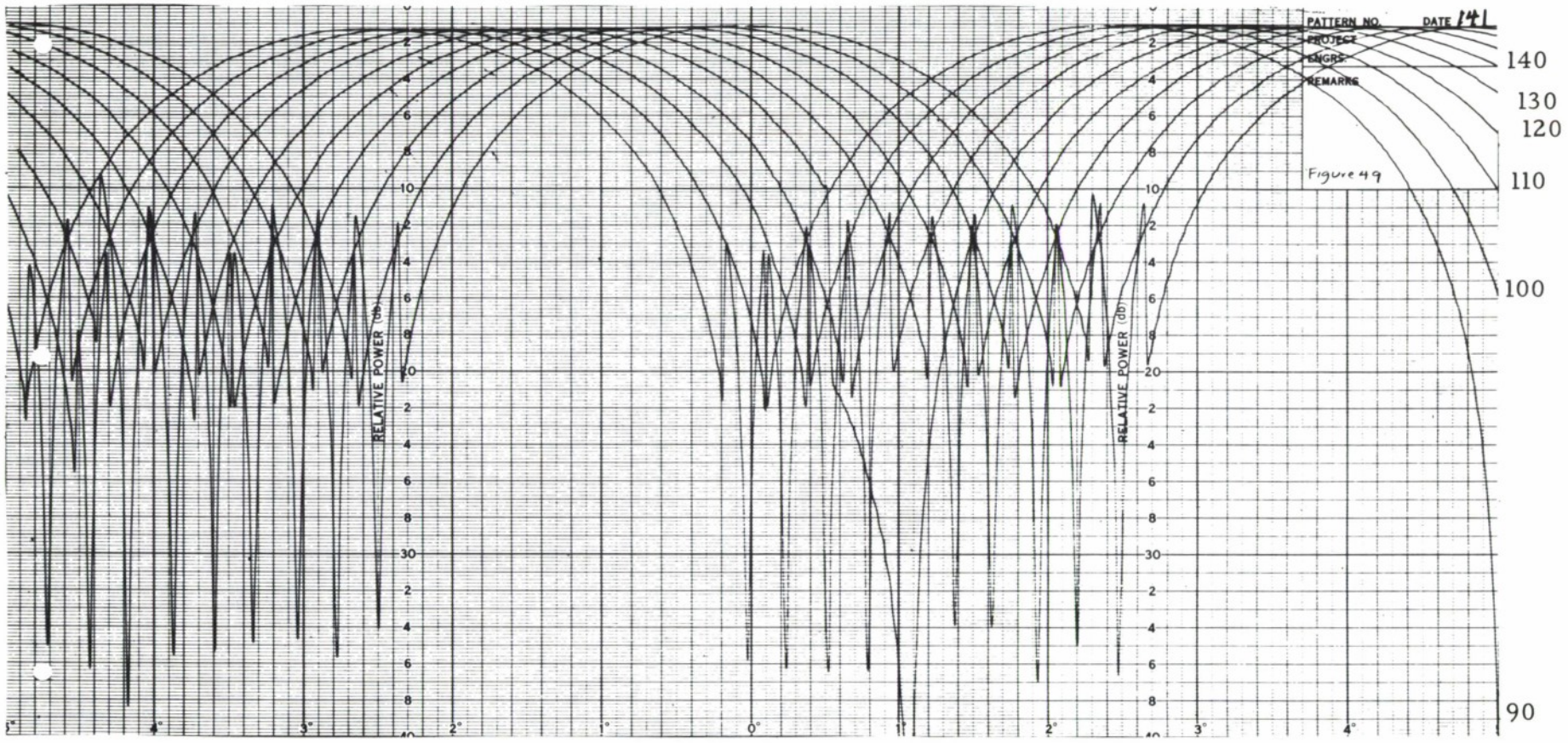

Figure 50. Polarization Patterns at 3 GHz for Transmitter in Forward Position. Patterns are taken at 10° Intervals from 90° to 180°.

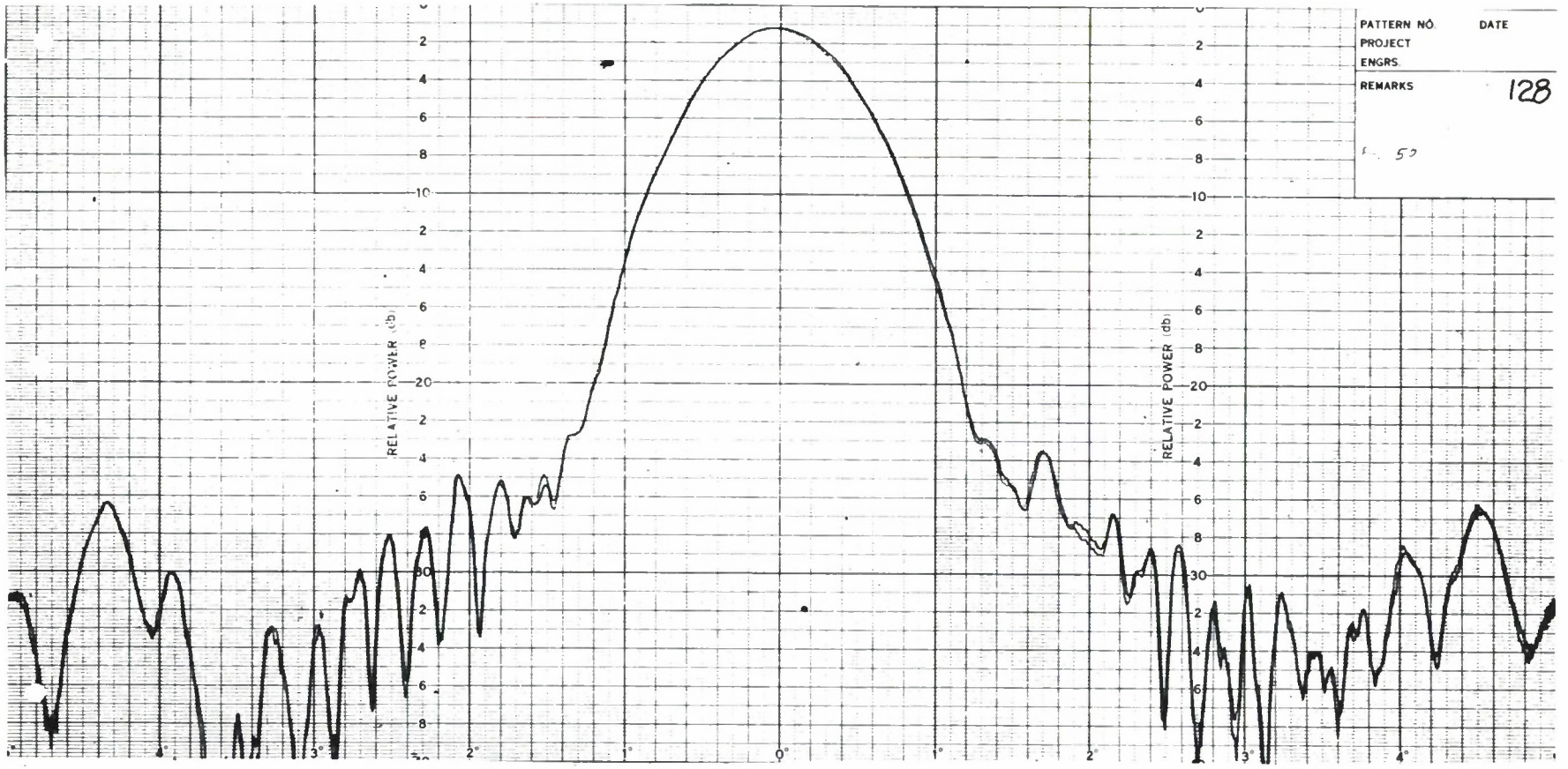

Figure 51. 360° Azimuth Patterns with and without Absorber on Model Tower Pan Cover. The Transmit Antenna was vertically Polarized and in Rearmost Position.

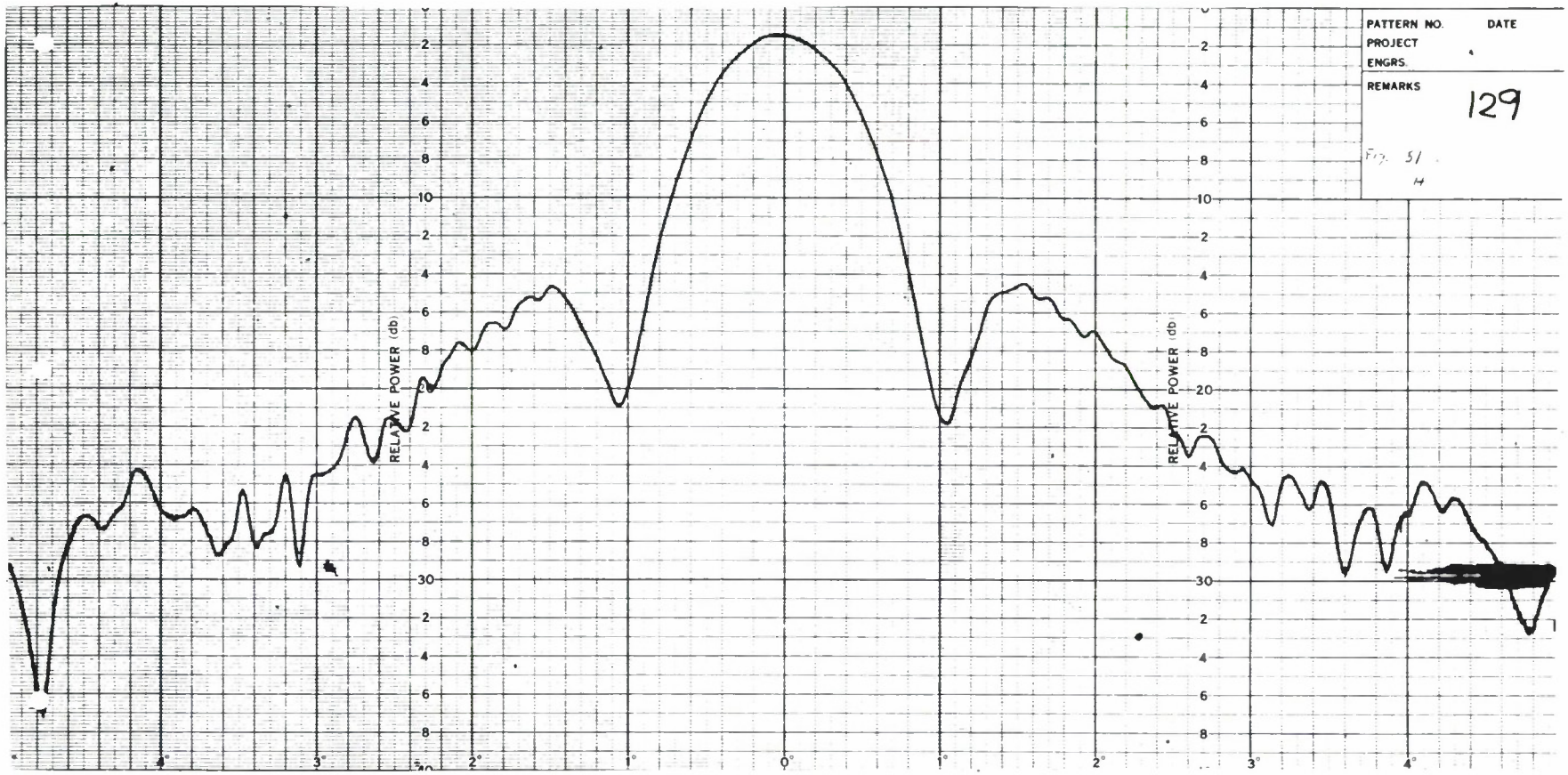

Figure 52. 360° Azimuth Patterns with and without Absorber on Model Tower Pan Cover. The Transmit Antenna was Horizontally Polarized and in Rearmost Position.

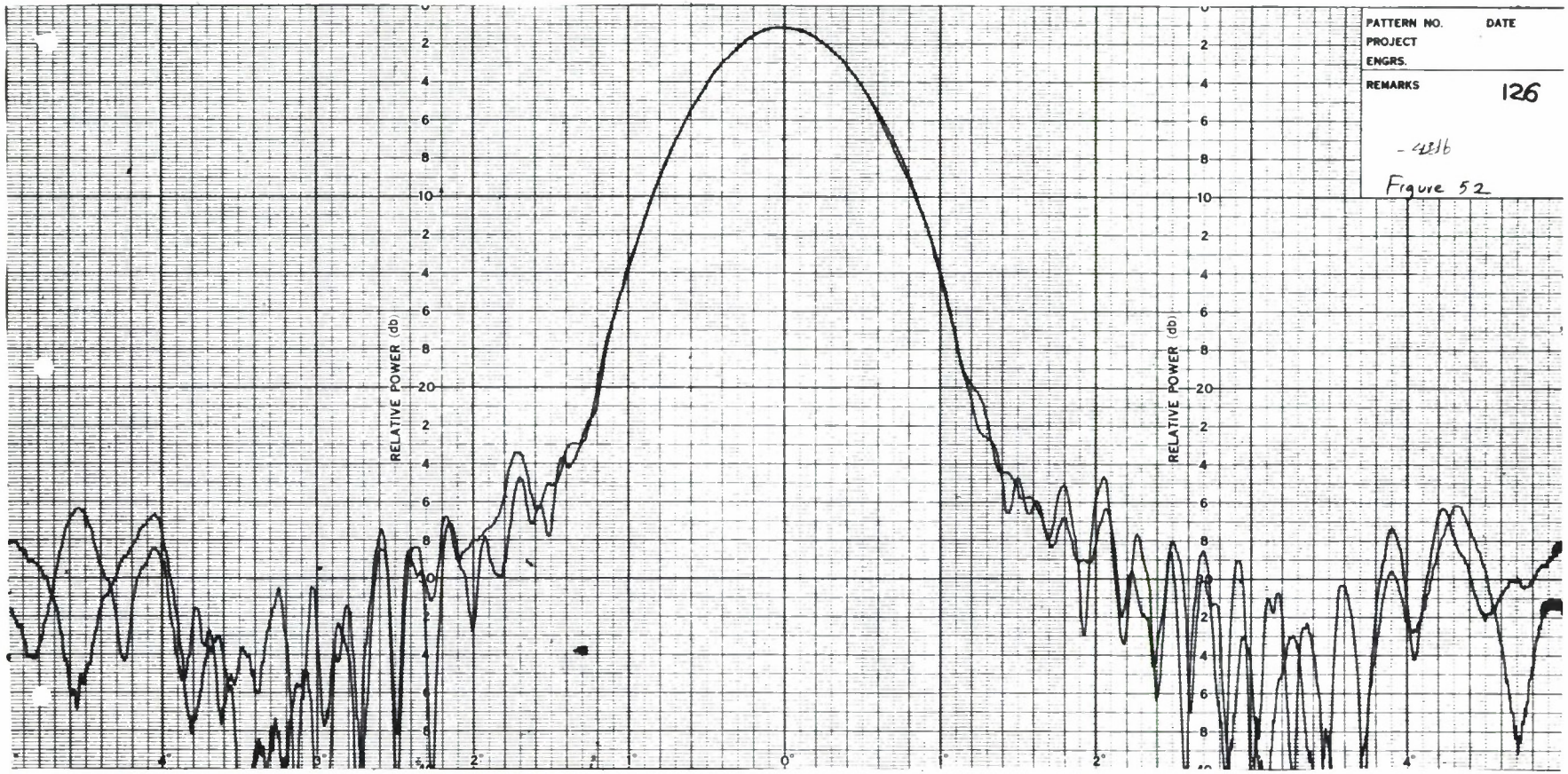

Figure 53. 360° Azimuth Pattern Comparison at Vertical Polarization. Transmitter was in Rearmost Position.

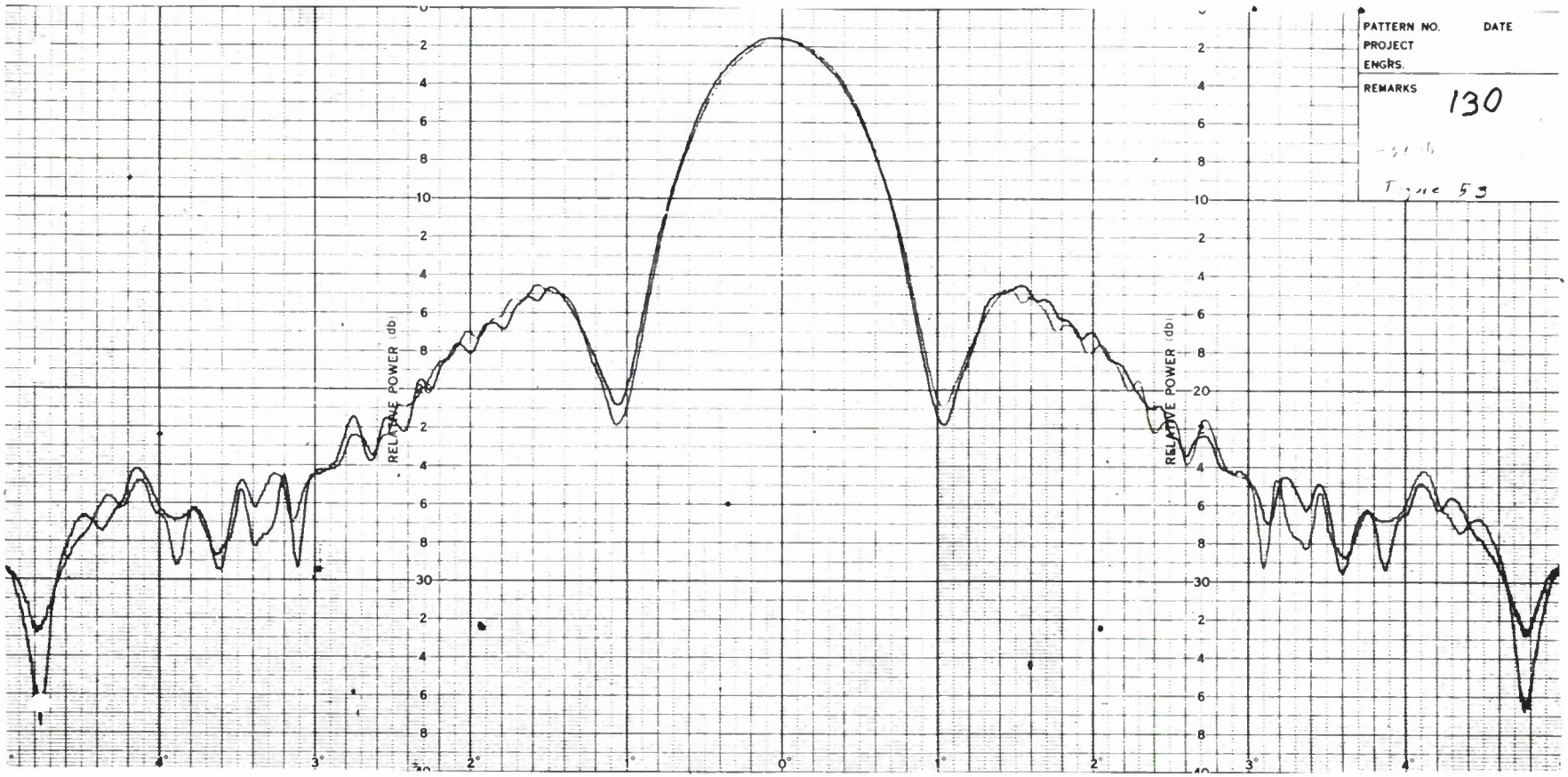

Figure 54. 360° Azimuth Pattern Comparison at Horizontal Polarization. Transmitter was in Rearmost Position.

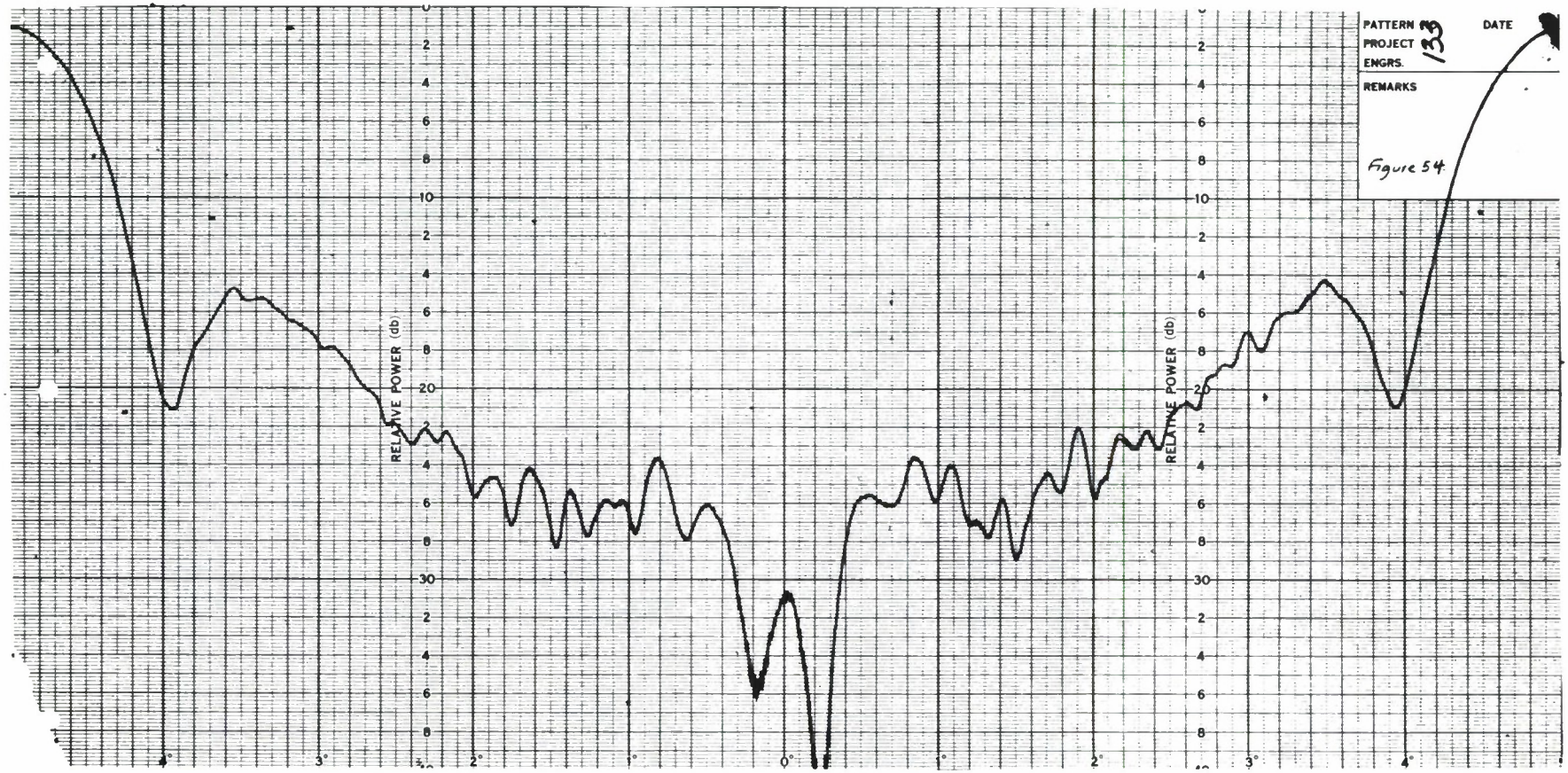

Figure 55. 360° Azimuth Patterns with and without Absorber in Transmit Antenna Slot. Transmit Antenna was in Rearmost Position.

The transmit antenna was positioned at the rear stop and patterns were made with and without absorbing material in the slot; as can be seen in the figure, the patterns are identical. This indicates that the absorbing material in the throat of the chamber is not reflecting a significant amount of energy into the quiet zone as it was at 250 MHz. One would expect a large section taken out of a strongly specularly reflecting surface to change the level of the interference pattern. This is probably due to the increased efficiency of the absorber at 3.0 GHz in conjunction with the increased directivity of the transmit antenna.

Measurements made with the transmitter positioned at the front of the slot showed essentially the same extraneous signal levels as those made with it positioned at the rear. These patterns are shown in Figures 56 and 57 for horizontal and vertical polarizations, respectively.

4.2.3 Field Probe Measurements

The field probe measurements shown in the following sections were made with a high resolution potentiometer in the recorder thus expanding the scale such that the smallest division on the ordinate now represents 0.05 dB. Figure 58 (a) and 58 (b) represent vertical cuts across the quite zone at horizontal and vertical polarization, respectively. Here again, the two cuts in each figure represent cuts with and without absorber on the model tower pan cover. The reflections from the pan appear to be on the order of -35 dB with respect to the direct path signal. A definite low pitch ripple is seen in figure 58 (b) representing a narrow angle reflection. It was shown in Equation (2.7) that the direction of an extraneous signal could be related to the period of the ripple and to the wavelength by

$$d = \frac{\lambda}{\sin \theta}$$

where d is the period and θ is the angle from which the reflection comes. A smooth curve was dotted in on the figure in order to emphasize the ripple.

The period of the ripple is about 2 feet, which corresponds to a direction of about 10 degrees off the axis. This is the region of specular reflection from

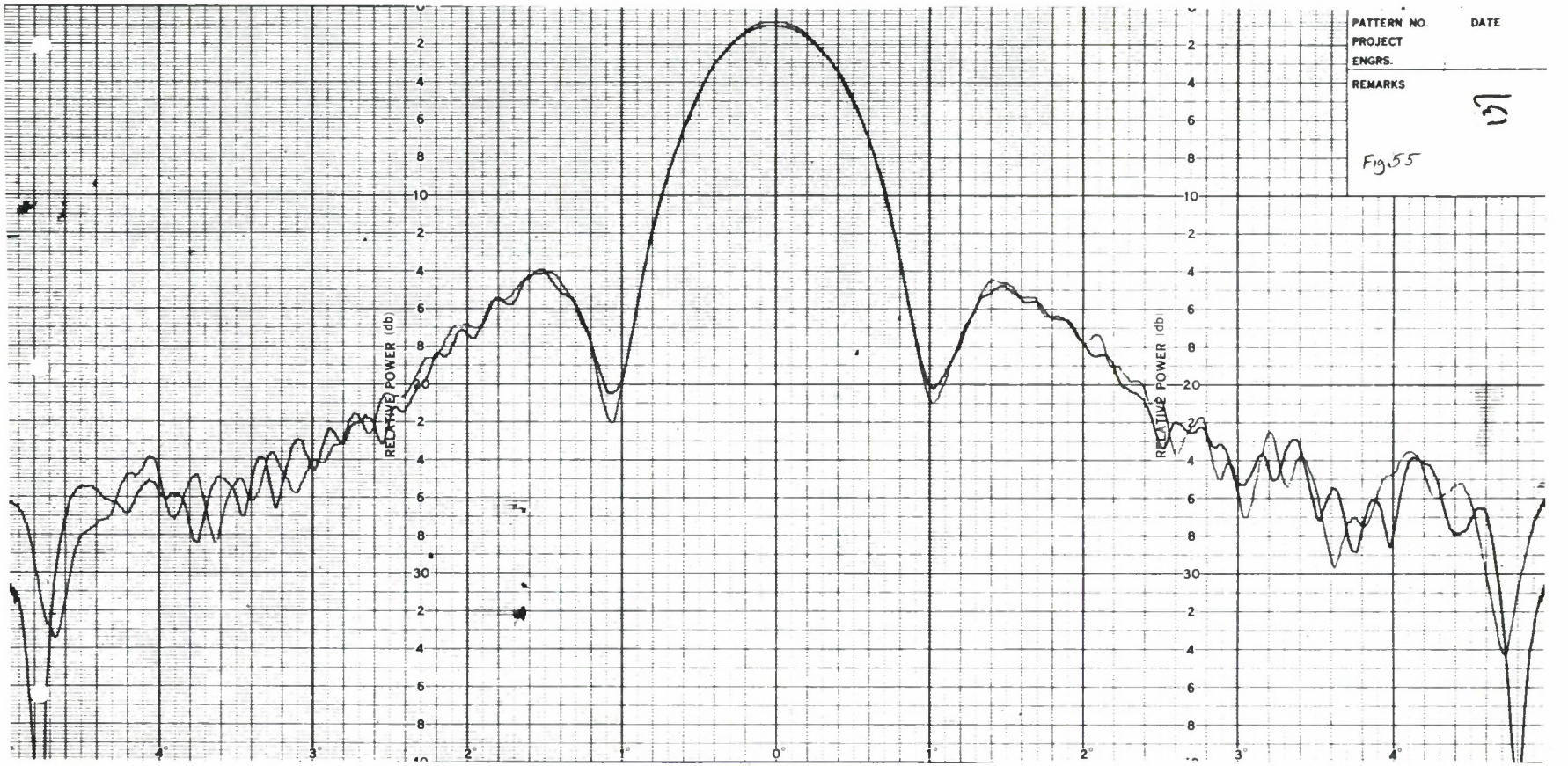

Figure 56. 360° Azimuth Pattern Comparison for Horizontal Polarization. Transmitter is in Forward Position.

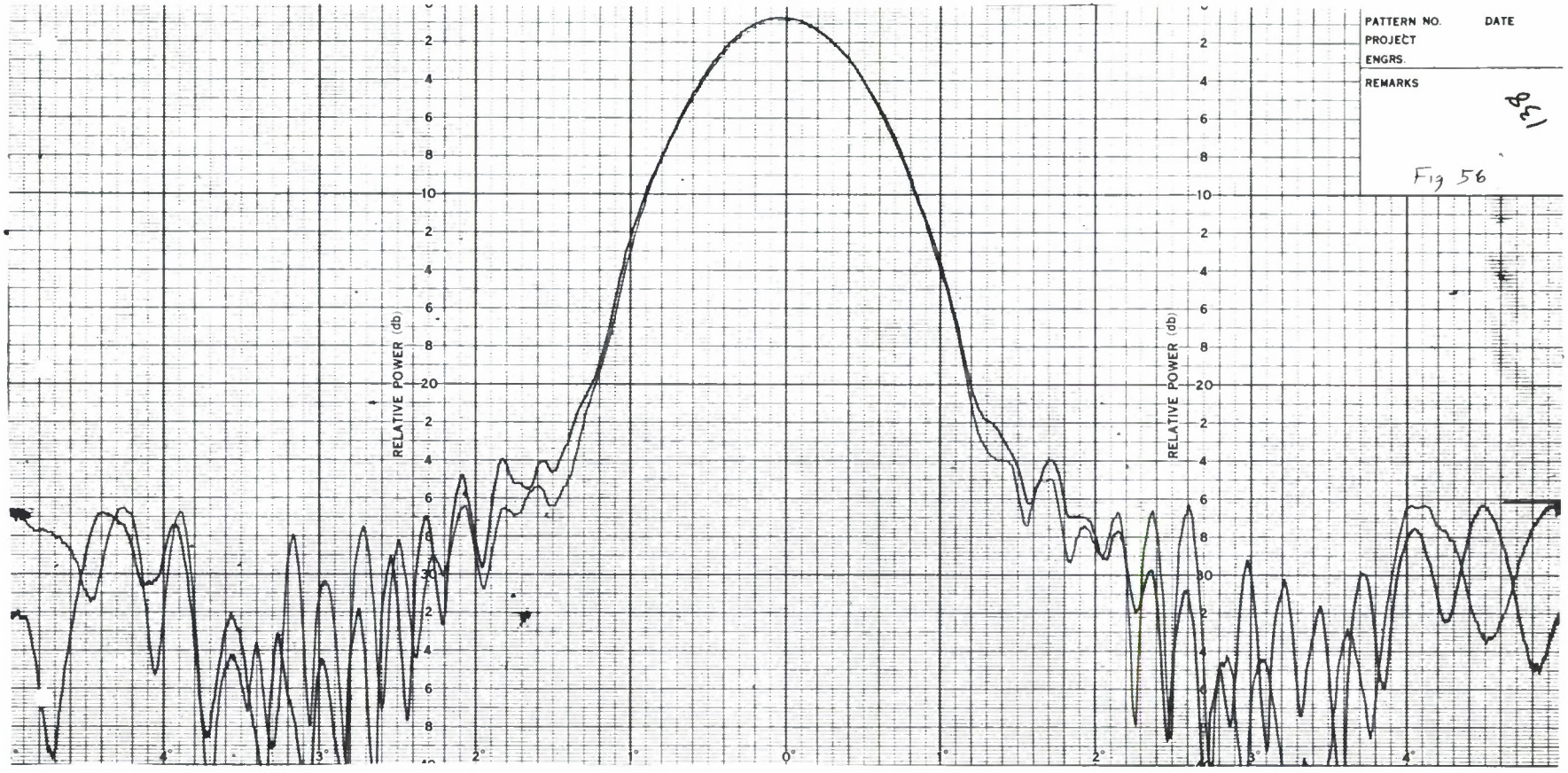

Figure 57. 360° Azimuth Pattern Comparison for Vertical Polarization. Transmitter is in Forward Position.

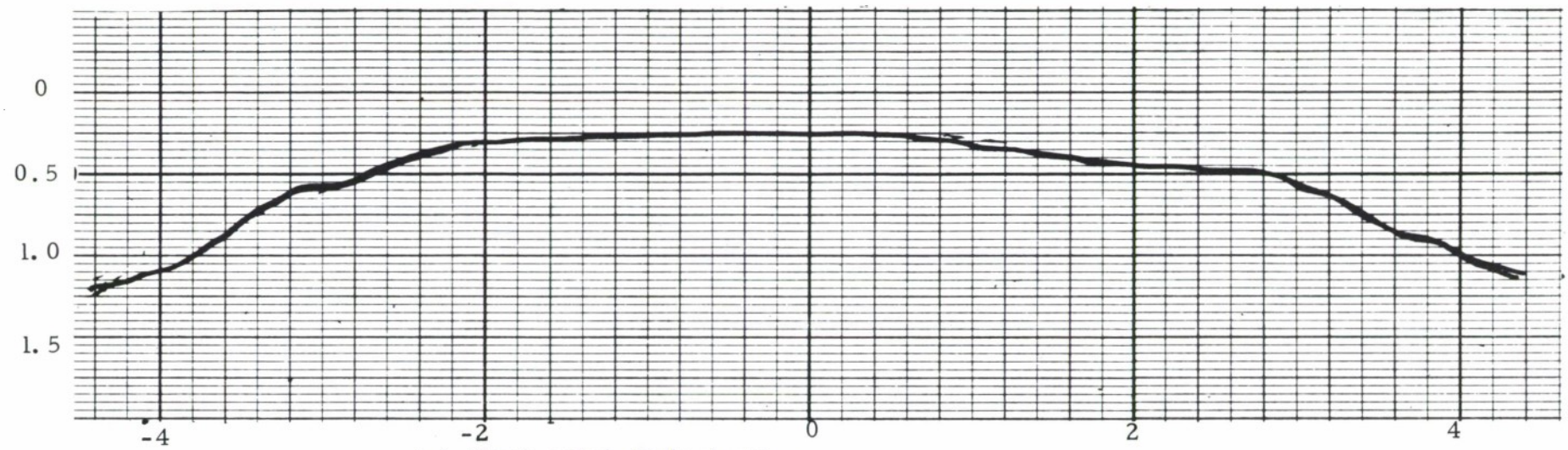

(a) Horizontal Polarization

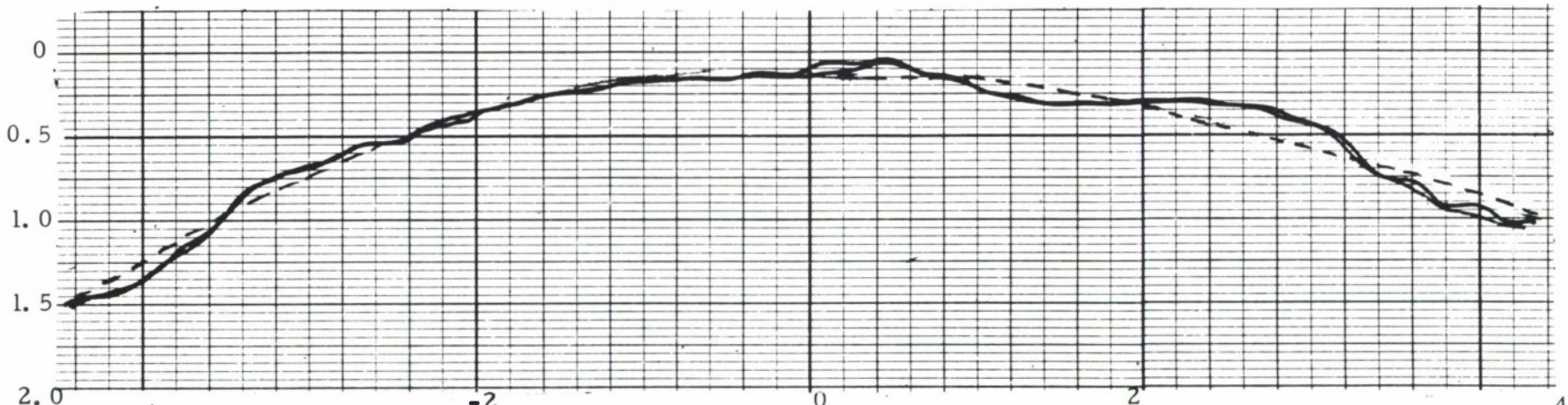

(b) Vertical Polarization

Figure 58. Vertical Field Probe Cuts at 3 GHz with and without Absorber on Model Tower Pan Cover. The Transmitter was in the Forward Position.

the throat of the chamber. The reflection level is about -35 dB with respect to the direct path signal. This specular effect was not really in evidence in Figure 58(a) at horizontal polarization. It is clearly visible at 2.2 GHz for horizontal polarization, however, as can be seen in Figure 59. This reflection level is about 40 dB below the direct path signal. The transmit antenna was in its most forward position for Figures 58(a), 58(b), and 59.

This raises the question as to where the transmitter should be placed in this particular frequency range. Figures 60 and 61 shed much light on this area. Probe measurements are shown in these figures at frequencies from 2.2 GHz to 4.0 GHz in 0.2 GHz increments. They are all vertical probes at horizontal polarization. In Figure 60, the transmitter was placed in its full forward position. Reflection levels seem to be about 40 dB down at 2.2 GHz and become less and less as the frequency increases until relatively smooth plots occur at 4.0 GHz. Note how the beamwidth of the transmit horn is starting to decrease markedly at the upper frequencies.

In Figure 61, the transmitter was placed in its rearmost position and the reflection levels are severe at the lower frequencies. Due to the poorly defined taper, the magnitude of the variations are not easily discernible, but a reasonable estimate would be about 1.0 dB peak to peak. This corresponds to a reflection level about 25 dB down. The cuts smooth out consistently with increasing frequency, but those cuts in Figure 60 represent cleaner aperture fields at all frequencies in this range. A set of horizontal cuts at horizontal polarization are shown in Figure 62 at frequencies from 2.4 GHz to 4.0 GHz. These were also made with the transmitter in its full forward position.

A longitudinal probe through the quiet zone revealed the variation shown in Figure 63(a). The period of the ripple showed that the source of energy was coming from an angle of 90°. By covering various areas with absorber, it was discovered that this energy was coming from the pit containing the positioner. When the entire pit was covered with absorber, the plot in Figure 63(b) was recorded. Strips of shielding are exposed at the edges of the absorber as is the edge of the turntable and these are likely to be sources of reflections. The reflections were determined to be at a level of -28 dB relative to direct path by measuring the ripple with the horn looking straight at the reflections and correcting for the gain levels, thus permitting higher resolution of the signal.

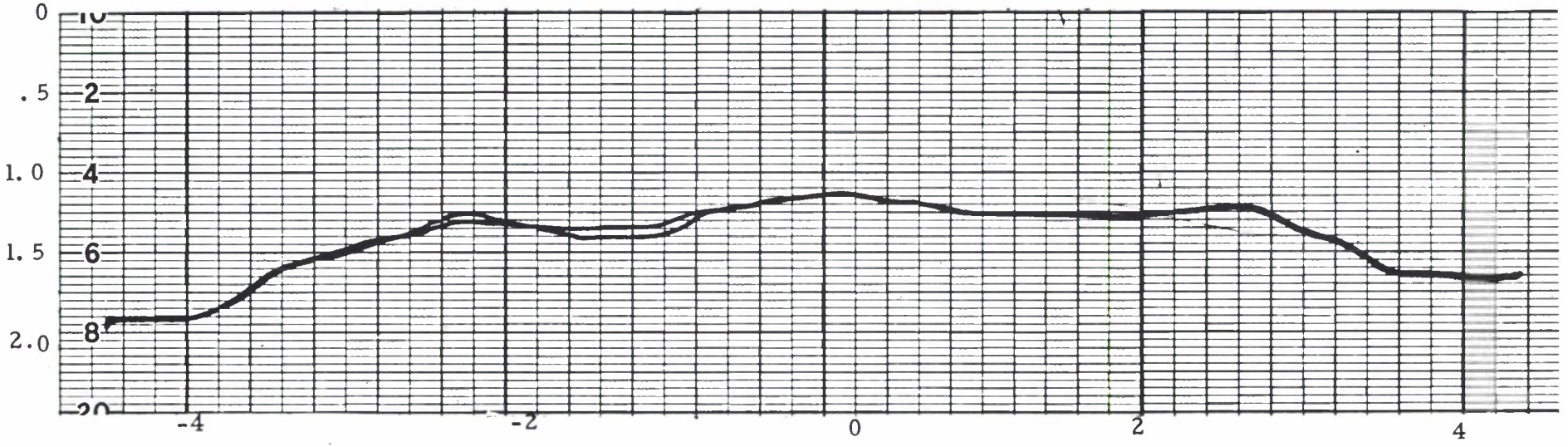

Figure 59. Vertical Field Probe Cuts at 2.2 GHz. The transmitter was in the Forward Position. Cuts were made at 90° and 270° Polarizations.

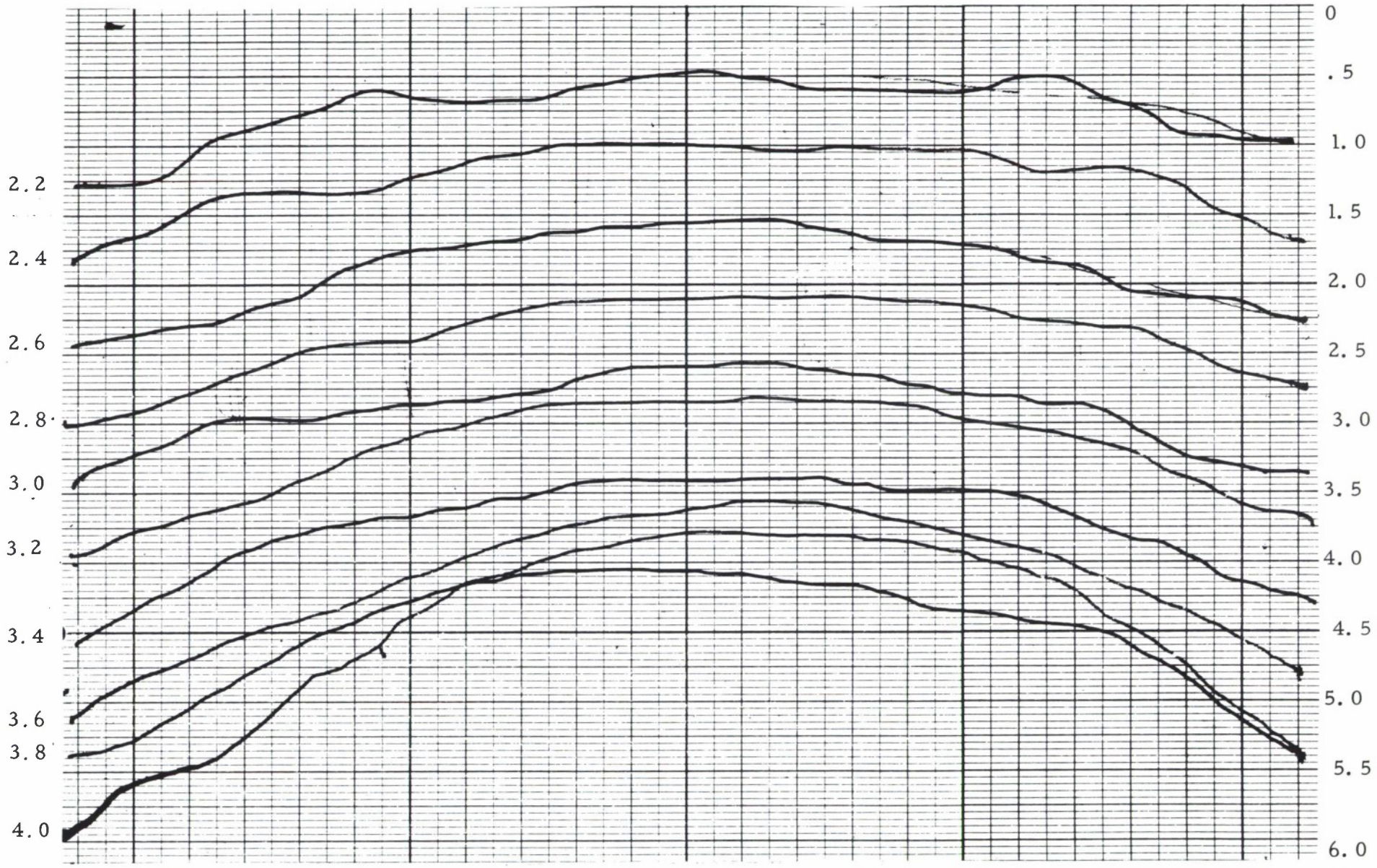

Figure 60. Vertical Field Probe Cuts as a Function of Frequency at 0.2 GHz Intervals from 2.2 GHz to 4.0 GHz. The Transmitter was in its Forward Position and Horizontally Polarized. The numbers to the left of each curve identifies the frequency at which that curve was taken. The ordinate scale is identified on the right.

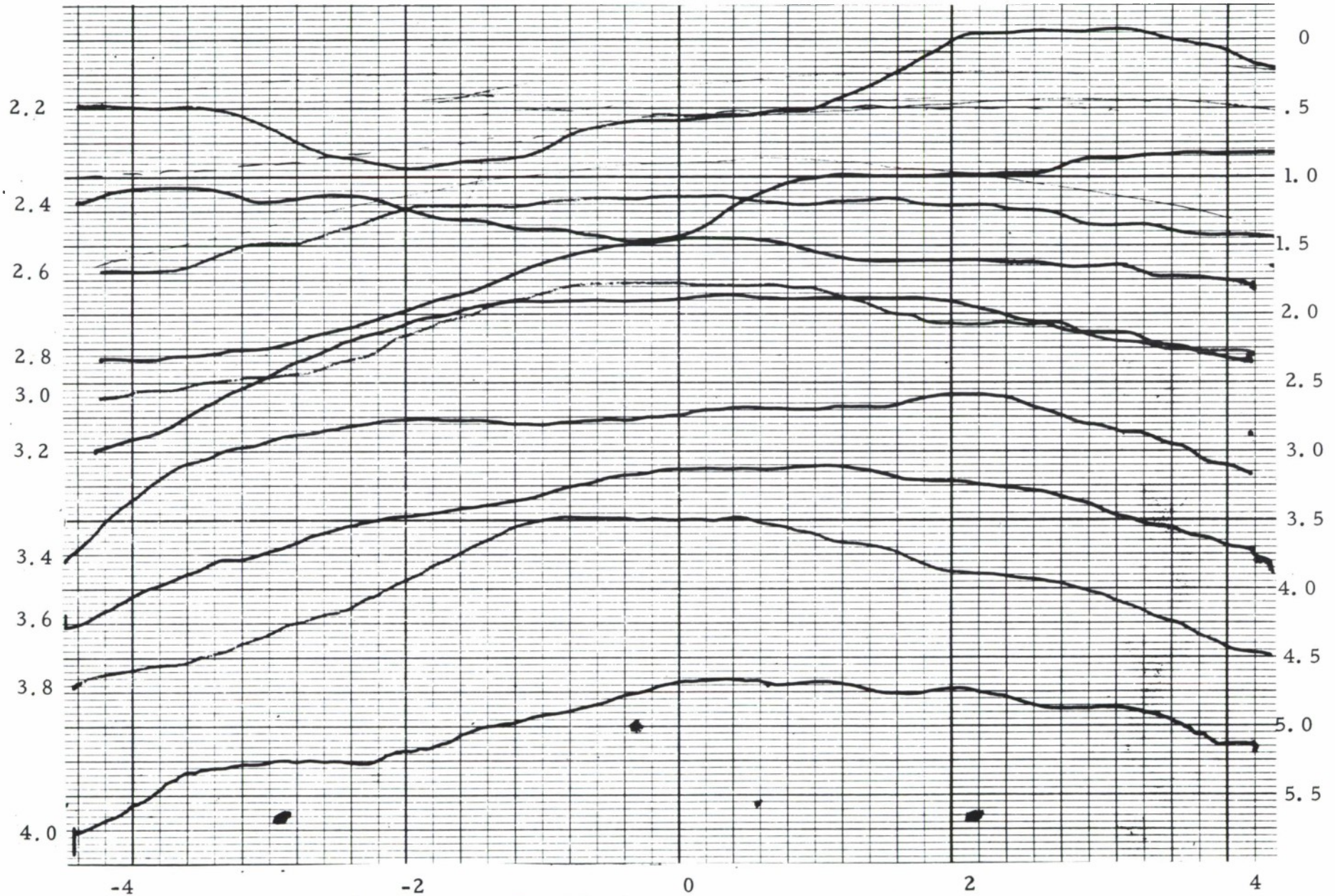

Figure 61. Vertical Field Probe Cuts as a Function of Frequency at 0.2 GHz Intervals from 2.2 GHz to 4.0 GHz. The Transmitter was in its Rearmost Position and Horizontally Polarized. The numbers to the left of each curve identifies the frequency at which that curve was taken. The ordinate scale is identified on the right.

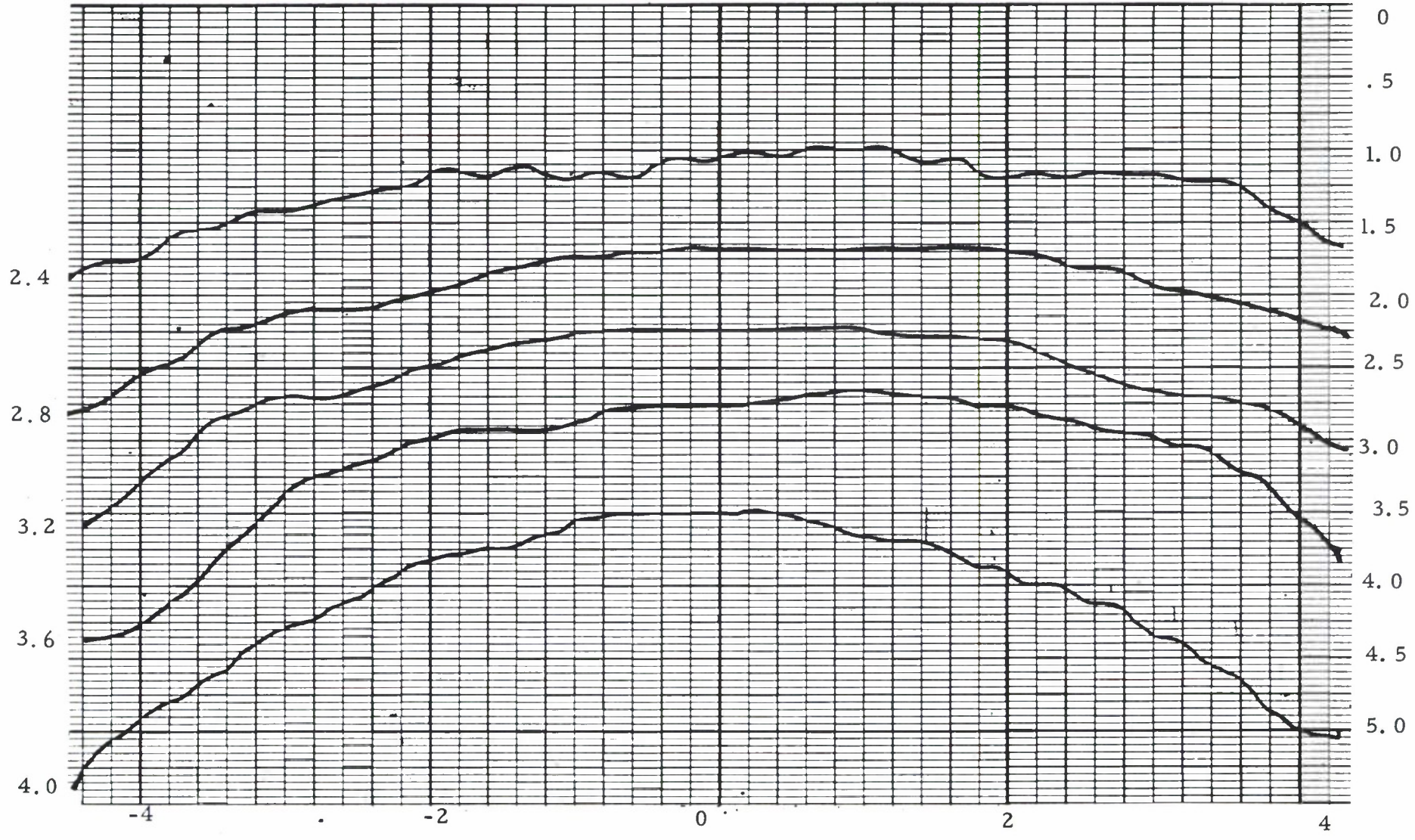

Figure 62. Horizontal Field Probe Cut as a Function of Frequency at 0.4 GHz Intervals from 2.4 GHz to 4.0 GHz. The Transmitter was in its Forward Position and Horizontally Polarized. The numbers to the left of each curve identifies the frequency at which that curve was taken. The ordinate scale is identified on the right.

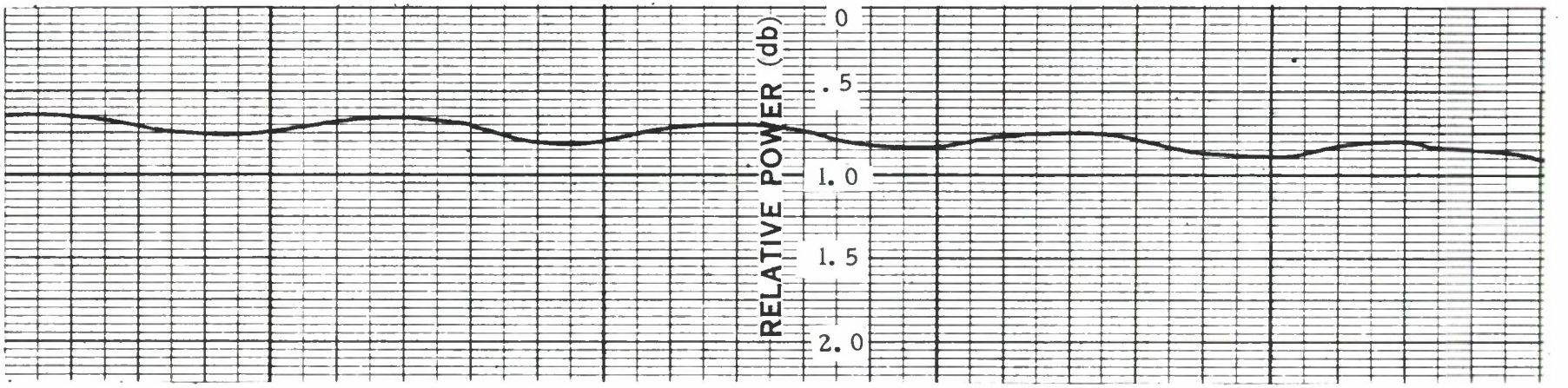

(a) Pit Uncovered.

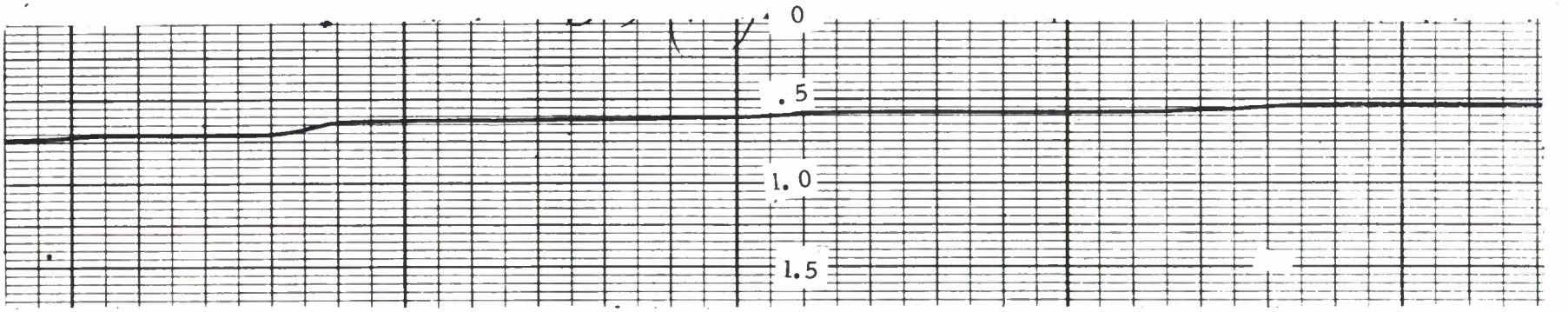

(b) Pit Blocked by Absorber.

Figure 63. Longitudinal Field Probe Cuts Showing Effects of Reflections from Pit.

4.3 10 GHz Measurements

Measurements were made at 10 GHz using a modified Scientific-Atlanta Model 12-8.2 standard gain horn. The horn was shortened to provide a half power beamwidth of approximately 30° in both planes. The transmit antenna was a Model 12-8.2 standard gain horn. Due to extended evaluation time at 3.0 GHz, measurements at this frequency were limited to polarization measurements, longitudinal field probe measurements, and pattern comparison measurements.

4.3.1 Polarization Measurements

Figures 64 and 65 present polarization patterns with the transmit antenna positioned at the front of the chamber slot. Figure 64 is for polarizations from 0° to 90° taken in 10° intervals and the same information is presented in Figure 65 for 90° to 180° polarizations. Null depths in both figures are about 45 dB. A change of 0.6 dB was observed in the peak level in Figure 64 versus 0.2 dB in Figure 65.

Similar patterns are shown in Figures 66 and 67 when the transmitter was positioned in the rearmost position. In this case, essentially no change in the maximum signal level was observed in either figure. The null depths were again about 45 dB.

4.3.2 Pattern Comparison Measurements

A 360° azimuth pattern comparison is shown in Figure 68. The extraneous signal evidenced in this pattern is about 48 dB below the direct path signal. This is based upon the differences in pattern levels about 17 dB down on the main lobe and substantiated by the differences just off the edge of the main lobe and in the back lobe area.

Figures 69 and 70 are 360° conical comparisons (i.e., those made by rotating the head axis through 360°) taken at ±5° and ±30° in azimuth respectively. Figure 69 shows a difference of 0.2 dB at the pattern peaks, which corresponds to a reflection level 39 dB below the direct path signal. A sidelobe difference of 2.0 dB at a point 10 dB below the pattern maximum as seen in Figure 70 indicates a reflection level about 39 dB down. It should be reemphasized, however, that pattern comparisons are intended to assess reflection levels over

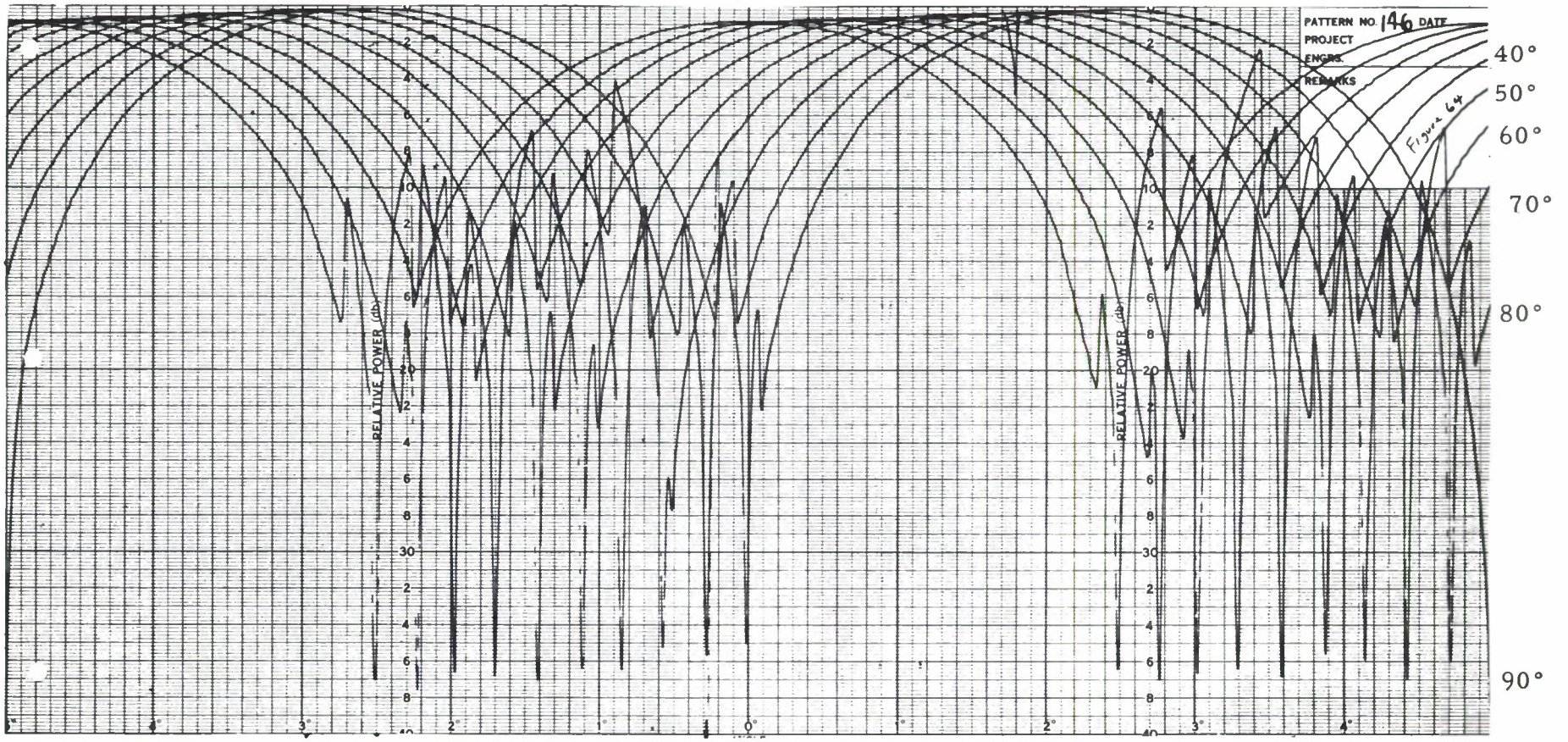

Figure 64. Polarization Patterns at 10 GHz with Transmitter positioned in the Forward Position. Patterns were taken at Transmit Antenna polarizations from 0° to 90° at 10° Intervals.

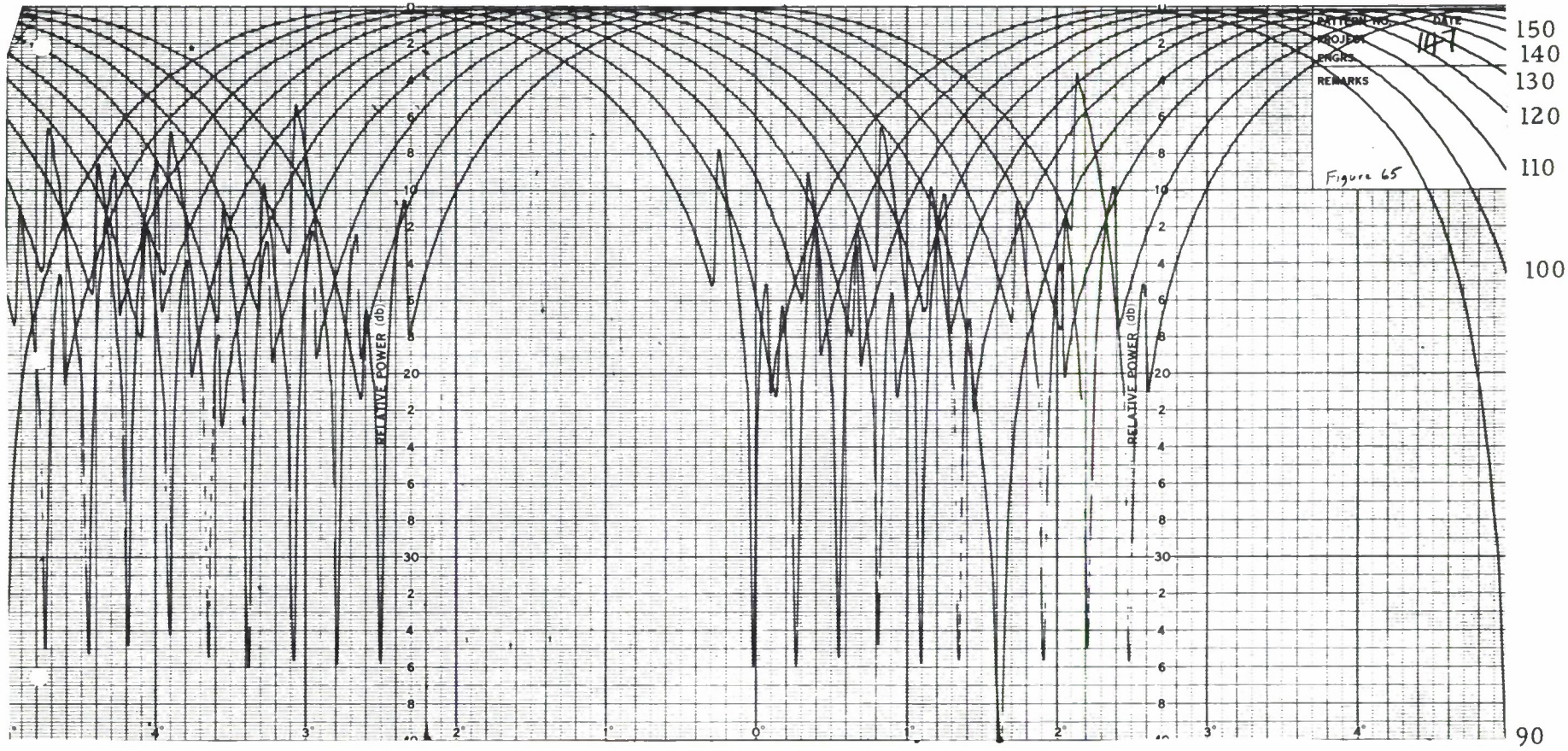

Figure 65. Polarization Patterns at 10 GHz with Transmitter Positioned in the Forward Position. Patterns were taken at Transmit Antenna Polarizations from 90° to 180° at 10° Intervals.

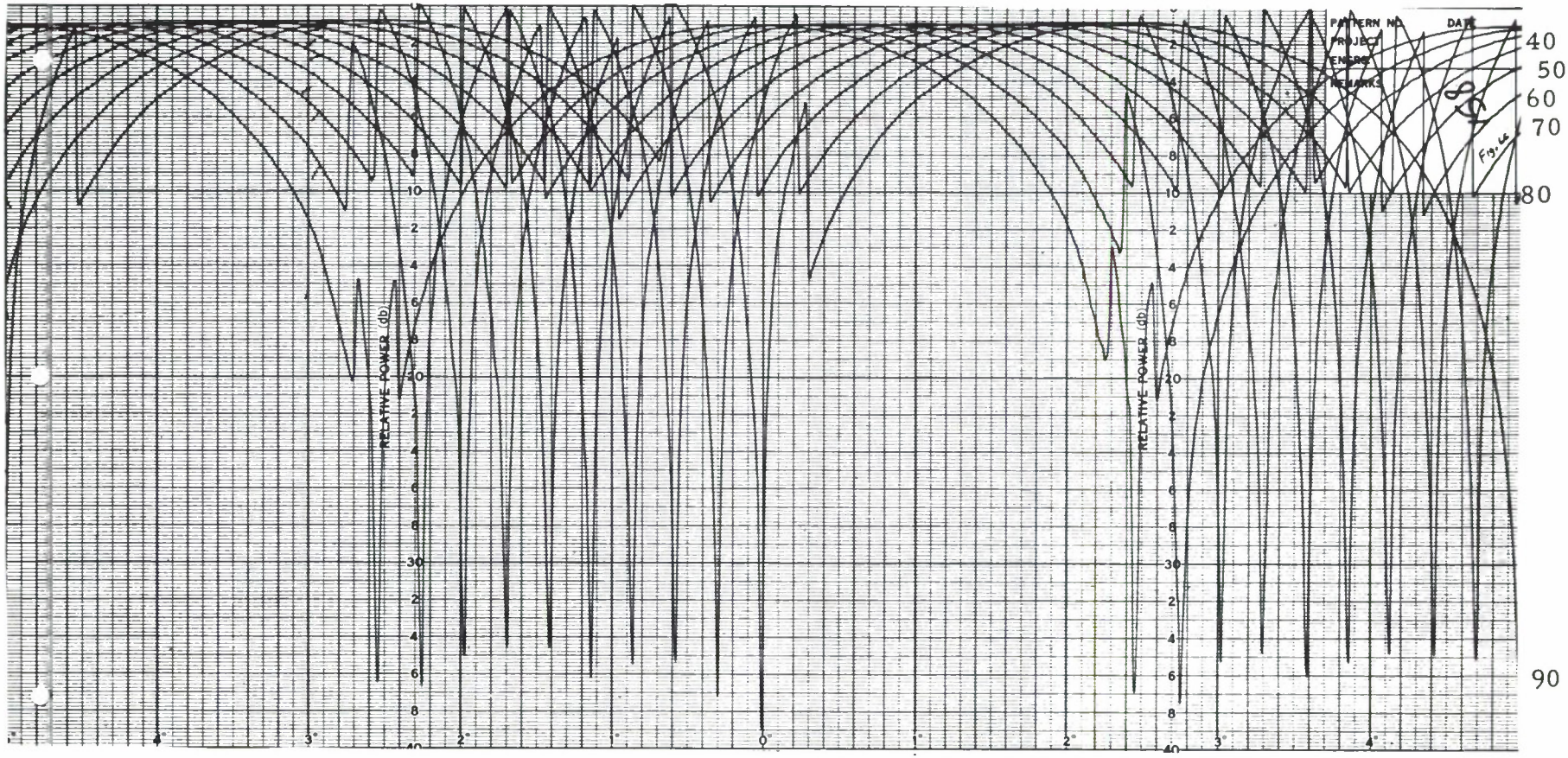

Figure 66. Polarization Patterns at 10 GHz with Transmitter Positioned in the Rearmost Position. Patterns were taken at 10° Intervals in Polarization from 0° to 90°.

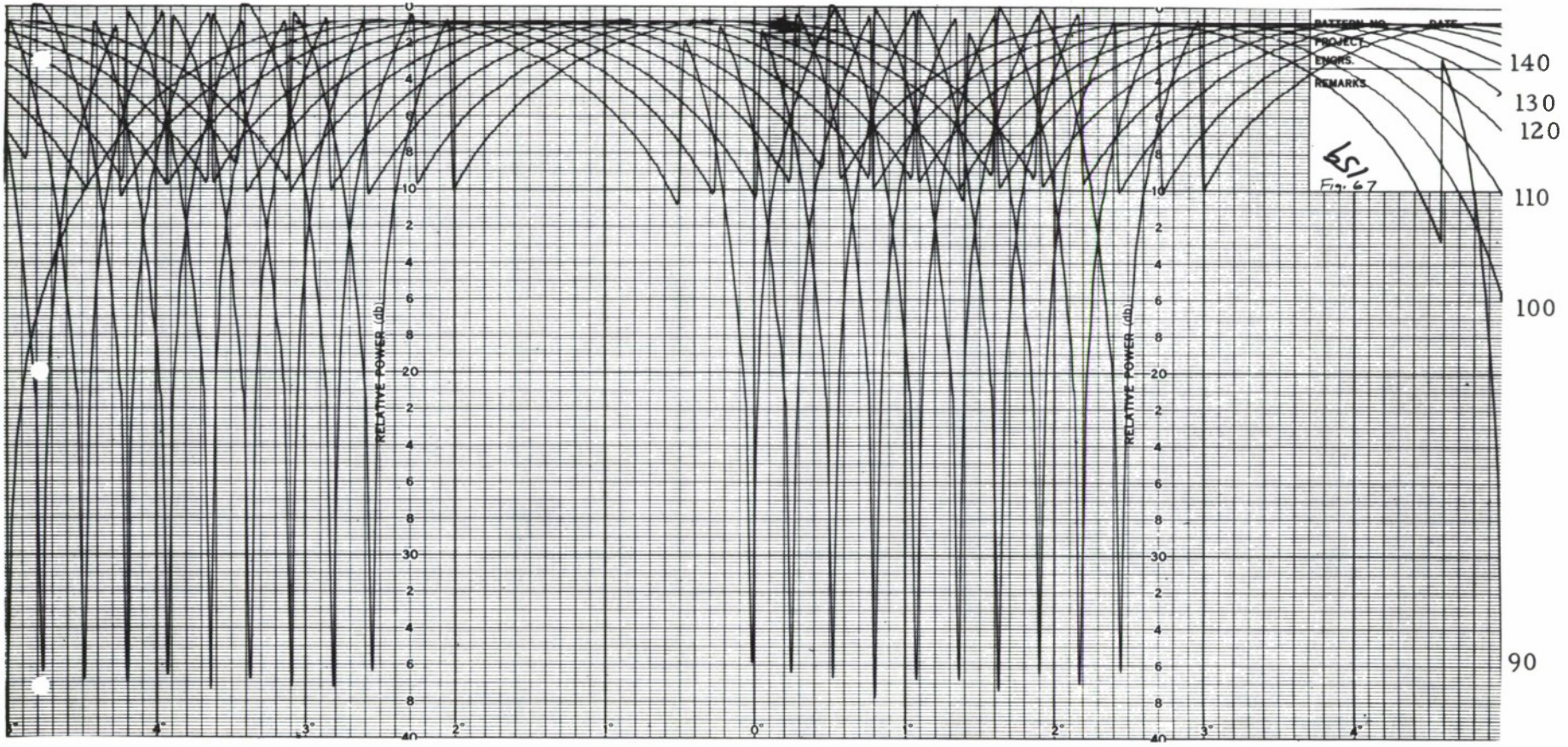

Figure 67. Polarization Patterns at 10 GHz with Transmitter Positioned in Rearmost Position. Patterns were taken at 10° Intervals in Polarization from 90° to 180°.

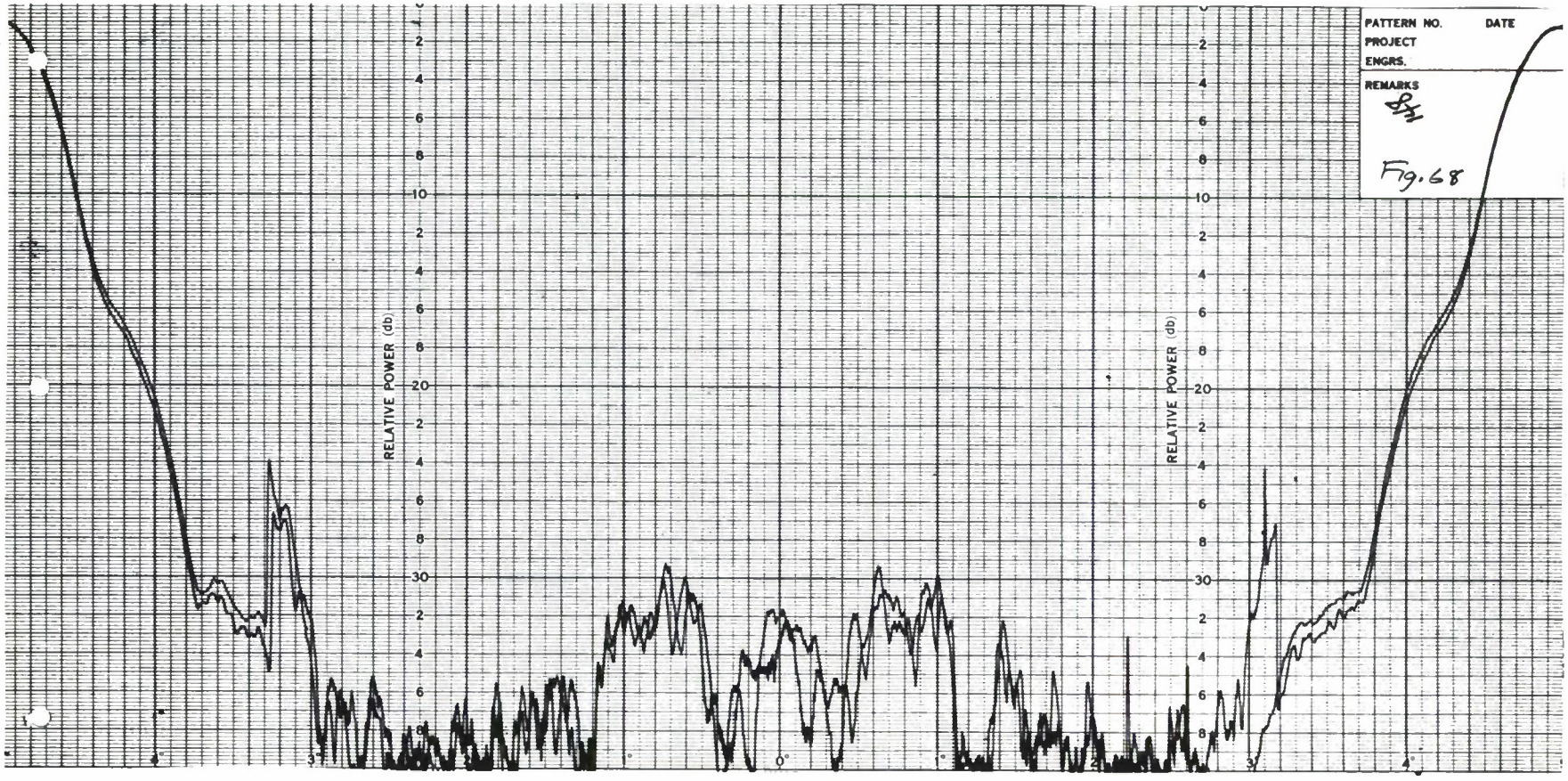

Figure 68. 360° Azimuth Pattern Comparison at 10 GHz For Vertical Polarization. Transmit Antenna was in the Forward Position and Vertically Polarized.

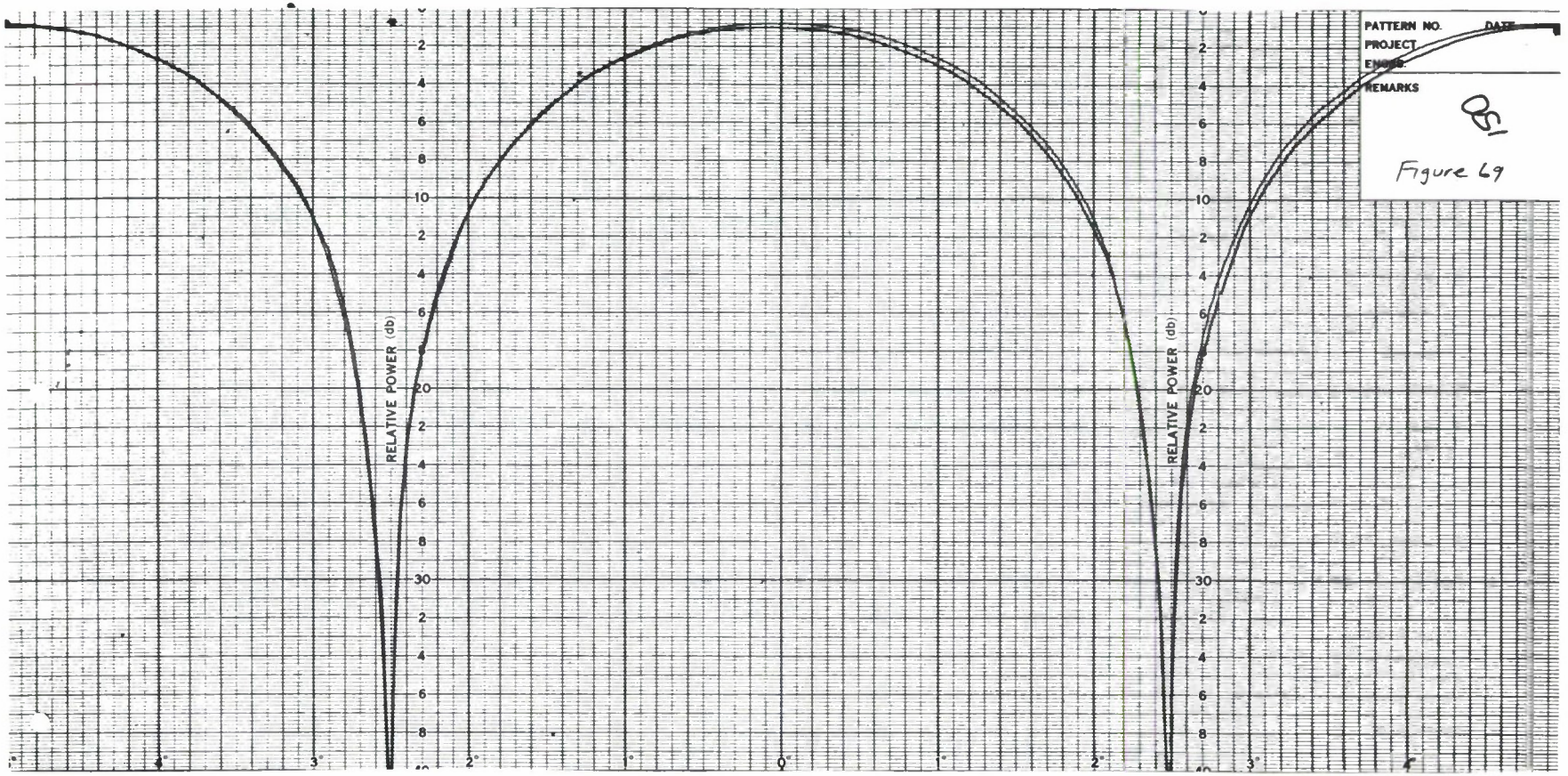

Figure 69. 360° Conical Pattern Comparison at Azimuth Settings of ±5°. Transmit Antenna was in the Forward Position and Vertically Polarized.

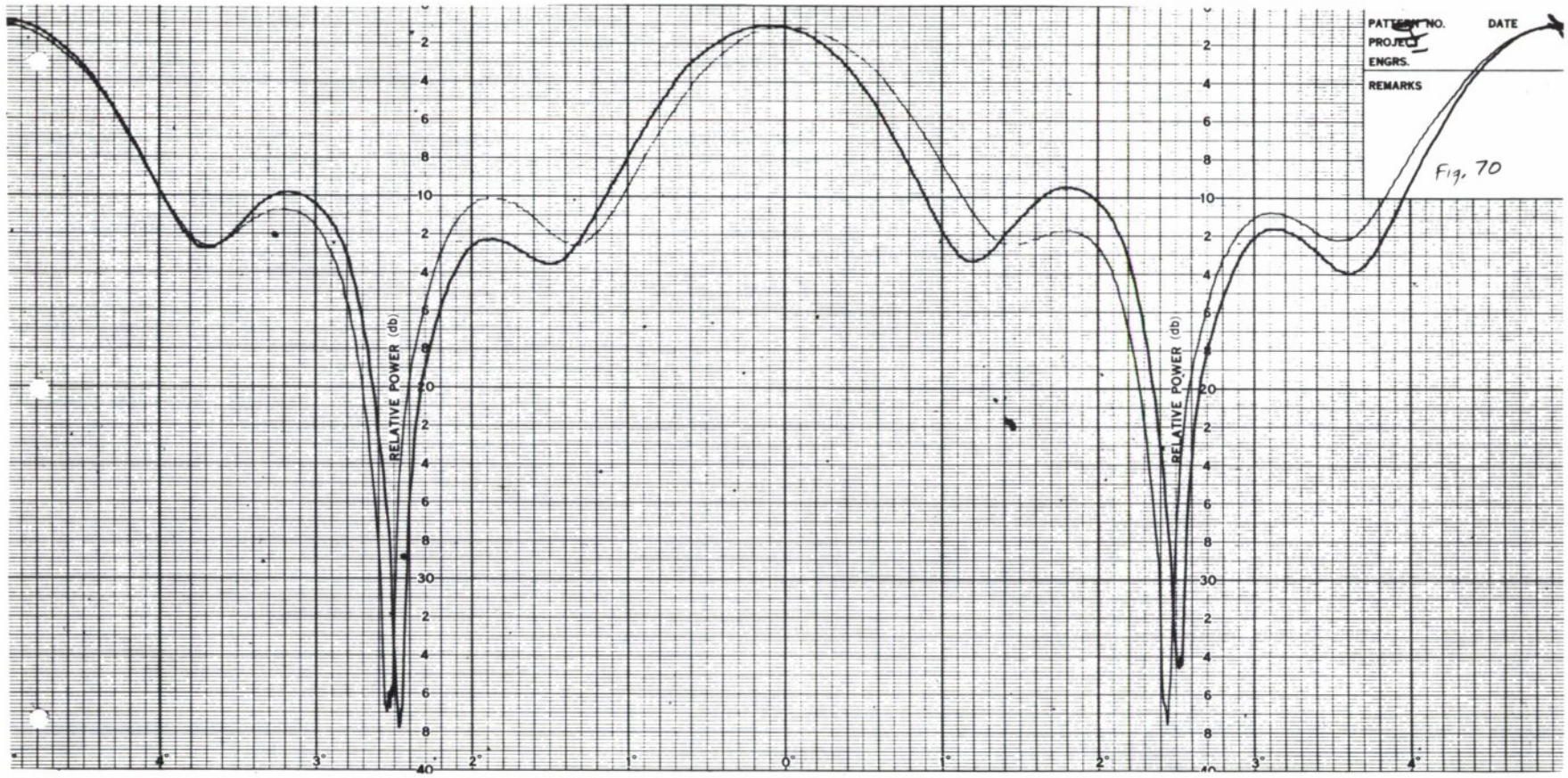

Figure 70. 360° Conical Pattern Comparison at Azimuth Settings of ±30°. Transmit Antenna was in the Forward Position and Vertically Polarized.

wide angle areas when phasing differences in the lobular structure of the antenna can integrate reflections into the pattern and allow an integrated assessment not present in Figure 70. Figure 69, on the other hand, showed a shift in the peak level of the beam and is considered reliable.

Figures 68, 69, and 70 are all taken with the transmit antenna at the front position and at vertical polarization. A conical comparison cut is shown in Figure 71 in which it was placed in the rearmost position at vertical polarization. The patterns were made at azimuth positions of ±20°. The null positions are displaced by about 7° as a result of the asymmetry. Note the definite distortion of the pattern in that the pattern which starts out at the lower level near the peak of the beam shifts over to the higher level at about 0.5 dB down on the pattern. This rules out the possibility of an incorrect synchro setting between patterns causing the difference in level. The pattern differences here again represent reflection levels only about 30 dB below the direct path signal. The indicated abscissa positions of ±80° differ in level by 4.0 dB. Four decibels peak to peak variation actually correspond to -13 dB signal level, but this was at a point approximately 17 dB down on the beam, which could provide gain to the reflected signal. Four tenths decibels difference at 36° to the right occurs at about 2.0 dB down on the beam and represents about -35 dB reflected signal level.

4.3.3 Field Probe Measurements

The only field probe measurements made at this frequency were longitudinal ones. The measurements represented in Figure 72 were made with the transmit antenna in its full forward position. The upper curve is for horizontal polarization, the lower for vertical. As in previous longitudinal probes the abscissa was on a time base on the recorder since no synchro information is available from the longitudinal drive on the model tower, which was driven at a constant rate. For this reason, the scales on these cuts vary from cut to cut and can only be established by dividing the entire length of the chart by the total length of travel. The slight ripple present, which represents reflections about 60 dB down has a pitch corresponding to 12°, or the specular zone. Figure 73 was made with the transmit antenna at the rear of the chamber and is essentially a repeat of Figure 72 in that the reflections were again about 60 dB down and coming from the same area.

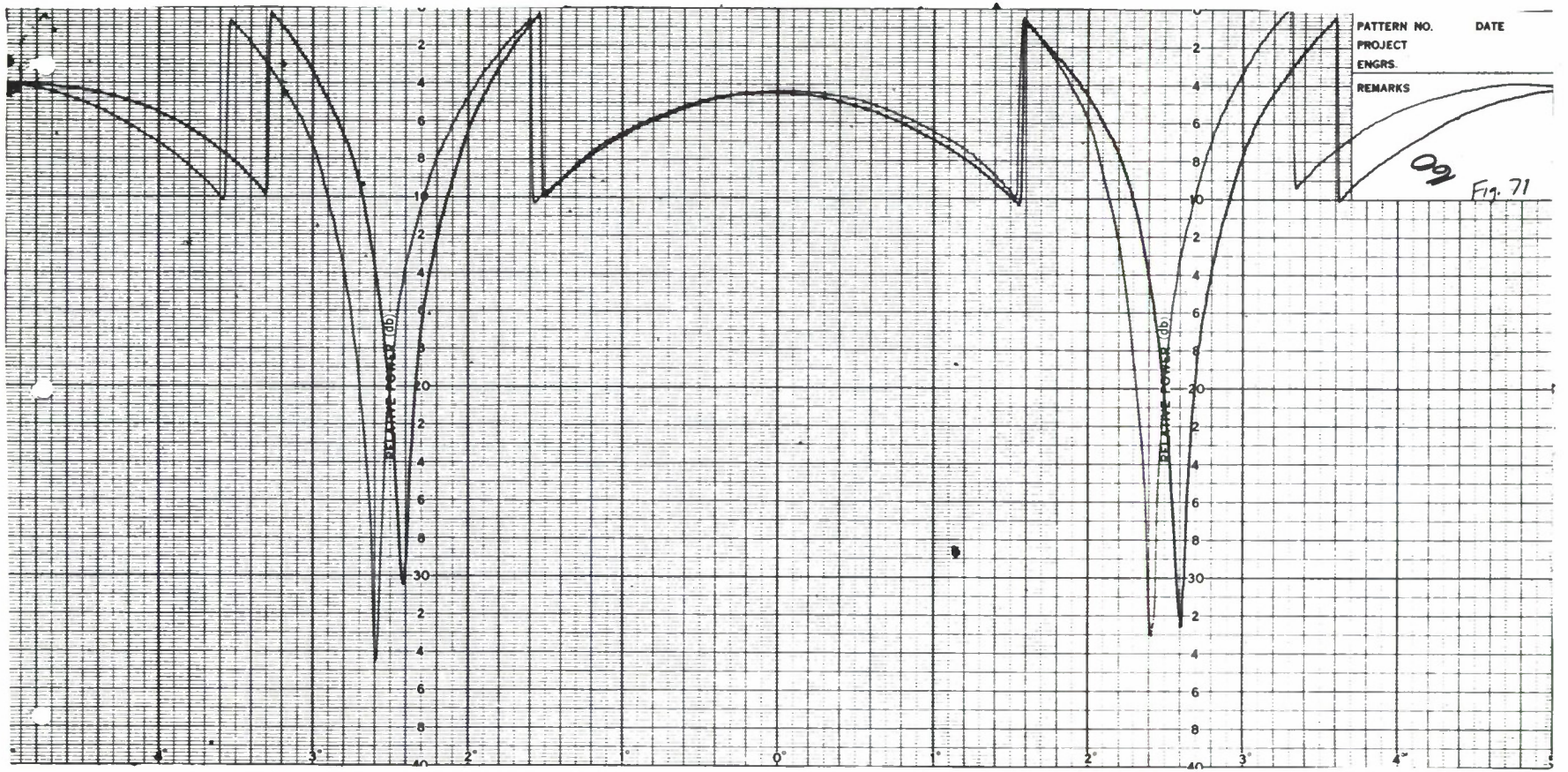

Figure 71. 360° Conical Pattern Comparison at Azimuth Settings of ±20°. The Transmit Antenna was in the Rearmost Position and Vertically Polarized.

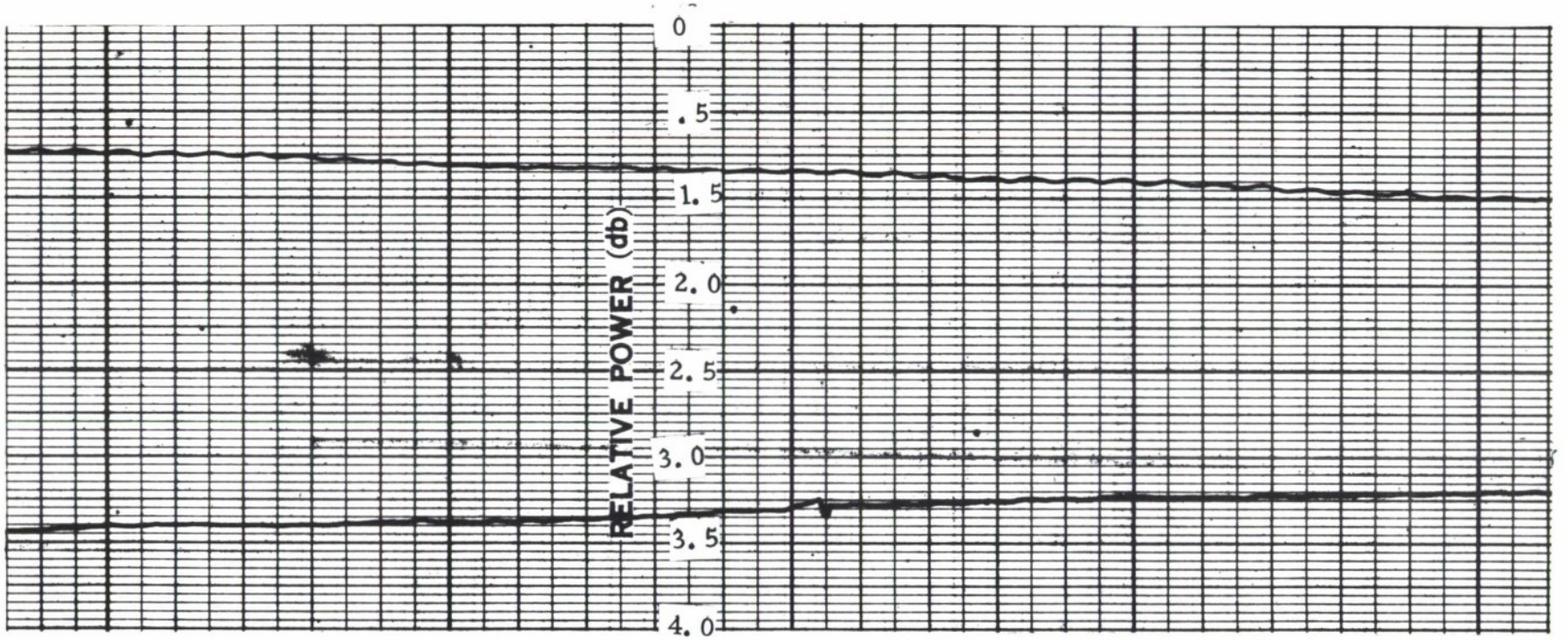

Figure 72. Longitudinal Field Probe Measurements with Transmitter in Forward Position. Upper Curve is For Horizontal Polarization, the Lower is for Vertical.

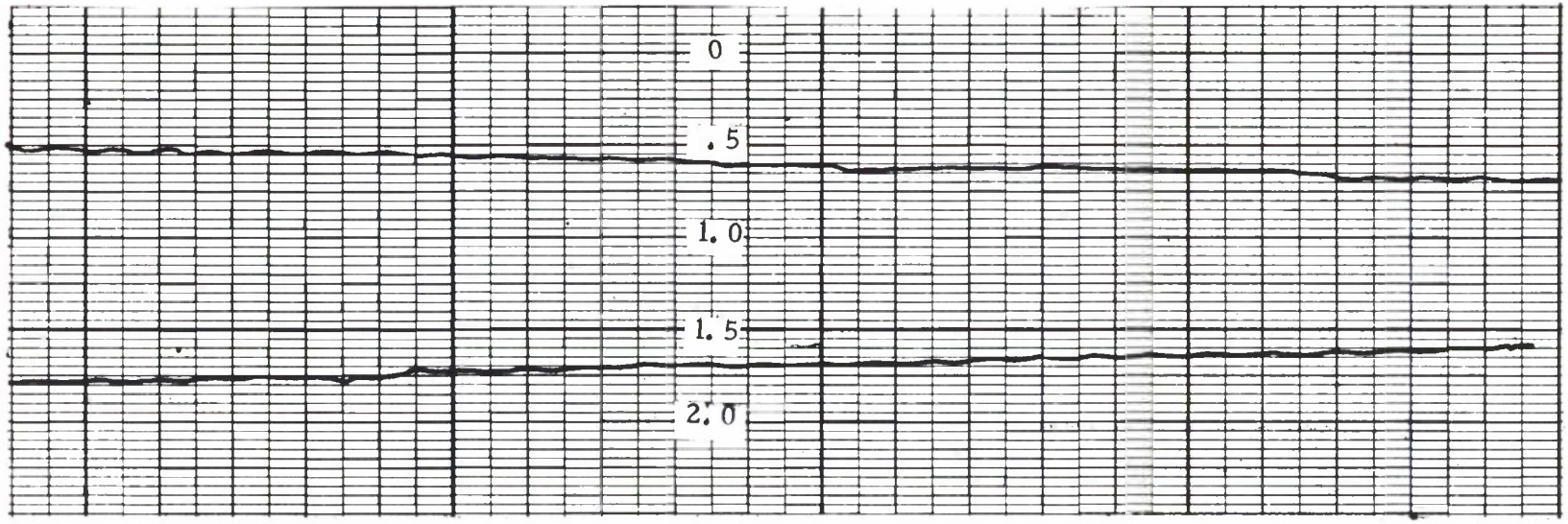

Figure 73. Longitudinal Field Probe Measurements with Transmitter in the Rearmost Position. Upper Curve is for Horizontal Polarization, the Lower is for Vertical.

5.0 CONCLUSIONS AND RECOMMENDATIONS

The analytical and experimental program described above was directed toward evaluation of the performance of the MIT Lincoln Laboratory anechoic chamber from the viewpoint of typical antenna measurement objectives. Particular parameters of concern as measured in the specified quiet zone were the polarization characteristics, the reflected energy level, and the stability of the apparent phase center of the source of radiation. The chamber was evaluated at three representative frequencies within its specified operational range of 250 MHz to 10 GHz. The first, 250 MHz, was indicative of the low frequency performance and corresponded to the low frequency evaluation conducted by Secoa, Inc. upon completion of the chamber. The second frequency, 3 GHz, coincided with the mid-range frequency of the Secoa tests, and was of particular interest in that this frequency is within the transitional band between true tapered chamber performance and quasi free-space chamber performance. The previous tests had shown 3 GHz to be the most troublesome frequency in terms of meeting specified performance criteria. The highest frequency at which tests were made was 10 GHz, which coincided with the high frequency measurements made by Secoa, and was representative of the free-space region of operation for this chamber.

The analytical work performed prior to the evaluation was quite helpful in gaining an understanding of the reflection mechanism in the tapered region upon which the operation of the tapered chamber is dependent. The chamber performed differently in each of the frequency ranges tested; these differences are discussed in the following sections.

5.1 250 MHz Operation

At 250 MHz, it was shown that the field incident upon the test areas in the plane normal to the line-of-sight was basically a smoothly varying interference pattern exhibiting a single peak at the center of the quiet zone. This interference pattern consisted of the phasor addition of direct-path energy through the primary beam of the transmit antenna and specular reflections from the tapered walls of the throat of the chamber. The relative field ampltude rolled off approximately 0.2 dB two feet to either side of the center of the quiet zone and 0.8 dB four feet to either side of the center of the quiet zone. Antennas less than four feet across would be illuminated by a field with an amplitude taper less than 0.2 dB.

A commonly accepted rule of thumb for uniform illumination in high-accuracy antenna tests is that the amplitude taper across the test aperture be less than or equal to 0.25 dB.

Interference at a level of -23 dB relative to the direct-path signal was observed due to wide angle reflections from the flat metal slide cover on the model tower base. Covering this reflecting surface with absorber during measurements eliminated it as a detectable source of interference. It is recommended that this surface be so covered for all antenna measurements. High-level reflections from the metal slide cover were detected at higher frequencies as well. It should be noted that since chamber evaluations are commonly performed before the positioning equipment is installed, it is important that some additional measurements be made after its installation.

Pattern comparison measurements performed after the slide cover was shielded detected additional wide angle reflected signals at levels of approximately -45 dB with respect to the direct-path signal level. The effects of such interference would be most noticeable in the measurement of sidelobes of an antenna. For example, a maximum error of 1 dB could result in the measurement of a sidelobe level 20 dB below the peak of the beam.

Polarization characteristics of the chamber were quite good at 250 MHz. Differences in the maximum power transfer as a function of polarization were no greater than 0.1 dB for fixed relative polarizations of the linearly polarized transmitting (YAGI) and receiving (LPA) antennas. These small deviations were attributed to the composite effects of minor roll-axis misalignments, source level instability and chamber asymmetry. The measured axial ratio of the field over the quiet zone was found to be a function of the position of the transmitting antenna along the longitudinal axis of the chamber, particularly for the diagonal (45° and 135° from vertical) linear polarization orientations. This result further substantiated the simultaneous effects of independent causes of position dependence, such as chamber asymmetries and geometrical misalignments, and demonstrated a nominal axial ratio range of 30 dB to 40 dB. In cases where extreme polarization purity is required for various orientations of linear transmit antennas, particular care should be taken in making the transmit antenna axis, the positioner polarization axis and the longitudinal chamber axis colinear.

The phase center of the transmitting array formed by the source antenna and its images was consistently within 1.5 to 3.5 milliradians of the axis of rotation of the transmit polarization positioner. The assumption of a phase center along the chamber axis should provide a sufficiently good boresighting reference for most of the antennas likely to be tested at that frequency. However, if a more accurate reference is needed for a particular boresighting requirement, then calibration of the apparent phase center location could be performed as a part of the measurement procedure.

5.2 3 GHz Operation

For frequencies in the range of about 3 GHz, specular reflection from the throat of the chamber was measured at a level of about -35 dB with respect to the direct-path signal when the transmit antenna was placed at the front of the slot. This reflected energy was clearly in evidence in the transverse field probe measurements, and from its periodicity was shown to be incident from an angle of about 10 degrees from the line of sight which corresponded to the calculated specular region in the tapered section. The level of these reflections was substantiated by pattern comparison measurements. These reflections were minimized by placing the transmit antenna at the forward limit of the slot. When the transmit antenna was placed in the rearmost limit of the slot, reflection levels as high as -25 dB were detected. The -35 dB extraneous signal level could result in pattern level errors as large as 0.3 dB near the peak of the beam. Wide angle interference from the side and back walls of the rectangular section of the chamber of the order of -42 dB was also detected by pattern comparison measurements during this evaluation.

Energy reflected from the specular regions in the tapered section could constitute a problem at frequencies for which the wavelength is short enough to cause a cyclic variation in the field across a test antenna, whereas at frequencies below about 500 MHz the wavelength is long enough that the resulting interference pattern from the same specular region gives a smooth taper across the quiet zone. The period of the interference pattern at 3 GHz for example is approximately 1.8 feet, whereas the period at 250 MHz is approximately 22 feet. (See equation 2.18). The basic difference in operational characteristics at the two frequencies is the separation in wavelengths achievable between the transmit antenna and the chamber walls. At the rear stop, the antenna's phase center was on the order of one wavelength from the walls at 250 MHz. At 3 GHz, however, moving the antenna to the same rear stop would position its phase center on

the order of 10 wavelengths from the wall. This large separation of the source antenna from its images results in a high pitched interference pattern. Better results were obtained at 3 GHz when the source antenna was brought to the front of the slot, thereby increasing the angle of incidence as measured from the wall, hence decreasing the reflection coefficient. This decrease in reflection coefficient had a more pronounced effect than did increasing the separation of the source from its images.

Reflections from the model tower slide cover were again observed at 3 GHz. At this frequency, they were about -35 dB with respect to the direct-path signal. Further interference was also detected in the region of the pit containing the positioner. This interference came from the pit itself and not from the slide cover. It was at a level of about -28 dB with respect to the direct path signal. Shielding this pit from direct-path radiation by placing absorber panels in front of it eliminated this region as a detectable source of interference.

Polarization characteristics at this frequency were essentially independent of the location of the transmit antenna. At the rearward and forward limits of the transmit antenna location, measured axial ratios employing waveguide horn antennas were approximately 45 dB as a function of polarization tilt angle.

5.3 10 GHz Operation

The reflected signal levels observed from the tapered section were about 60 dB below the direct-path signal. This significant decrease in the reflected energy level from that observed to be coming from that region at 3 GHz was due to a combination of two things. First the transmit antenna used at 10 GHz had a much narrower beamwidth than the one used at 3 GHz thus allowing a lesser amount of energy to reach the specular zone. Secondly, the absorbing material was more effective at the higher frequency. The 18 inch pyramids looked quite large to the 10 GHz radiation and large portions of them were exposed to essentially normal incidence thereby providing greater attenuation for the shorter wavelengths.

Wide angle reflections documented with pattern comparison measurements showed extraneous signal levels 45 to 50 dB below that of the direct-path signal. Reflections of this magnitude could contribute errors of 1 dB or less to sidelobe levels 20 dB below the peak of the beam.

Polarization characteristics of the chamber were excellent at this frequency. The measured axial ratios employing waveguide horn antennas remained essentially constant with transmit polarization tilt angle. The axial ratios were approximately 45 dB for the rearward and forward limits of the transmit antenna position.

DOCUMENT CONTROL DATA - R&D

(Security classification of title, body of abstract and indexing annotation must be entered when the overall report is classified)

1. ORIGINATING ACTIVITY *(Corporate author)* Scientific-Atlanta, Inc. under Purchase Order No. A-1007 to Lincoln Laboratory, M.I.T.	2a. REPORT SECURITY CLASSIFICATION Unclassified 2b. GROUP None

3. REPORT TITLE

Experimental Evaluation of the Massachusetts Institute of Technology Lincoln Laboratory Anechoic Chamber

4. DESCRIPTIVE NOTES *(Type of report and inclusive dates)*

Final Report

5. AUTHOR(S) *(Last name, first name, initial)*

Hickman, T.G. and Lyon, T.J.

6. REPORT DATE	7a. TOTAL NO. OF PAGES	7b. NO. OF REFS
June 1968	114	None

8a. CONTRACT OR GRANT NO.	9a. ORIGINATOR'S REPORT NUMBER(S)
AF 19(628)-5167 b. PROJECT NO. 649L c. d.	None 9b. OTHER REPORT NO(S) *(Any other numbers that may be assigned this report)* ESD-TR-69-65

10. AVAILABILITY/LIMITATION NOTICES

This document has been approved for public release and sale; its distribution is unlimited.

11. SUPPLEMENTARY NOTES	12. SPONSORING MILITARY ACTIVITY
None	Air Force Systems Command, USAF

13. ABSTRACT

This report presents the results of an analytical and experimental program directed toward evaluation of an 84-foot tapered anechoic chamber at M.I.T. Lincoln Laboratory. The program was cooperatively funded by Lincoln Laboratory under Contract AF 19(628)-5167 and Scientific-Atlanta, Inc.; the experiments and analyses were conducted by the Research and Analysis Group of Scientific-Atlanta with the support and assistance of Lincoln Laboratory personnel under the direction of Mr. L.J. Ricardi and the direct supervision of Mr. D.J. Frediani, Jr. Emphasis of the program was placed on documentation of the chamber capabilities at representative frequencies in terms of typical required antenna measurement objectives.

14. KEY WORDS

anechoic chamber
antennas
antenna design